BIOCHEMICAL AND MECHANICAL CUES FOR OSTEOGENIC INDUCTION OF STEM CELLS ON PAPER BASED SCAFFOLDS

A Thesis Submitted to
the Graduate School of Engineering and Sciences of
İzmir Institute of Technology
in Partial Fulfillment of the Requirements for the Degree of

DOCTOR OF PHILOSOPHY

in Bioengineering

by
Özge KARADAŞ

December 2019
İZMİR

ACKNOWLEDGMENTS

I would like to express my deepest gratitude to my supervisor Assoc. Prof. Dr. Engin Özçivici for his continuous guidance, advice, support, encouragement, insight and understanding throughout the research.

I am also grateful to Prof. Dr. Laoise McNamara from National University of Ireland, who accepted me as a short term fellow and provided me every kind of support for using all of the instruments and facilities in her lab. Special thanks to Dr. Jessica Schiavi who shared all of her valuable experiences and advices with me. Extra thanks for her help in solving my problems outside the lab as well. I must also mention Dr. Juan Alberto Panadero Perez who helped me in RT-PCR studies performed in Chapter 4 and thank to him for his valuable guidance

Dr. Johanna Melke deserves special thanks for her extreme help in the assembly of the bioreactor and for the amazing accompany during my stay in Ireland.

I would also like to thank to my past and present dissertation committee members Assoc. Prof. Dr. Ferda Soyer, Prof. Dr. Neşe Atabey, Asst. Prof. Dr. H. Cumhur Tekin Prof. Dr. Ataç Sönmez, Asst. Prof. Dr. Ozan Karaman, Asst. Prof Dr. Nur Başak Sürmeli and Assoc. Prof. Dr. Güneş Özhan Baykan.

I am especially grateful to Assoc. Prof. Dr. Gülistan Meşe and Assoc. Prof. Dr. Özden Yalçın Özuysal for their valuable advices during lab meetings and my research group members Öznur Baskan, previous member Melis Olçum Uzan, Müge Anıl İnevi, Öykü Sarıgil, special thanks to Yağmur Ünal for sharing her experiences and discussions about optimization studies and Umur Ayaz and Gizem Batı Ayaz for their help in formatting of the thesis. I would like to express my special thanks to Burcu Fıratlıgil Yıldırır, who encouraged me to apply for EMBO fellowship and motivated me throughout my PhD. My previous office mate Ceren Tabak Buru also deserves a thank for her motivation and support.

I would like to thank warmly Uğur Yurdakul, who suffers all of my whims and supports my decisions.

The biggest thanks are for my family. My parents Ayten and Bahri Karadaş were always by my side throughout my life and I felt their support every single day. I would like to thank to my sister Ceyda Karadaş as well for all the moments we share.

ABSTRACT

BIOCHEMICAL AND MECHANICAL CUES FOR OSTEOGENIC INDUCTION OF STEM CELLS ON PAPER BASED SCAFFOLDS

Tissue engineering aims to produce functional constructs with living cells that can fully integrate with the tissue when inserted into the body. Design of the scaffold and the choice of cell type that will be used for production of the tissue engineering construct are very important for the success of the application. For bone tissue engineering, incorporation of substances with antimicrobial properties can supply additional benefits. This dissertation seeks answers for two discrete questions in different chapters: Do carnosol and carnosic acid, phenolic antimicrobial compounds extracted from plants have cytotoxic effect on bone tissue derived cells and do the culture conditions (monolayer or 3D) effect the response of cells (Chapter 2); and how do application of a single type of mechanical force (vibration) and a combination of two forces (vibration plus fluid shear) affect the osteogenesis of tissue engineering constructs (Chapters 3 and 4)? The results of this research demonstrated that carnosol and carnosic acid had bacteriostatic effect at 60 μg/mL but this concentration value was highly cytotoxic for bone tissue derived cells. Nevertheless, when the same cells were incubated under 3D culture conditions their cytotoxic tolerance was higher. The supportive role of mechanical forces on osteogenic differentiation of stem cells on 3D scaffolds prepared by using filter paper, on the other hand, was demonstrated with the increase in osteoblastic gene expression, immunocytochemical staining and detection of mineralization by Alizarin red S staining and quantification. In conclusion this research showed the importance of biochemical and biomechanical cues on osteogenesis.

ÖZET

KAĞIT TABANLI DOKU İSKELELERİNDE KÖK HÜCRELERİN OSTEOJENİK FARKLILAŞMASI İÇİN BİYOKİMYASAL VE MEKANİK İŞARETLER

Doku mühendisliği canlı hücrelerden oluşan, doku işlevini yerine getirebilen ve vücuda yerleştirildiği zaman dokunun bir parçasıymış gibi görev yapabilen parçaları laboratuvar ortamında üretmeyi hedefler. Bu amaçla kullanılacak doku iskelesi ve hücre türünün seçimi uygulamanın başarılı olabilmesi için büyük önem arz etmektedir. Kemik doku mühendisliği için bu yapıya antimikrobiyal özellik taşıyan bileşenlerin ilave edilmesi üretilen doku parçasının işlevselliğini arttıracaktır. Bu tez çalışması iki önemli soruya cevap arayan farklı bölümlerden oluşmaktadır: Tezin 2. bölümünde antimikrobiyal özellikleri bulunan ve bitkilerden izole edilen karnosol ve karnosik asit fenollerinin kemik doku kaynaklı hücreler üzerindeki toksik etkileri ve hücre kültürü yönteminin (doğrudan kültür kabında ya da 3 boyutlu ortamda) hücrelerin toksik etkiye verecekleri yanıtı nasıl değiştireceği araştırılırken 3. ve 4. bölümlerde dışarıdan uygulanan titreşim ve kayma gerilimi fiziksel kuvvetlerinin, filtre kağıdından yapılan doku iskeleleri üzerine ekilmiş kök hücrelerin kemik hücrelerine farklılaşmasındaki rolü incelenmiştir. Elde edilen sonuçlara göre fenolik bileşiklerin 60 μg/mL konsantrasyonda Gram negatif bakteriler üzerinde büyümeyi durdurucu etkisi bulunduğu fakat bu konsantrasyonun kemik kaynaklı hücreler için fazla toksik olduğu sonucuna varılırken, hücreler 3 boyutlu ortamda kültüre alındığında kültür kabına kıyasla daha yüksek fenol konsantrasyonlarında canlılıklarını sürdürebildikleri gözlenmiştir. Diğer bölümlerde ise doku iskeleleri üzerindeki kök hücrelere uygulanan mekanik kuvvetlerin osteojenik farklılaşma üzerindeki olumlu etkisi gen ekspresyonu, immüno boyama teknikleri ve mineral oluşumunun saptanmasıyla belirlenmiştir. Özet olarak bu çalışmayla biyokimyasal ve biyomekanik etkenlerin kemik oluşumu üzerindeki önemi gösterilmiştir.

Dedicated to my mom and dad…

TABLE OF CONTENTS

LIST OF FIGURES x

LIST OF TABLES xiv

CHAPTER 1. BACKGROUND AND SIGNIFICANCE 1

1.1. Structure and Function of Bone 1

1.2. Bone Modeling and Remodeling 5

1.3. Bone Tissue Engineering 7

1.3.1. Cell Sources for Bone Tissue Engineering 8

1.3.2. Scaffolds 9

1.3.2.1. Filter Paper as a Scaffold Material 11

CHAPTER 2. CYTOTOXIC TOLERANCE OF HEALTHY AND CANCEROUS BONE CELLS TO ANTI-MICROBIAL PHENOLIC COMPOUNDS DEPEND ON CULTURE CONDITIONS 13

2.1. Biochemical Cues 13

2.1.1. Bone Infections and Commonly Used Antibiotics for Treatment 15

2.1.2. Natural Phenolic Compounds as Antimicrobial Agents 16

2.1.2.1. Carnosol 17

2.1.2.2. Carnosic Acid 18

2.1.3. Phenolic Compound Delivery in Tissue Engineering Applications 19

2.1.4. The Approach of the Study 20

2.2. Methods 21

2.2.1. Determination of Antimicrobial Properties 21

2.2.2. Cell Culture 22

2.2.3. Determination of Effective Carnosol and Carnosic Acid Concentration 23

2.2.4. Carnosol and Carnosic Acid Treatment for Cells on Filter Paper Scaffolds 24

2.2.5. Statistical Analyses 24
2.3. Results 25
2.3.1. Determination of Antimicrobial Properties 25
2.3.2. Determination of Effective Carnosol and Carnosic Acid Concentration 25
2.3.3. Carnosol and Carnosic Acid Treatment for Cells on Filter Paper Scaffolds 28
2.4. Discussion 30

CHAPTER 3. LOW INTENSITY MECHANICAL VIBRATIONS ENHANCE OSTEOGENESIS OF MESENCHYMAL STEM CELLS ON PAPER BASED SCAFFOLDS 36
3.1. Biomechanical Cues 36
3.1.1. Effect of Mechanical Forces on Bone at Tissue Level 36
3.1.2. Effect of Mechanical Forces on Bone at Cellular Level 37
3.1.3. Signal Transduction Pathways in Mechanotransduction 38
3.1.4. Mechanical Loading of Cells in Vitro 41
3.1.5. Low Magnitude High Frequency Vibration 42
3.2. Methods 44
3.2.1. Generation of Stable Cell Lines Through Viral Infection 44
3.2.2. Cell Culture and Osteogenic Induction 45
3.2.3. Application of Low Magnitude Mechanical Signals (LMMS) 46
3.2.4. Determination of Cell Viability on Whatman Paper 46
3.2.5. Total RNA Isolation from Paper Scaffolds and RT-PCR 47
3.2.6. Determination of Mineralization on Whatman Paper 48
3.2.7. Quantification of Alizarin Red S Staining Through Cetylpyridinium Chloride (CPC) Extraction 49
3.2.8. Total Protein Isolation and Determination of the Amount from Cells on Paper Scaffolds 49
3.2.9. FTIR Analyses for Detection of Mineralization 49
3.2.10. Statistical Analyses 50
3.3. Results 50
3.3.1. Generation of Stable Cell Lines Through Viral Infection 50

3.3.2. Determination of Cell Viability 51
3.3.3. Determination of Osteogenic Differentiation 53
3.3.3.1. Determination of Osteogenic Gene Expression 53
3.3.3.2. Determination of Mineralization 55
3.3.3.3. Detection of Extracellular Matrix Components by FTIR..... 55
3.4. Discussion 56

CHAPTER 4. BIOREACTOR BASED CONTINUOUS APPLICATION OF MECHANICAL SIGNALS TO MESENCHYMAL STEM CELLS ON PAPER BASED SCAFFOLDS ENHANCE MINERALIZATION..... 62
4.1. Bioreactors in Bone Tissue Engineering..... 62
4.1.1. Perfusion Bioreactors..... 63
4.2. Methods..... 65
4.2.1. Experimental Design for the Perfusion/Vibration Bioreactor 65
4.2.2. Total RNA Isolation from Bioreactor Samples and RT-PCR..... 68
4.2.3. FTIR Analyses for Detection of Mineralization 69
4.2.4. Detection of Scaffold Mineralization with Micro Computed Tomography (μCT)..... 69
4.2.5. Immunostaining for Osteogenic Differentiation Markers 70
4.2.6. Statistical Analyses..... 71
4.3. Results..... 71
4.3.1. The Effect of Mechanical Stress on the Differentiation of MSCs at Gene Expression Level 71
4.3.2. Micro Computed Tomography (μCT) Analyses for Detection of Mineralization..... 73
4.3.3. Immunostaining for Osteogenic Differentiation Markers 75
4.3.4. Alizarin Red S Staining for Detection of Mineralization 77
4.3.5. FTIR Analyses for Detection of Mineralization..... 77
4.4. Discussion 79

CHAPTER 5. CONCLUSION 82

CHAPTER 6. REFERENCES 84

LIST OF FIGURES

Figure **Page**

Figure 1.1. Structure of cortical and trabecular bone [3] 2

Figure 1.2. Organization of molecular components in bone tissue [9]. 3

Figure 1.3. Bone remodeling phases (Figure was drawn using Biorender software) [25]. 6

Figure 1.4. Main constituents of tissue engineered constructs (Figure was drawn using Biorender software) [25] 8

Figure 2.1. Structure of carnosol [90] 17

Figure 2.2. Structure of carnosic acid [96] 18

Figure 2.3. Anti-microbial activity of carnosol and carnosic acid on S. aureus, S. epidermidis, E. coli, and K. pneumoniae. Increasing concentrations of both carnosol and carnosic acid decreased the growth of S. aureus. Both phenolic compounds decreased the growth of S. epidermidis. Growth inhibition of S. epidermidis was not concentration dependent for carnosol, but carnosic acid effected the same organism in a concentration dependent manner. Both carnosol and carnosic acid did not have any inhibitory effect on growth of E. coli and K. pneumoniae. 26

Figure 2.4. Changes in cell viability of D1 ORL UVA bone marrow stem cells, HS-5 bone marrow cells, and Saos-2 osteosarcoma cells in a) monolayer culture for 3 days, b) monolayer culture for 3 days with 7 days prior conditioning in osteogenic medium, and c) culture for 3 days in 3D paper based scaffold. *$p \leq 0.05$ for viability at 72 h compared to 24 h calculated by ANOVA followed by Tukey's post hoc test. 1,2: differences in viability of cell type at 72 h calculated by ANOVA followed by Tukey's post hoc test. 27

Figure 2.5. Effect of carnosol treatment on monolayer cultured cell viability for 24, 48 and 72 h for a) D1 ORL UVA, b) HS-5, and c) Saos-2 cells. Effect of carnosic acid treatment on monolayer cultured cell viability for 24, 48, and 72 h for d) D1 ORL UVA, e) HS-5, and f) Saos-2 cells. †$p \leq 0.05$; ‡$p \leq 0.01$; *$p \leq 0.001$ for each time point compared to negative control calculated by ANOVA followed by Dunnett's post hoc test. 29

Figure **Page**

Figure 2.6. Effect of carnosol treatment on osteogenic conditioned monolayer cultured cell viability for 24, 48, and 72 h for a) D1 ORL UVA, b) HS-5, and c) Saos-2 cells. Effect of carnosic acid treatment on osteogenic conditioned monolayer cultured cell viability for 24, 48, and 72 h for d) D1 ORL UVA, e) HS-5, and f) Saos-2 cells. †$p \leq 0.05$; ‡$p \leq 0.01$; *$p \leq 0.001$ for each time point compared to negative control calculated by ANOVA followed by Dunnett's post hoc test. 30

Figure 2.7. Effect of carnosol treatment on 3D cultured cell viability for 24, 48, and 72 h for a) D1 ORL UVA, b) HS-5, and c) Saos-2 cells. Effect of carnosic acid treatment on 3D cultured cell viability for 24, 48, and 72 h for d) D1 ORL UVA, e) HS-5, and f) Saos-2 cells. †$p \leq 0.05$; ‡$p \leq 0.01$; *$p \leq 0.001$ for each time point compared to negative control calculated by ANOVA followed by Dunnett's post hoc test. 31

Figure 3.1. Transmission of the mechanical loads from ECM to intracellular space (The figure was drawn using Bio render software [25]) 40

Figure 3.2. WNT/β-catenin pathway in MSC differentiation (The figure was drawn using Bio render software [25]) 40

Figure 3.3. pMIG viral vector map 44

Figure 3.4. Vibration platform and the computer system 46

Figure 3.5. D1 ORL UVA cells that were infected with EGFP carrying PMIG retroviral vector. Left: phase contrast, right: fluorescent microscope images. Scale bar: 100 μm 51

Figure 3.6. The viability of D1 ORL UVA cells on filter paper scaffolds was determined via MTT test. Cell viability under a) normal growth and b) ostogenic induction conditions during 10 days. *$p \leq 0.05$; **$p \leq 0.01$; ***$p \leq 0.001$ for each cell density and each time point compared to control calculated by Student's t-test. 52

Figure 3.7. Fluorescent microscope images of D1 ORL UVA-EGFP cells showing proliferation of cells on filter paper scaffolds; a) day 1, b) day 7, c) day 14 and d) day 21after cell seeding. Magnification, 4X. 53

Figure **Page**

Figure 3.8. Gene expression levels of D1 ORL UVA stem cells that were either induced with application of vibration or with osteogenic induction medium treatment after 14 days. OCN expression was found to be higher for OC and OV groups, whereas ALP expression was lower for all groups compared to GC group. a, b, c: differences in gene expression level between groups calculated by ANOVA followed by S-N-K post hoc test. $p \leq 0.05$. GC: growth control, OC: osteogenic control, GV: growth vibration, OV: osteogenic vibration 54

Figure 3.9. a) Phase contrast micrographs of D1 ORL UVA cells in tissue culture plates, stained with Alizarin red on day 14 (Magnification 10X). Red color indicates calcium deposits. b) Quantification of Alizarin red S (ARS) staining by CPC extraction. a, b, c: differences in dissolved ARS dye concentration between groups calculated by ANOVA followed by S-N-K post hoc test. GC: Growth control, GV: Growth vibration, OC: Osteogenic control, OV: Osteogenic vibration 59

Figure 3.10. a) Stereomicroscope images of D1 ORL UVA cells seeded on paper scaffolds, incubated in regular growth medium or osteogenic induction medium and stained with Alizarin red on days 14 and 21. Red color indicates calcium deposits. b) Quantification of Alizarin red S (ARS) staining by CPC extraction. a, b, c: differences in dissolved ARS dye concentration between groups calculated by ANOVA followed by S-N-K post hoc test. GC: Growth control, GV: Growth vibration, OC: Osteogenic control, OV: Osteogenic vibration 60

Figure 3.11. FTIR spectra of filter paper samples with D1 ORL UVA stem cells that were incubated in regular growth media or osteogenic media for 14 and 21 days with vibration or under static conditions. a) Spectra of each sample and the empty paper without cells, b) spectra of samples after the spectrum of empty paper was subtracted from each. GC: Growth control, GV: Growth vibration, OC: Osteogenic control, OV: Osteogenic vibration 61

Figure 4.1. Schematic representation of custom made vibration/perfusion bioreactor [214]. 64

Figure 4.2. Parts of perfusion/vibration bioreactor and the controlling unit 66

Figure 4.3. a) Serial connection of sample holes. White circles show two successive holes that are connected to each other, and red arrows show the connector tubing. Media bottles. Medium is perfused through the system and returns back to the same bottle. The sample chamber and the screws. The chamber consists of 4 sample holes. 67

Figure **Page**

Figure 4.4. Gene expression levels of D1 ORL UVA stem cells that were either incubated in the bioreactor with regular growth medium or osteogenic medium (Br-g and Br-o), or under static culture conditions (St-g and St-o) after 19 days. OPN expression was found to be higher whereas Runx 2 and ALP expressions were lower for Br-o and Br-g compared to St-g group. a, b,: differences in gene expression levels between groups calculated by ANOVA followed by S-N-K post hoc test. 72

Figure 4.5. μCT images of the scanned paper samples. St-g: Static growth, Br-g: Bioreactor growth, St-o: Static osteogenic, Br-o: Bioreactor osteogenic 73

Figure 4.6. Histograms of each sample. St-g: Static growth, Br-g: Bioreactor growth, St-o: Static osteogenic, Br-o: Bioreactor osteogenic 74

Figure 4.7. Expression of bone specific protein osteopontin (OPN) was detected by immunocytochemical staining. Samples were stained for OPN (red) on day 19 (14 days in vibration/perfusion bioreactor and 5 days in tissue culture plate before transferring into bioreactor, or 19 days in tissue culture plate for static condition) and counterstained with DAPI (blue) for nucleus. More OPN signal was detected for the samples incubated in the bioreactor compared to static cultures. Scale bar represents 10 μm. 75

Figure 4.8. Production of bone specific protein bone sialoprotein 2 (BSP 2) was detected by immunocytochemical staining. Samples were stained for BSP 2 (red) on day 19 (14 days in vibration/perfusion bioreactor and 5 days in tissue culture plate before transferring into bioreactor, or 19 days in tissue culture plate for static condition) and counterstained with DAPI (blue) for nucleus. The signal for BSP 2 was found higher in osteogenic induction group, whether the samples were incubated in the bioreactor or under static culture conditions. Scale bar represents 20 μm for the left column, 50 μm for the right column. 76

Figure 4.9. Stereomicrographs of Alizarin red S stained samples. Samples incubated in standard growth medium under static conditions (St-g) and in the bioreactor (Br-g) were not stained, but the ones incubated in osteogenic induction medium (Br-o) and (St-o) stained positively for calcium deposition. 77

Figure 4.10. FTIR spectra of the samples between 450 and 1800 cm^{-1} wavenumbers. All of the samples had the same spectra with empty paper (Ep), except Br-o. a) Spectra of all samples demonstrating the distinct peaks of Br-o sample. b) Spectra of all samples after the spectrum of empty paper was subtracted. 78

LIST OF TABLES

Table **Page**

Table 2.1. Colony forming units (cfu)/mL results for *E.coli*, *S.aureus, K. pneumoniae* and *S. epidermidis*. 21

Table 2.2. IC50 values (μg/ml) of carnosol and carnosic acid calculated after 72h treatment of D1 ORL UVA, HS-5 and Saos-2 cells for different culture conditions. The values in parenthesis are μM equivalents of the concentrations..... 32

Table 3.1. Sequences of forward and reverse primers used for RT-qPCR reactions..... 48

Table 4.1. Sequences of forward and reverse primers used for RT-qPCR reactions..... 69

Table 4.2. Bone volume (BV) values of the samples obtained by μCT scans..... 74

Table 4.3. BMDD parameters calculated from the histograms of the samples 74

CHAPTER 1

BACKGROUND AND SIGNIFICANCE

1.1. Structure and Function of Bone

Bone is a dynamic living tissue which is renewed throughout life. Bone has various functions such as providing structural support to the body for posture and movement, protecting the vital organs from trauma, housing bone marrow as a stem cell pool and transmission of sound waves for hearing. In addition to these it is a reservoir for calcium, phosphate, bicarbonate and amino acids and it also has metabolic functions such as regulation of energy and mineral metabolism [1].

Bone tissue can be categorized into five groups according to the shape of the bones in the human body. These are long, short, flat, irregular and sesamoid bones [2]. The length of long bones is more than their width and they are cylindrical shaped. They move with muscle contraction. Short bones are only found in the wrists and ankles. They have almost equal dimensions in length, width and thickness and they provide support with a limited movement capability. Flat bones are usually thin bones and they are found in the skull, ribs and shoulders. Their primary role is to protect internal organs. Irregular bones have shapes that are not easily defined such as the facial bones forming sinuses and the vertebrae that protects the spinal cords from compression. Finally, sesamoid bones are only found in patellae and have a shape like a sesame seed. Their function is to protect tendons from compressional forces.

Bone is comprised of a dense layer, which is called as cortical (or compact) bone and a porous layer, cancellous (or trabecular or spongy) bone at the macroscopic level. Cortical bone has a more ordered structure than trabecular bone and it is the dense layer which covers all bones and surrounds the bone marrow. Cortical bone is composed of osteons, which are concentric cylindrical structures with the hollow Haversian canals in the center. Blood vessels and nerve fibers are situated in the Haversian canals. These canals are surrounded by compact mineral matrices called lamellae. Osteocytes reside in

the lamellae and their dendritic structures are connected through canaliculi for transport of blood and biochemical signals (Figure 1.1).

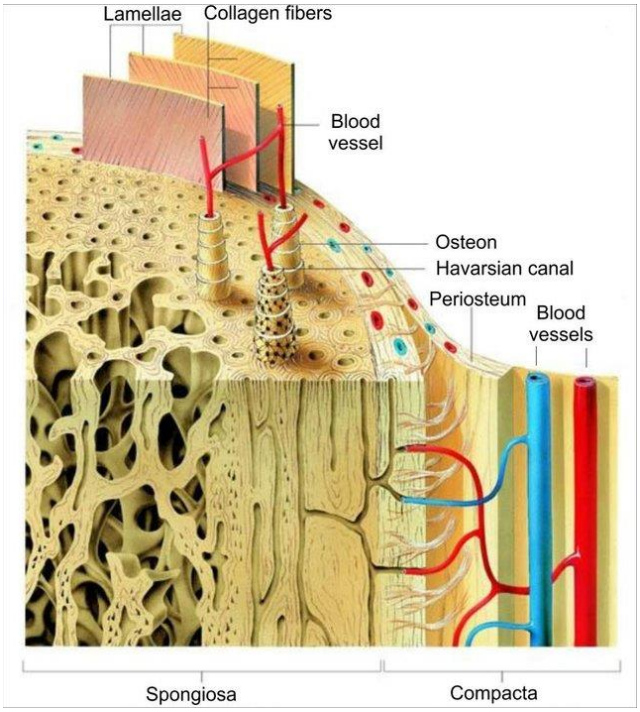

Figure 1.1. Structure of cortical and trabecular bone [3]

Trabecular bone has a higher surface area per volume ratio, so it responds to mechanical loads faster than the cortical bone with a higher metabolic activity [4]. Since the trabecular bone directly contacts with the bone marrow and blood flow with a larger surface area, bone turnover is higher than cortical bone [5].

Periosteum, which is the membranous outermost layer of all bones, except joints of long bones is a bilayer structure with a fibrous outer layer and a cambium layer. Fibrous layer provides the structural integrity whereas cambium layer is responsible for osteogenic capacity. Outer layer consists of blood vessels and the inner layer contains mesenchymal stem cells, progenitor cells, osteoblasts and fibroblasts within a collagenous matrix. Periosteum and its precursor perichondrium have two main functions; appositional growth of long bones during development and fracture healing [6].

Bone has a hierarchically organized composite structure. At nanometer level it is composed of organic collagen fibers and inorganic carbonated apatite nanocrystals. The inorganic component of bone constitutes 60-65% of its weight and 20-25% of it is composed of organic molecules, mainly collagen type I. Bone also contains small amounts of hydrogen phosphate, sodium, magnesium, citrate, potassium and carbonate ions in the mineral structure [7, 8]. Collagen gives tensile strength and hydroxyapatite crystals provide stiffness to compression. Organic components of bone also contain type III and type V collagen and non-collagenous proteins such as proteoglycans and glycoproteins, osteocalcin and osteonectin. Among these, osteonectin (SPARC) osteocalcin and osteopontin (bone sialoprotein 1, BSP 1) and BSP 2 are responsible for cell attachment and calcium and apatite binding. Osteocalcin is also chemotactic for monocytes and regulates bone formation. The remaining is composed of water that is bound to the collagen fibers or unbound water that moves within canalicular channels. The content of calcium is lower but water is higher in trabecular bone compared to cortical bone (Figure 1.2).

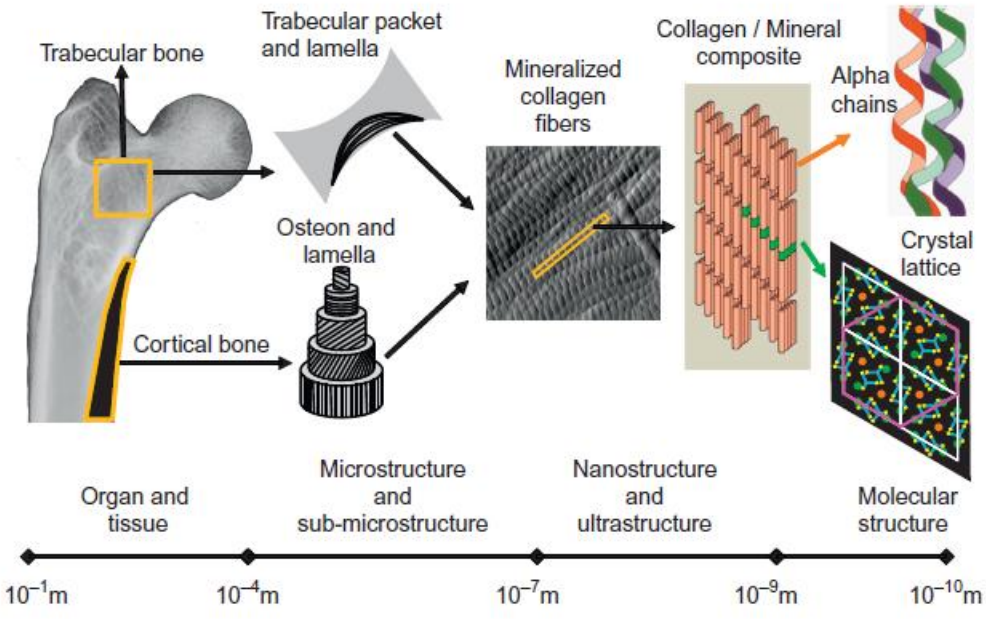

Figure 1.2. Organization of molecular components in bone tissue [9].

Bone tissue is composed of different cell types with distinct functions. Osteoblasts are single-nucleated cells that are derived from MSCs. They are responsible for the formation of new bone by directly playing a role in ECM synthesis and mineralization and indirectly in bone resorption by their paracrine effects on osteoclasts. The proliferation and differentiation of osteoblast progenitors are regulated by hormones, cytokines and growth factors and by hedgehog and WNT signaling pathways [10]. Osteoblasts are cuboid in shape and they are secretory cells with well-developed rough endoplasmic reticulum and large Golgi complexes. Osteoblasts secrete a mixture of matrix proteins which are not yet mineralized called as "osteoid" [11]. Organic and inorganic phosphate sources together are needed for further mineralization of osteoid [12]. Fate of osteoblasts are determined according to the needs of the tissue. Osteoblasts may die as a result of apoptosis after completion of their lifespan or they can turn into quiescent bone lining cells or lose most of their organelles and are trapped into mineralized matrix and become osteocytes [13]. Bone lining cells are the flat cells that cover the bone surface with osteoblastic lineage and they have osteogenic capacity [13, 14]. They are connected to each other via gap junctions and they also have important roles in maintenance of mineral homeostasis by adjusting ion flux [14].

Osteocytes are derived from osteoblasts and they are the most abundant cells in bone [15]. Some osteoblasts are buried inside the osteoid and before mineralization of the osteoid they have a transition in their shapes from cuboid to dendritic processes [16]. They connect with neighboring osteocytes and the lining cells on the surface and osteoblasts through these processes. After mineralization they get stuck in the matrix and reside there until the end of their lifespan. When osteoblasts terminally differentiate into osteocytes, they lose most of their organelles and their ability to produce ECM and their nucleus to cytoplasm ratio increases [17]. They are the main sensors of mechanical stimuli in bone and they have important roles in bone modeling and remodeling through communication with osteoblasts and osteoclasts [16].

Mononuclear osteoclasts are terminally differentiated and derived from the same precursors as macrophages and they form multinuclear osteoclasts by fusion [18]. After formation of multinucleated cells they resorb the calcified matrices in coordination with osteoblasts [19]. They degrade bone by adhering to bone matrix and secreting acidic and lytic enzymes [20]. They have other functions than bone resorption such as participating

in immune responses, secretion of cytokines and regulation of osteoblastic cell functions and migration of hematopoietic stem cells from bone marrow to blood stream [19].

Each bone cell type is responsible from the maintenance of bone tissue by anabolic and catabolic reactions and as a result of these reactions bone alters throughout life and adapts to the environmental conditions which will be discussed more thoroughly in the following section.

1.2. Bone Modeling and Remodeling

Bone modeling usually occurs in children and it is less evident in adults except fracture healing, and the aim is to reshape the bone or increase bone mass [21]. First, precursor cells are recruited and activated for differentiation upon osteoblasts for bone formation or osteoclasts for bone resorption to normalize local bone strain by increasing or decreasing bone mass. Osteoblasts and osteoclasts do not work simultaneously; they work separately on different bone surfaces. Modeling always takes place on preexisting bone tissue [21]. Modeling and remodeling processes are different from each other. Bone remodeling, on the other hand, is a sequential formation and resorption process occur at the same site of the bone by osteoblasts and osteoclasts. The aim of remodeling is to replace the old bone and form the new tissue for the maintenance or a slight decrease in bone mass [21]. Remodeling of bone can be divided into two types, physiological remodeling and adaptive remodeling. Physiological remodeling is the resorption and formation processes without altering the shape of bone for the maintenance of the skeletal tissue. Adaptive remodeling occurs as a result of mechanical loading and changes the shape, strength and density of the bone [4]. Remodeling cycle consists of a series of events in which osteoblasts and osteoclasts communicate with each other. The combination of osteoblasts, osteoclasts and blood capillaries that work together for the renewal of bone is called as “basic multicellular unit (BMU)” [22]. The remodeling of bone is a five step process. It starts with the activation phase in which osteoclast precursors in the blood stream are recruited and activated. In the second phase, which is resorption, osteoclasts adhere to bone surface and form a ruffled membrane to increase their secretory surface and degrade bone matrix via proteases and matrix metalloproteinases and an increase in

local acidity [23]. This step ends with the programmed cell death of osteoclasts to prevent excess degradation. The next step is reversal, in which osteoclasts stop resorbing bone and formation of new bone starts by osteoblasts. The mechanism underlying this step is not well understood yet [21, 24]. The next step, formation, is divided into two phases. In the first phase of this step non-mineralized protein mixture osteoid is secreted by osteoblasts and in the second phase the osteoid is mineralized by the coordination of calcium and phosphate concentrations and mineralization inhibitor proteins such as osteopontin [24]. In the final step, termination, after completion of mineralization osteoblasts whether die as a result of apoptosis, or they become lining cells or osteocytes (Figure 1.3).

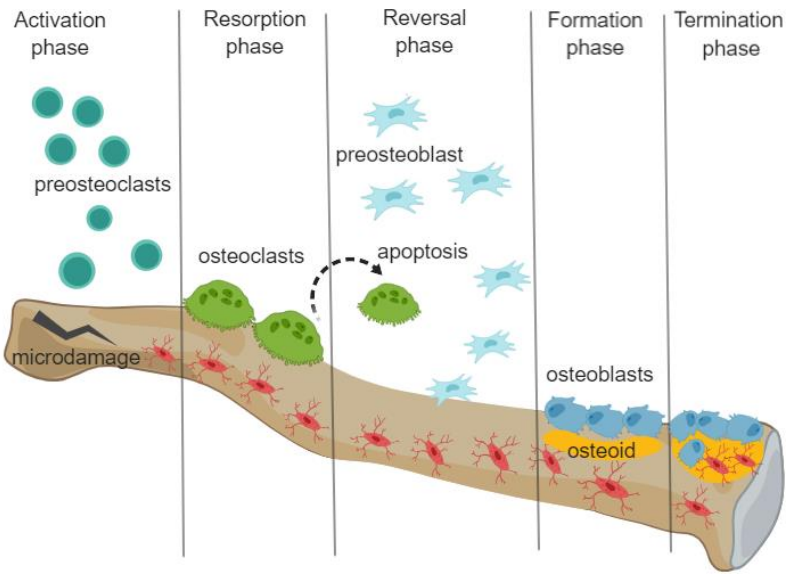

Figure 1.3. Bone remodeling phases (Figure was drawn using Biorender software) [25].

If the remodeling is targeted, it occurs at a specific site to repair a damaged or old bone and this process is directed by osteocytes. However, if the remodeling is non-targeted it occurs as a result of systemic changes such as the alteration of hormone concentrations and it is not site-specific [24].

1.3. Bone Tissue Engineering

Bone can recover the minor defects by remodeling throughout the life of an individual. However, some cases such as accidents, tumor resection surgeries, osteoporotic fractures or tissue loss due to osteonecrosis may lead to fractures that cannot be repaired by the tissue itself. These are defined as the 'critical sized defects' [26]. In clinic, for the treatment of these types of defects usually bone grafts or implants made up of various metallic or polymeric materials are used. Even though these systems have successful outcomes for the treatment of bone defects they also have some drawbacks. Autografts (patient's own tissue taken from a healthy part of the body) might cause donor side morbidity or allografts (tissue transplanted from another person) and xenografts (tissue transplanted from another species) might be rejected by the patient's immune system [27]. Metallic implants are widely used for joint replacement, but they cause stress shielding since their stiffness values are generally much higher compared to the bone [28]. Polymeric grafts, on the other hand, have some advantages such as tunable mechanical properties, scaffold architecture and degradation time, but at the same time they might release residues that can cause immune reactions as a result of biodegradation. These drawbacks of the traditional treatment methods yield a need for developing new technologies.

Tissue engineering is an emerging field of science that has been developing especially for the last decades. The main principle of tissue engineering depends on formation of functional tissues in vitro. To achieve this goal, three main constituents are needed; scaffolds, cells and biochemical or physical signals (Figure 1.4).

An ideal bone tissue engineering construct should match the mechanical strength of the bone, integrate with the healthy tissue and allow vascularization. Each component of the construct should be selected meticulously for the success of the application to meet ideal design criteria. Detailed information about the types of each component is given in the following sections.

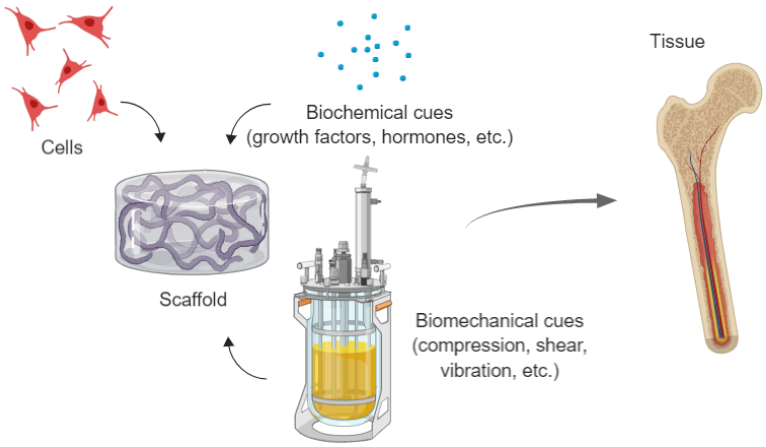

Figure 1.4. Main constituents of tissue engineered constructs (Figure was drawn using Biorender software) [25].

1.3.1. Cell Sources for Bone Tissue Engineering

Osteoblasts and osteocytes are the main regulatory cells for bone deposition, so osteoblasts and precursor cells are considered as the primary cell sources for bone repair studies. Stem cells, on the other hand, can proliferate for a long time *in vitro* and are mostly preferred because of their differentiation potential into different lineages upon stimulation. Bone marrow mesenchymal stem cells (BM-MSCs) are the most preferred stem cell source because of their high osteogenic potential [29]. It was reported lately that periosteum also contains skeletal stem cells with higher regenerative potential than BM-MSCs [30, 31]. Adipose tissue derived stem cells are also used very commonly as an alternative to BM-MSCs because of the ease in isolation and their survival capacity in low oxygen and glucose conditions which is a problem often encountered when growing cells in 3D scaffolds *in vitro* [29]. Stem cells isolated from discarded tissues as a result of surgical operations such as oral cavity derived stem cells have gained importance lately [32]. Skin is another important stem cell source by being easily accessible and the non-invasive isolation procedures of the cells. In addition, these cells do not cause oncogenesis after transplantation [33]. Another non-invasive stem cell source that is obtained from a discarded tissue is the umbilical cord. Especially, the connective tissue of the umbilical cord, called as Wharton's jelly, is a potential cell source for bone tissue engineering applications [34]. Menstrual blood derived endometrial stem cells are also a non-invasive

cell source with osteogenic differentiation potential which was discovered almost a decade ago [34-36]. In addition to adult stem cells, embryonic stem cells are also used for tissue engineering. However, because of difficulty in expansion of these cells *in vitro* and some ethical issues regarding their use adult stem cells are more intensely used for tissue engineering applications [37, 38].

Other than primary cells isolated from tissues, cell lines that are transformed by viruses to make them immortal or non-transformed cell lines are also commonly used for bone tissue engineering applications. Depending on the needs of the research various cell lines at different differentiation stages and isolated from different species such as mouse, rat or human can be used. Among these cells, most widely used ones are osteosarcoma derived cell lines with osteoblastic phenotype ROS 17/2.8 and UMR 106 (rat), MG-63 and SaOS-2 (human) or non-transformed cell lines MC3T3-E1 (newborn mouse calvaria) and UMR 201 (neonatal rat calvaria) [39]. MLO-Y4 cell line derived from murine long bone is another commonly used cell line with osteocytic characteristics [39]. D1 ORL UVA cell line, which was used in all experimental designs throughout this research, is derived from mouse bone marrow stromal cells and can differentiate into osteogenic lineage rapidly [40]. This cell type is capable of expression of osteoblastic genes, as well as alkaline phosphatase production and *in vitro* mineralization [41]. Another cell line used in this thesis, HS-5, is a transformed cell line and derived from human bone marrow stroma. HS-5 cells have the functional marrow characteristics and represent the bone marrow microenvironment [42].

1.3.2. Scaffolds

A scaffold in tissue engineering is the mechanical support that holds the cells together. There are plenty of different scaffold designs in the literature and especially with the developments in 3D printing and bioprinting technologies it is even possible to produce organs outside the body [43]. In order to encounter the needs of the specific tissues, scaffolds should have some properties. Primarily a scaffold must be biocompatible; the material itself and its degradation products should not evoke immune response in the body [44]. The surface chemistry and topography of the scaffold are very

important for cell attachment and differentiation [45, 46]. Porosity and pore size distribution, shape and interconnectivity of the pores are also very important for the nourishment of the cells through infiltration and for vascularization [47]. Biodegradability is another important parameter. If the degradation rate of the scaffold is correlated with the formation of new tissue, the mechanical forces acting on the scaffold can be transferred to the newly formed tissue in time due to deposition of the new tissue. If a scaffold material can be digested by the enzymes of the body or via through simple hydrolysis upon implantation, this prevents the need for a second surgery for the removal of the implant [48].

A plethora of different materials, synthetic or natural, have been used for the design of bone tissue engineering scaffolds up to now. Polyesters such as polylactic acid (PLA), polyglycolic acid (PGA), their copolymer polylactide-co-glycolide (PLGA) and poly(ε-caprolactone) (PCL) are the most widely preferred synthetic polymers because of their biocompatibility and tunable properties [48, 49]. Ceramics are another class of materials used for scaffold production in bone tissue engineering. The inorganic component of bone, hydroxyapatite (HAP), is also a ceramic. Tricalcium phosphate (TCP), bioactive ceramics like calcium phosphates, glass ceramics and low silica glasses are commonly used because of their ability to bond with bone [50, 51].

Natural biomaterials, on the other hand, are very commonly used in scaffold production because of their biocompatibility. There are also some drawbacks of using natural materials such as the difficulty in modification of the physicochemical and mechanical properties, the difference in chemistry or purity of the material from batch to batch or source to source and the risk of viral contamination [52]. Collagen, gelatin, ECM components such as proteoglycans, chitosan, silk fibroin and poly(hydroxyalkanoate)s are the most widely used natural scaffold materials for bone research. Another important natural material is cellulose, because of its abundance, low cost, tunability of mechanical properties and surface chemistry. It is the most abundant biopolymer in the world and it can be obtained from various species from plants to bacteria [53]. Paper is a product of cellulose and in this research filter paper (Whatman no 114) was used as a scaffold material. A detailed information about filter paper and its applications are given in the next section.

1.3.2.1. Filter Paper as a Scaffold Material

Since its invention paper has been used for various applications. Together with the advancements in technology many types of papers with different physical and mechanical properties have been produced. Filter paper (Whatman) contains only cellulose without any additional binders in its structure [54]. In biotechnology field, paper has been used as disposable high throughput analytical test systems, biosensors, electronic devices and recently cell and tissue culture platforms because of its biocompatibility, ease of modifications, low cost and being commercially available [55].

In one of the studies, paper was used for screening the cytotoxic effect of chemical compounds on human breast cancer cells via high throughput testing [56]. Researchers formed cell seeding spots on the paper by separating these regions with hydrophobic borders like a 96-well plate, and stacked these patterned papers to form layered structures. This allowed the researchers to study the cytotoxic effect of the chemical compounds at different depths of the culture by peeling the layers and observing the layers like 2D gel layers.

In another study a very similar system to the one described above was used to study cardiac ischemia [57]. They seeded cardiomyocytes and cardiac fibroblasts on separate layers of patterned papers and stacked them, and a limited access of nutrients and oxygen was provided unidirectionally. This system allowed the researchers to study how nutrient and oxygen deficiency affect cardiomyocytes and how the migration of fibroblasts is dependent on release of cytokines from ischemic cardiomyocytes. A very similar coculture system was also used for investigation of interactions between human lung tumors and fibroblasts [58].

It was also demonstrated that paper is a very promising scaffold material for bone tissue engineering applications, especially for centimeter size defects. The researchers seeded MLO-A5 osteoblasts in collagen I to paper scaffolds folded into different shapes inspired of origami based folding techniques and incubated cells in osteogenic differentiation medium for 21 days. They reported that osteoblasts mineralized *in vitro* and expressed bone specific marker osteocalcin [54].

In another research, paper based origami inspired scaffolds were used for trachea tissue engineering [59]. The researchers chemically modified the paper surfaces and

coated the papers with PLL. The cells were seeded in alginate hydrogel and the paper scaffolds were folded in different shapes. The paper scaffolds with cell and hydrogel mixtures were implanted in rabbits with trachea defects and it was reported that after 4 weeks engineered tissues replaced the native ones without stenosis.

In our research filter paper (Whatman 114) was used for detection of cytotoxic effect of two natural phenolic compounds carnosol and carnosic acid in 3D cell culture on D1 ORL UVA, HS-5 and SaOs-2 cell lines (Chapter 2) [60]; as a cell seeding platform for determination of osteogenic differentiation of D1 ORL UVA stem cells upon mechanical stimulation through application of vibration in 3D cell culture (Chapter 3); and as a scaffold for determination of osteogenic differentiation of D1 ORL UVA stem cells in a perfusion/vibration bioreactor (Chapter 4).

Two of the main components of a tissue engineered construct, scaffold and cell types were discussed in this chapter. A deeper information about the last component biochemical and biomechanical cues will be given in chapters 2 and 3, respectively.

CHAPTER 2

CYTOTOXIC TOLERANCE OF HEALTHY AND CANCEROUS BONE CELLS TO ANTI-MICROBIAL PHENOLIC COMPOUNDS DEPEND ON CULTURE CONDITIONS

2.1. Biochemical Cues

The last component of a tissue engineered construct in addition to cells and scaffolds is the signaling cues that are biochemical (soluble factors such as growth factors, cytokines, enzymes, small molecules, etc.) or biophysical (mechanical, electrical, thermal, magnetic, acoustic, etc.) in nature. Growth factors are organic molecules that stimulate the growth, proliferation and differentiation of cells [61]. Biomolecules that regulate the cellular events such as growth factors, cytokines and morphogenes bind to cell surface receptors and initiate molecular signals that lead to cellular responses such as proliferation, differentiation, migration and apoptosis. Regulation of cellular events by biomolecules is concentration dependent and pico or nanomolar concentrations of these molecules are sufficient enough to evoke cellular activities [62]. Naturally, ECM binds and release these biomolecules to orchestrate the cell and tissue function at the right spatial and temporal conditions [63]. In order to mimic this behavior of ECM, biomolecules are usually delivered within controlled release systems for *in vitro* tissue engineering applications.

Some of the most commonly used growth factors in bone tissue engineering are bone morphogenetic proteins (BMPs), transforming growth factor β (TGF-β), fibroblast growth factor (FGF), vascular endothelial growth factor (VEGF), insulin-like growth factor (IGF), and platelet-derived growth factor (PDGF) [64].

TGF-β superfamily proteins have important roles in growth, differentiation and ECM production in bone. BMPs are a subgroup of TGF-β family. BMP-2, BMP-4 and BMP-7 are the most frequently used proteins among this group for bone tissue engineering applications. Induction of osteogenic differentiation by BMPs has a species

specific effect. When they are introduced *in vitro* they induce osteoblast differentiation in rodents, however this is not the case for human bone formation [65, 66]. In addition to that BMPs might cause tumorigenesis [66].

FGFs and PDGF are responsible for the proliferation of mesenchymal cells [67]. FGFs and VEGFs also have important roles in angiogenesis. In addition to blood vessel formation VEGFs also take place in endochondral and intramembraneous ossificiation and bone remodeling [68].

IGFs are important in the maintenance of skeletal mass and collagen type I production, and has significant roles in bone remodeling and age-related osteoporosis [62, 67]. They are also responsible for maintenance, proliferation, differentiation and ECM production of *in vitro* cultured osteoblasts [69]. Production and responsiveness of IGF-1 are increased upon mechanical loading of osteoblasts and osteocytes [70].

For *in vitro* bone tissue engineering applications, some bioactive agents other than growth factors are also used to trigger the differentiation of MSCs into osteoblastic lineage. Among these agents, dexamethasone, β-glycerophosphate and ascorbic acid are the most commonly used differentiation agents.

Dexamethasone, which is a synthetic glucocorticoid, is very commonly added to osteogenic induction media. However, while inducing osteoblastic differentiation glucocorticoids inhibit the proliferation of osteoblastic cells [71]. Nevertheless, if used within the physiological range (10 nM) the inhibitory effect is prevented and when combined with ascorbic acid its adverse effect on collagen synthesis of cells is also reverted back [65].

Another component of a standard osteogenic induction medium is ascorbic acid. Ascorbic acid has a role in the hydroxylation of proline and lysine amino acids in collagen as a cofactor [72, 73]. Ascorbic acid induces MSC proliferation and ECM secretion *in vitro* while stimulating mineralization and ALP activity induction [74, 75]. Ascorbic acid 2-phosphate, which is the more stable derivative of ascorbic acid is commonly preferred for osteogenic medium preparation [72].

β-glycerophosphate is another component utilized as *in vitro* inorganic phosphate source that is hydrolyzed by ALP enzyme [65]. The mineralization of osteoblastic cells is stimulated by the released phosphate ions by ALP enzyme [75].

Even though glucocorticoids are commonly used for induction of osteogenesis, their cytotoxic effect on MSCs is also reported [76]. Previous studies performed by our

group also verified that D1 ORL UVA mouse bone marrow MSCs can undergo osteoblastic differentiation in the absence of dexamethasone [77, 78]. Because of this, osteogenic media used throughout this research were supplemented with ascorbic acid and β-glycerophosphate without dexamethasone.

2.1.1. Bone Infections and Commonly Used Antibiotics for Treatment

Bone infection, which is also known as osteomyelitis, is a rare disease caused by certain bacteria strains, mycobacteria and fungi. Osteomyelitis can arise from surgical operations for implants, as a result of blood circulation from another infected part of the body or vascular insufficiency resulting from diseases such as diabetes, and the most common cause of osteomyelitis is *Staphylococcus aureus* type of bacteria [79]. The main treatment method for osteomyelitis is the removal of infected tissue via surgical operations and delivery of antibiotics parenterally or a combination of parenteral and oral administration at high doses due to poor vascularization of the bone tissue which might cause systemic toxicity [79, 80]. Fluoroquinolones, which are a class of antibiotics effective both on Gram positive and Gram negative bacteria, are the most widely used drugs for the treatment of osteomyelitis [81]. Ciprofloxacin, vancomycin, levofloxacin, clindamycin, rifampicin and amoxicillin are most commonly administered antibiotics of the fluoroquinolone classes in clinic [82]. Other than quinolones, beta-lactam agents such as penicillin are also very commonly preferred for the treatment [82]. Treatment of bone infections via antibiotics usually results with successful outcomes, but sometimes administration of the antibiotics with high doses might cause especially renal toxicity, or some patients might have allergic reactions to some antibiotics such as penicillin derivatives [83]. Because of these reasons, new antimicrobial agents with less toxic effects are under investigation by the researchers.

2.1.2. Natural Phenolic Compounds as Antimicrobial Agents

It is known that administration of antibiotics for different types of infectious diseases caused the formation of resistant bacterial strains against many antibiotics. To increase the efficiency of antibiotics and diminish their side effects, various synthetic and natural molecules have been tested in combination with antibiotics or alone, until now. The compounds that plants have evolved for multidrug resistance mechanisms of microorganisms can be utilized for production of new antibiotics [84]. Phenolic compounds, which are secondary metabolites isolated from several plants, are one of the most commonly studied of these groups. They are composed of aromatic rings which contain one or more hydroxyl or methoxyl groups in their chemical structures.

Phenolic compounds are usually found in herbs and plants and their consumption as a part of the human diet is recommended because of their antioxidant, anticarcinogenic, anti-hypertensive, anti-allergic and antimicrobial properties [85, 86]. For example, cranberry and bearberry contain antibacterial compounds which are effective on several pathogens such as *Escherichia coli, Bacillus subtilis* and *Staphylococcus aureus* in the treatment of urinary tract infections and garlic has antimicrobial and antiseptic effect on respiratory tract infections [84].

Flavonoids, another group of polyphenols which are mostly extracted from edible plants, are also free radical scavengers and antioxidants with antimicrobial, antihypertensive, antiallergic and anti-inflammatory properties [87]. Their intake as a part of diet has also preventive effect on various chronic diseases such as cardiovascular diseases [87].

Phenolic compounds from grape pomace are also reported to have synergistic effects on *S.aureus* and *E.coli* strains when used together with antibiotics via reducing the minimal inhibitory concentration (MIC), which is defined as “the lowest concentration of a compound which inhibits the visible growth of bacteria”, of several antibiotics such as β-lactam, quinolone, fluoroquinolone, tetracycline and amphenicol from 4 to 75 times [88].

2.1.2.1. Carnosol

Carnosol is a polyphenolic compound found in rosemary (*Rosmarinus officinalis*) and sage (*Salvia officinalis*) with anti-oxidant, anti-inflammatory, antimicrobial and anticarcinogenic properties [89-92] (Figure 2.1). It is reported that carnosol has anti-cancer and preventive properties in prostate, breast, skin, ovarian, colon and intestinal cancers and leukemia [90, 92]. The inhibitory effect of carnosol on angiogenesis is also studied [93]. Anti-metastatic properties of carnosol is also demonstrated and the efficacy on cancer cell growth inhibition is reported to be higher when the cells are grown in suspension rather than monolayer [92].

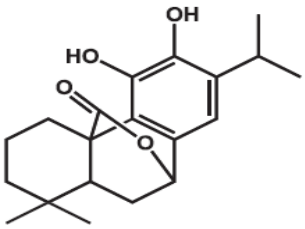

Figure 2.1. Structure of carnosol [90]

Anticarcinogenic properties of carnosol have been studied with various cancer and normal cell types and a wide range of different effective concentration values were reported. IC_{50} values of carnosol, which is defined as the concentration at which the cell viability decreased to the half of the population when compared to the control group, for MCF7 breast cancer cells in one study is reported as 25.6 μM [94], while in another study it was reported as 82 μM [90].

The IC_{50} value of carnosol was also studied for various cancer and normal cells and it was reported that low concentrations of carnosol is enough for reducing the cancer cell viability, but much higher concentrations are needed for normal cell viability reduction. In one of these studies IC_{50} value of carnosol was reported as 50 μM and 35.2

μM for BAEC and HUVEC epithelial cells, respectively, while these values were reported as 5.3 μM and 6.6 μM for HL60 (leukemia) and HT1080 (fibrosarcoma) cancer cells [93]. In another study, the effect of carnosol was studied on breast, ovarian and colon cancer models and it was reported that at concentrations lower than 25 μM, it had no effect on cell viability, while at concentrations higher than 50 μM the effect was dose and time dependent for cancer cells, but for normal cells, cell viability reduction was only observed at concentrations higher than 200 μM [92]. It is also stated that carnosol has an anti-proliferative effect by increasing intracellular cyclin B1 protein, which regulates the progression from G2 to M phase after promethaphase of mitosis by using adenocarcinoma cell line [95].

2.1.2.2. Carnosic Acid

Carnosic acid is also a polyphenolic compound found in rosemary and sage which has a similar chemical structure with carnosol (Figure 2.2).

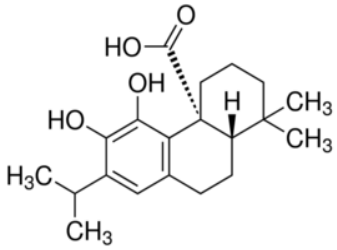

Figure 2.2. Structure of carnosic acid [96]

It has chemopreventive, antioxidant, antimicrobial, antiobesity, antiplatelet and antitumor activities [93, 96]. Carnosic acid may undergo an oxidative degradation and rearrangement cascade, which ends with the generation of other rosemary antioxidant compounds such as carnosol, rosmanol, galdosol and rosmariquinone [93].

Carnosic acid that is extracted especially from rosemary is reported to have anti-proliferative effects on various cancer cell lines such as HL-60 (myeloid leukemia), M14

and A375 (human melanoma), CaCo-2 (human colon carcinoma), HepG2 (hepatoma) and HCT-116 (colon cancer) and estrogen receptor negative human breast cancer cells by induction of G1 cell cycle arrest [97-99]. It was found that in RINm5F rat beta cells, carnosic acid is responsible for cell viability decrease due to apoptosis mediated by nitric oxide [99] and in human neuroblastoma IMR-32 cells, formation of these reactive oxygen species caused mytochondria dysfunction [100].

Research on antimicrobial properties of carnosic acid demonstrates that it is not effective on *E.coli* and *K. pneumoniae*, and minimal inhibitory concentration (MIC) values reported for *S. aureus* (ATCC 25923) and *S. epidermidis* (DSM 1798) were 64 μg/mL for both microorganisms [101].

2.1.3. Phenolic Compound Delivery in Tissue Engineering Applications

Delivery of drugs at a specific region in the body is very important to decrease the side effects of the drugs for the healthy cells and keeping their concentration at an elevated level. Many different controlled release systems have been designed in this regard to meet the desired criteria.

Tissue engineering scaffolds are also utilized as delivery vehicles, especially for antibiotics. Various polyphenolic compounds such as epigallocatechin-3-gallate (EGCG), quercitrin, extracts of green tea and red grape have reported to be inductive on osteoblast proliferation and mineralization, so recently delivery of polyphenols as implant coating or via tissue engineering scaffolds have started to be studied by different research groups [102].

In one of the studies, cryogels and electrospun fibers of silk fibroin were produced and Manuka honey, which is special to New Zealand and known for its antibacterial properties was loaded to these scaffolds and the antibacterial effect of honey on *E. coli* and *S. aureus* together with the cytotoxicity of the scaffolds on human dermal fibroblasts were studied and it was observed that the release of honey had partial or complete clearance of bacteria with no significant cytotoxic effect on fibroblasts [103].

In another research, poly (l-lactide-co-glycolide) (PLGA) nanofibrous scaffolds that carry quercetin flavonoid were produced and their cytocompatibility with KB epithelial cells and antimicrobial properties on *S.aureus* and *K. pneumoniae* were studied.

It was reported that scaffolds with 1wt% quercetin had good cytocompability [104]. Another phytochemical, icariin, which has angiogenic and osteogenic properties was loaded to tricalcium phosphate scaffolds to treat the osteonecrosis of the femur head of rabbits and it was reported that icariin can be used for the treatment of bone defects and prevention of femur head collapse [105].

In another research, naringin, a citrus flavonoid, was incorporated into poly(ε-caprolactone) (PCL) and poly(ethylene glycol)-block-poly(ε-caprolactone) (PEG-b-PCL) electrospun scaffolds to determine the differentiation and mineralization characteristics of MC3T3-E1 osteoblasts and it was observed that naringin release from scaffolds suppressed osteoclast formation and induced osteoblast proliferation and mineralization [106].

2.1.4. The Approach of the Study

Even dose studies for carnosol on various cancer cell types are studied, there is not much information on its effect for osteosarcoma in the literature. Osteosarcoma is a type of cancer that develops in bone tissue, most commonly in the metaphyseal regions of long bones especially during childhood and adolescence, but it may occur at any age. It is relatively rarely studied amongst other cancer types.

The current treatment of osteosarcoma involves a combination of surgery and chemotherapy, but scientists are still under investigation of new therapeutic molecules which will be effective on primary and metastatic tumor cells with least damage to normal cells [107].

In this research, the antimicrobial effect of phenolic compounds carnosol and carnosic acid were studied on commonly observed Gram positive and Gram negative bacteria types in bone infections, together with their cytotoxic effect on mesenchymal stem cells, bone fibroblasts and osteosarcoma cell lines. Since the behavior of cells in 2D and 3D are different, determination of the cytotoxic effect was tested in tissue culture plates and on Whatman paper scaffolds.

2.2. Methods

2.2.1. Determination of Antimicrobial Properties

The antimicrobial properties of carnosol and carnosic acid against *Escherichia coli* (ATCC® 25922™), *Staphylococcus aureus* (RSKK 1009; Refik Saydam National Type Culture Collection, Turkey), *Klebsialla pneumoniae* (FOR, DHA-2) and *Staphylococcus epidermidis* (NRRL B-4268) were determined by antimicrobial activity test. Briefly, all the bacteria were streaked on both nutrient agar (NA) and tryptic soy agar (TSA) plates. After 24h incubation at 37 ^{o}C, it was observed that for all types of bacteria used in this experiment, growth and colony formation on TSA were more efficient than on NA. One of the middle sized colonies from all bacteria types mentioned above were chosen and suspension culture was started by transferring each colony to tryptic soy broth. Suspension cultures were incubated at 37 ^{o}C for 24h, and the bacteria that were proliferated from single colonies were streaked on TSA plates once more. All bacteria types were diluted 10^5 times and colony forming units (cfu) per milliliter were calculated by spreading 100 µL suspension on TSA plates. 24h later colonies from 10^5 diluted samples were counted and cfu/mL results were as given in Table 2.1.

Table 2.1. Colony forming units (cfu)/mL results for *E.coli*, *S.aureus*, *K. pneumoniae* and *S. epidermidis*.

Bacteria	**Colony Number**	**cfu/mL**
E.coli	26	2.6×10^7
S. aureus	67	6.7×10^7
K. pneumoniae	20	2×10^7
S. epidermidis	30	3×10^7

Antimicrobial activity was determined by choosing three different carnosol or carnosic acid concentrations (18, 30 and 60 µg/mL) depending on the cell viability results. In order to obtain these concentrations, three carnosol and carnosic acid stock solutions were prepared from the main 5 mg/mL stock that was dissolved in DMSO, with 120, 60 and 36 µg/mL concentrations by diluting the main stock with broth. A multiple well plate with 96 wells was used as the test platform and 10^6 cfu/mL bacteria for each bacteria type were used.

One colony from each bacteria was chosen and transferred into Pepton water to adjust the turbidity to 0.5 McFarland. In order to standardize antimicrobial tests 0.5 McFarland is accepted as the average turbidity of $150x10^6$ cells/mL bacterial concentration independent of bacteria type. The total volumes in each well of the plate were consisting of 80 µL broth, 100 µL of each carnosol or carnosic acid concentration and 20 µL of bacteria. Positive and negative controls were bacteria grown in tryptic soy broth and Pen/Strep (100 IU/ml Penicillin and 100 µg/ml Streptomycin), respectively. Since carnosol and carnosic acid are dissolved in DMSO, to see if DMSO has any toxic effect on the growth of bacteria, broth containing the same amount of DMSO as the highest carnosol or carnosic acid solution was also tested. The assay plate was incubated at 37 ºC and 120 rpm for 24h, by measuring the absorbance (Thermo Scientific, VarioSkan, USA) at 600 nm with 2h intervals.

2.2.2. Cell Culture

D1 ORL UVA mouse bone marrow stem cells, SaOs-2 human osteosarcoma cells and HS-5 human bone marrow stroma cells were used for *in vitro* cell culture studies. For culture of cells, Dulbecco's Modified Eagle Medium (DMEM) with 4.5 g/L D-glucose, L-glutamine and sodium pyruvate (Gibco, USA) supplemented with 10% FBS (Biological Industries, USA) and 1% Penicillin/Streptomycin (Pen/Strep) (Biological Industries, USA) (DMEM high glucose complete medium) was used as the growth medium. All of the cells were incubated in a humidified incubator with 5% CO_2 at 37 ºC.

2.2.3. Determination of Effective Carnosol and Carnosic Acid Concentration

The concentration dependent effect of carnosol and carnosic acid on different bone tissue derived cell lines was determined by MTT (3-(4,5-Dimethylthiazol-2-yl)-2,5-Diphenyltetrazolium Bromide) assay. Stock solutions of carnosol (Sigma-Aldrich, Germany) and carnosic acid (Sigma-Aldrich, Germany) with 5 mg/mL concentration were prepared by solubilizing the lyophilized powders with DMSO, and dilutions were made from these stock solutions by the addition of culture medium. DMSO volume was kept equal in each concentration. Cells were seeded at a density of 10^4 cells/well in 96 well plates. The next day after cell seeding, media of the cells were replaced with the media containing varying carnosol or carnosic acid concentrations (0, 6, 18, 30, 42 and 60 μg/mL). The viability of cells was determined by MTT (Amresco, USA) assay after 24, 48 and 72 h treatment with carnosol or carnosic acid. In this method, water soluble MTT is converted into insoluble formazan by the metabolically active cells and the amount of formazan produced is directly proportional to the number of living cells. For cell viability assay, the media of cells in 96 well plates were replaced with 100 μL growth media that contains 10% (v/v) MTT in final volume and the cells were incubated for 4 h at 37 ºC and 5% CO_2. The media were discarded and formazan crystals formed by the living cells were solubilized with 100 μL DMSO. Absorbance of the samples were measured at 570 and 650 nm wavelengths with a spectrophotometer (Thermo Fisher Scientific, Multiscan Spectrum, USA).

MTT test was also applied for the same cell types after one week osteogenic induction. Cells were seeded at a density of 10^3 cells/well for osteogenic induction. After 24 h, growth media of cells were replaced with osteogenic induction media (10 mM β-glycerophosphate (Sigma-Aldrich, Germany), 50 μg/mL ascorbic acid (Sigma-Aldrich, Germany) and DMEM high glucose complete medium) and the cells were incubated with this medium for one week. Then MTT test was applied according to the procedure above.

Calculation of IC50 values were done assuming the viability of control groups as 100%, and considering the concentrations of phenolic compounds that yield 50% cell survival depending on the MTT absorbance values [93, 108].

2.2.4. Carnosol and Carnosic Acid Treatment for Cells on Filter Paper Scaffolds

Whatman filter paper (Grade 114, Merck, Germany) was used as the support for 3D cell culture. Before cell seeding papers were cut according to the bottom surface area of the wells of a 96-well plate with a puncher. Then sterilization of papers were done by immersing them in 90% ethanol for 30 min, removing the ethanol and leaving them in the laminar flow hood overnight for drying [54]. Collagen type I was diluted to 2.5 mg/mL from 3.7 mg/mL stock solution [54]. Briefly, for preparing 1 mL solution, 800 µL collagen type I with 3.7 mg/mL concentration was diluted with 100 µL DMEM (1X) and 100 µL DMEM (10X) and 200 µL NaOH (with an initial concentration of 100 mM) was added. For cytotoxicity analysis cells were seeded within collagen, at a concentration of 10^4 cells/paper in 2 µL volume for 96 well plates and MTT assay was performed according to the procedure above. Cell carrying paper scaffolds were transferred to a new plate before MTT assay to eliminate the false signals that might arise from the cells infiltrated to the plate surface. Collagen solution absorbed papers without any cells that were incubated under same conditions with the cell carrying samples were used as blank for MTT test.

2.2.5. Statistical Analyses

All the experiments were repeated in triplicates, and all results are displayed as the mean ± standard deviation. Statistical analyses for comparison between the groups were performed using ANOVA. In order to detect significant difference in growth, or to demonstrate the differences between cell types ANOVA followed by Tukey post hoc test was done. For viability change upon carnosol and carnosic acid applications, ANOVA followed by Dunnett's multiple comparison post hoc tests was applied and the dose is compared to negative controls. Levels of significance were reported for 5%, 1%, and 0.1%.

2.3. Results

2.3.1. Determination of Antimicrobial Properties

Antimicrobial effect of carnosol and carnosic acid was determined by treating *S. aureus* (Gram-positive), *S. epidermidis* (Gram-positive), *E. coli* (Gram-negative) and *K. pneumoniae* (Gram-negative) with different concentrations (18, 30 and 60 µg/ml) of these components for 24h. The growth of *S. aureus* was inhibited upon carnosol and carnosic acid treatment, and the growth of *S. epidermidis* was also suppressed to a limited extend (Figure 2.3). A stationary phase was observed for *S. aureus* and *S. epidermidis*, but only for *S. aureus*, the expected concentration dependent decline in the growth curve was observed (Figure 2.3). The growth curves obtained from the carnosol or carnosic acid treated bacteria samples demonstrated that Pen/Strep stopped the growth of all types of bacteria. Upon 24h treatment of *S. aureus* with carnosic acid, a stationary phase was observed for the control group; however, for 18 and 30 µg/mL carnosic acid treatment instead of a stationary phase, a prolonged lag phase was observed (Figure 2.3). When the concentration increased to 60 µg/mL, it was observed that the decrease in the growth was the same with Pen/Strep treated samples. This shows that, both phenolic compounds had a bacteriostatic effect on the Gram (+) bacteria used in this research.

2.3.2. Determination of Effective Carnosol and Carnosic Acid Concentration

Determination of cell viability for all bone tissue derived stem, normal and cancer cells showed that during 72h of incubation, there was a significant increase in cell number for 2D cultures compared to the first day. This increase was 162%, 65% and 47% for D1 ORL UVA, SaOs-2 and HS-5 cells, respectively (all $p<0.001$) (Figure 2.4a). At the end of 72h, the viable D1 ORL UVA cells were 58% and 79% higher than SaOs-2 ($p<0.01$) and HS-5 ($p<0.001$) cells, respectively. Upon application of osteogenic induction, the growth pattern of cells changed (Figure 2.4b). HS-5 cell number increased 31% ($p=0.02$)

and SaOs-2 cell number decreased 63% ($p<0.001$). The viability of D1 ORL UVA cells was similar to non-osteogenic conditions. Incubation of cells in 3D environment increased viable cell number for D1 ORL UVA (73%, $p=0.02$) and HS-5 (88%, $p=0.02$) cells, where cell growth was similar between cell types (Figure 2.4c).

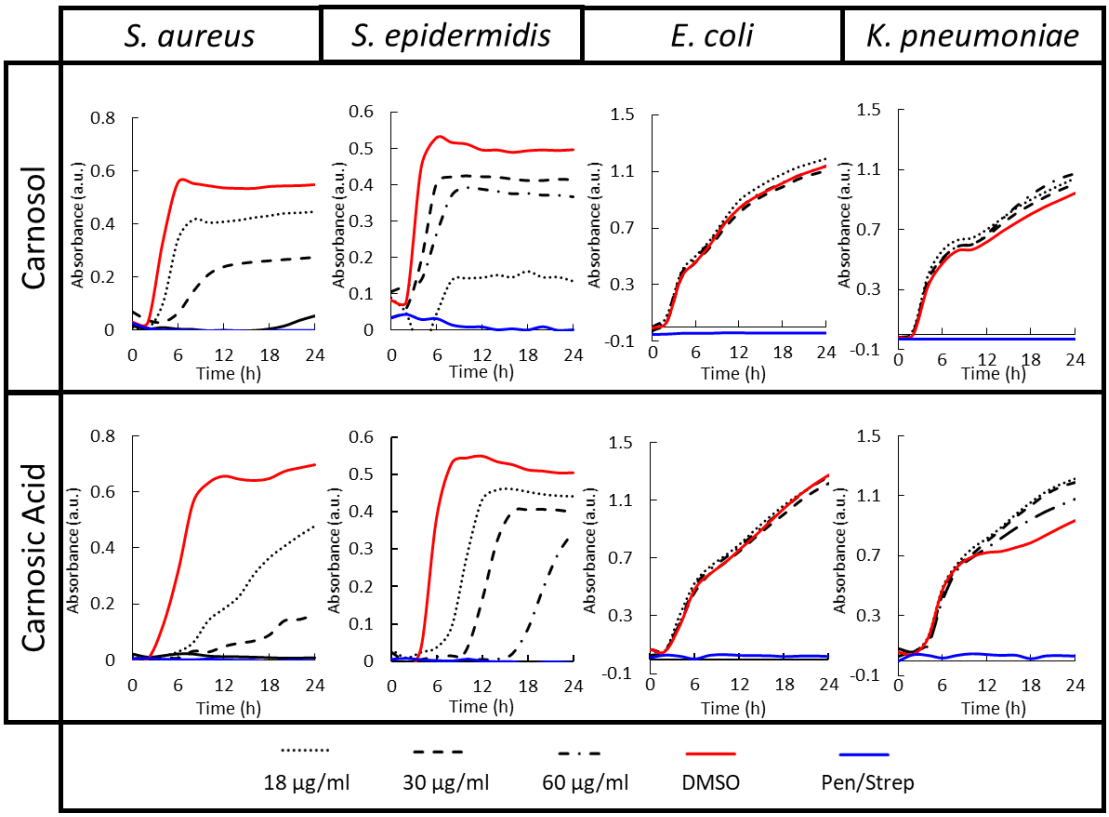

Figure 2.3. Anti-microbial activity of carnosol and carnosic acid on S. aureus, S. epidermidis, E. coli, and K. pneumoniae. Increasing concentrations of both carnosol and carnosic acid decreased the growth of S. aureus. Both phenolic compounds decreased the growth of S. epidermidis. Growth inhibition of S. epidermidis was not concentration dependent for carnosol, but carnosic acid effected the same organism in a concentration dependent manner. Both carnosol and carnosic acid did not have any inhibitory effect on growth of E. coli and K. pneumoniae.

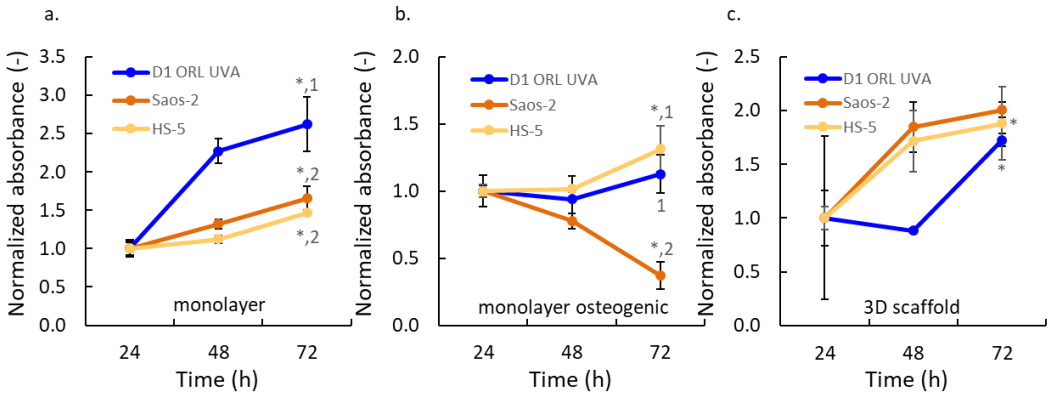

Figure 2.4. Changes in cell viability of D1 ORL UVA bone marrow stem cells, HS-5 bone marrow cells, and Saos-2 osteosarcoma cells in a) monolayer culture for 3 days, b) monolayer culture for 3 days with 7 days prior conditioning in osteogenic medium, and c) culture for 3 days in 3D paper based scaffold. *p ≤ 0.05 for viability at 72 h compared to 24 h calculated by ANOVA followed by Tukey's post hoc test. 1,2: differences in viability of cell type at 72 h calculated by ANOVA followed by Tukey's post hoc test.

According to the cytotoxicity determination results, the increasing concentration of carnosol caused a gradual decrease in D1 ORL UVA cell viability after 24h treatment. This decrease was 16%, 57%, 73% and 97% (all $p<0.05$) for 18, 30, 42 and 60 µg/mL concentrations, respectively (Figure 2.5a). Extended to 72h of exposure, the viability of D1 ORL UVA cells was 42%, 67%, 91%, 97% and 97% lower (all $p<0.001$) then negative controls for 6, 18, 30, 42 and 60 µg/mL concentrations, respectively. For HS-5 cells, a similar decrease in cell viability was observed after 24h treatment with carnosol. The decrease was 31%, 62%, 65% and 89% (all $p<0.05$) for 18, 30, 42 and 60 µg/mL carnosol concentrations, respectively (Figure 2.5b). When the treatment duration was extended to 72h, HS-5 viability was 19%, 68%, 92% and 96% lower (all $p<0.05$) than negative control group for 18, 30, 42 and 60 µg/mL concentrations, respectively. The effect of carnosol was more destructive for SaOs-2 cells after 24h treatment. The cell growth was 17%, 63%, 96%, 99% and 99% lower (all $p<0.001$) than the control group (Figure 2.5c). It was observed that 30 µg/mL carnosol concentration was extremely toxic for osteosarcoma cells. Carnosic acid treatment caused a concentration dependent decrease of viability for all cell types (Figure 2.5d-f). Cell viability trend of carnosic acid treated D1 ORL UVA cells was similar to carnosol treatment, but for HS-5 cells higher concentrations of

carnosic acid decreased cell viability more than carnosol. SaOs-2 cells, on the other hand, tolerated carnosic acid better until the highest concentration applied.

To induce osteogenic character of cells, before carnosol and carnosic acid treatment, all cell types were incubated in osteogenic induction medium for one week. Carnosol treatment for 24h under 2D cell culture conditions after osteogenic induction decreased viability of D1 ORL UVA cells 22%, 28%, 33% and 73% (all $p<0.05$) for 18, 30, 42 and 60 μg/mL concentrations, respectively (Figure 2.6a). At the end of 72h treatment after osteogenic induction, D1 ORL UVA cell number was 9% higher than the control group for 6 μg/mL concentration; however, 18, 30, 42 and 60 μg/mL carnosol concentrations decreased viability of these cells 42%, 67%, 91% and 97% (all $p<0.001$). Under the same conditions, carnosol treatment decreased HS-5 cell viability 30%, 41%, and 77% (all $p<0.001$) for 30, 42 and 60 μg/mL concentrations, respectively at 24h (Figure 2.6b). When the treatment duration was extended to 72h, the decrease in HS-5 cell viability was 20%, 51%, 70%, and 97% lower (all $p<0.001$) than non-treated group for 18, 30, 42 and 60 μg/mL concentrations, respectively. Similar to non-osteogenic conditions, carnosol had a more detrimental effect on SaO-2 cells at 72h. Cell viability decrease for these cells was 74%, 76%, 95%, 86% and 98% lower (all $p<0.001$) than the control group for 6, 18, 30, 42 and 60 μg/mL carnosol concentrations, respectively (Figure 2.6c). Carnosic acid treatment, on the other hand, caused significant cytotoxicity for all cell types. The cytotoxic effect of carnosic acid was seen at concentrations higher than 30 μg/mL for D1 ORL UVA and 18 μg/mL for HS-5 and SaOs-2 cells (Figure 2.6d-f).

2.3.3. Carnosol and Carnosic Acid Treatment for Cells on Filter Paper Scaffolds

Tolerance of D1 ORL UVA bone marrow stem cells to cytotoxic effect of carnosol was higher when these cells were cultured on 3D scaffolds (Figure 2.7a). HS-5 cell viability under 3D cell culture conditions was also higher than 2D culture at low concentrations, but 74%, 87% and 93% decrease (all $p<0.001$) was observed for 30, 42 and 60 μg/mL carnosol concentrations after 72h treatment, respectively (Figure 2.7b).

Sensitivity of SaOs-2 cells upon carnosol treatment on 3D scaffolds was higher; 18%, 35%, 88%, 96% and 86% decrease in viability (all $p<0.001$) for 6, 18, 30, 42 and 60 µg/mL concentrations was observed at 72h, respectively (Figure 2.7c). As for carnosol treatment, D1 ORL UVA cells had a higher tolerance upon carnosic acid treatment under 3D cell culture conditions (Figure 2.7d). Carnosic acid was found to be toxic at concentrations higher than 30 µg/mL for HS-5 and SaOs-2 cells (Figure 2.7e,f).

Different than the other cell types, D1 ORL UVA cell number increased upon treatment with 6 µg/mL (271%, $p<0.05$) and 18 µg/mL (230%, $p<0.05$) carnosol for 48h, and for the same carnosic acid concentrations at 72h (186% for 6 µg/mL and 171% for 18 µg/mL, $p<0.05$).

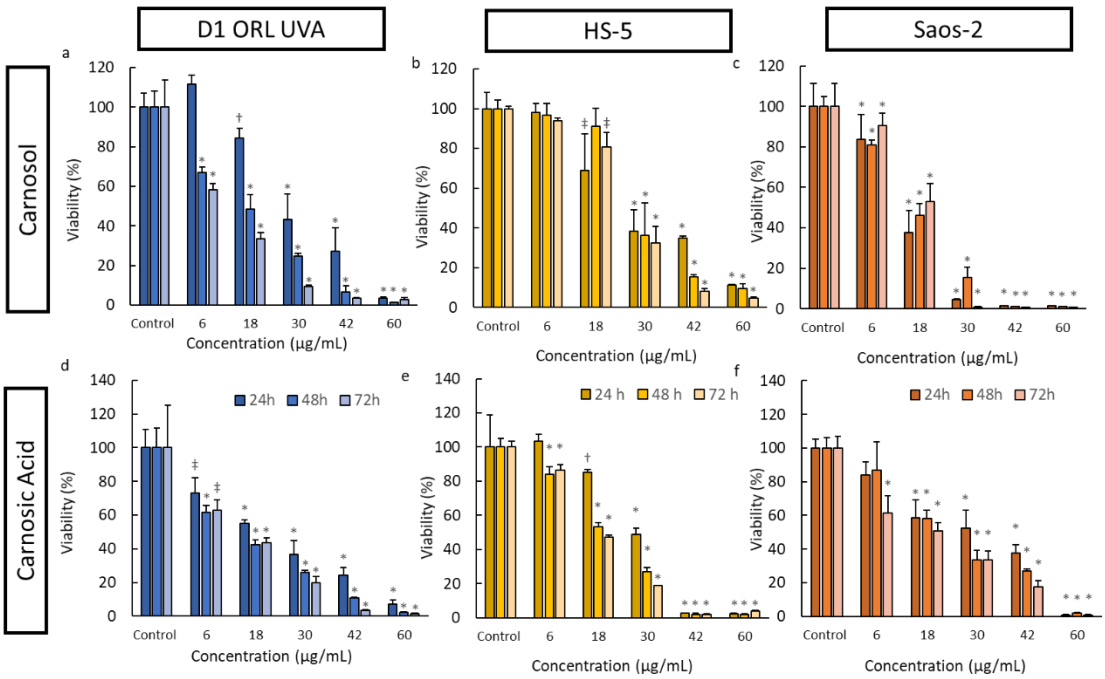

Figure 2.5. Effect of carnosol treatment on monolayer cultured cell viability for 24, 48 and 72 h for a) D1 ORL UVA, b) HS-5, and c) Saos-2 cells. Effect of carnosic acid treatment on monolayer cultured cell viability for 24, 48, and 72 h for d) D1 ORL UVA, e) HS-5, and f) Saos-2 cells. †$p \leq 0.05$; ‡$p \leq 0.01$; *$p \leq 0.001$ for each time point compared to negative control calculated by ANOVA followed by Dunnett's post hoc test.

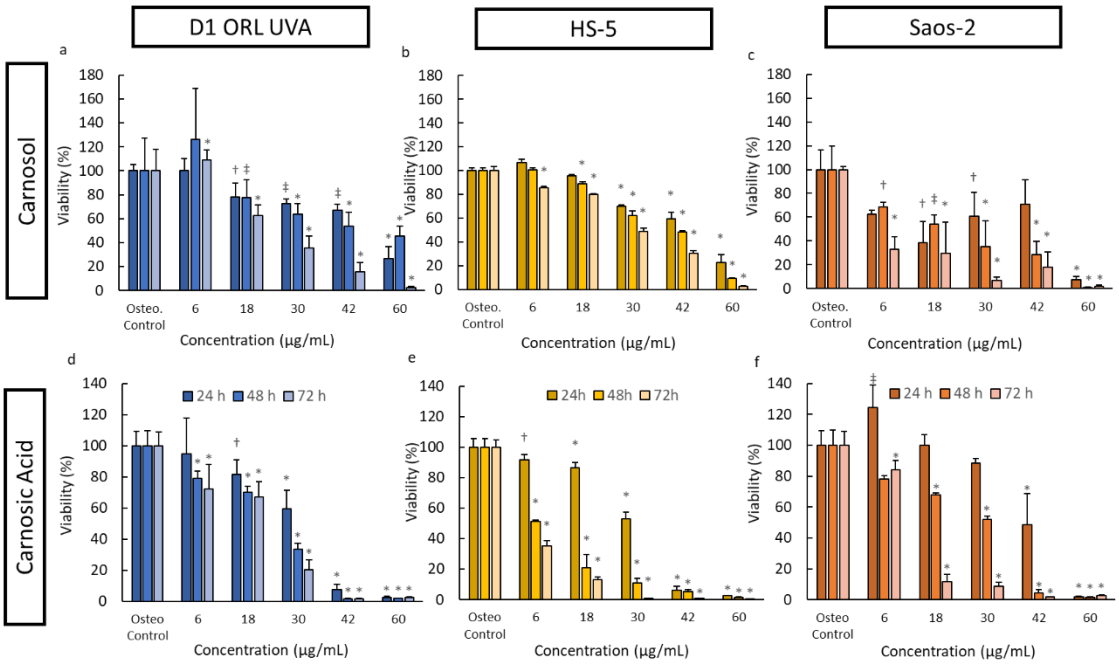

Figure 2.6. Effect of carnosol treatment on osteogenic conditioned monolayer cultured cell viability for 24, 48, and 72 h for a) D1 ORL UVA, b) HS-5, and c) Saos-2 cells. Effect of carnosic acid treatment on osteogenic conditioned monolayer cultured cell viability for 24, 48, and 72 h for d) D1 ORL UVA, e) HS-5, and f) Saos-2 cells. †$p \leq 0.05$; ‡$p \leq 0.01$; *$p \leq 0.001$ for each time point compared to negative control calculated by ANOVA followed by Dunnett's post hoc test.

2.4. Discussion

Plant extracts are commonly used in drug and food industry as anti-cancer and anti-microbial agents and nutritional supplements. Carnosol and carnosic acid are natural phenolic compounds isolated from several plants and very frequently used as anti-oxidants (E392) in food industry with the approval of European Union, Japan and China [96, 109]. In this research, we studied the anti-microbial properties and cytotoxic effect of both compounds on various bone tissue derived cell lines for bone tissue engineering applications. According to our results, despite the similarities in their chemical structures of both compounds, carnosol was found to be less cytotoxic and had more efficient anti-microbial effect than carnosic acid.

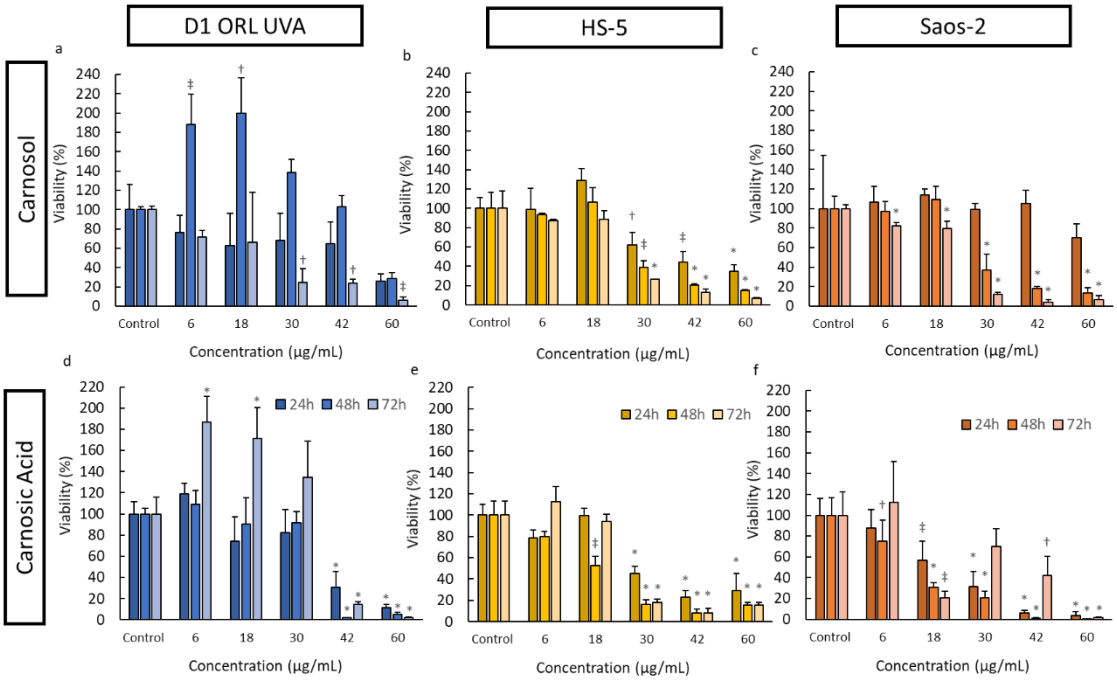

Figure 2.7. Effect of carnosol treatment on 3D cultured cell viability for 24, 48, and 72 h for a) D1 ORL UVA, b) HS-5, and c) Saos-2 cells. Effect of carnosic acid treatment on 3D cultured cell viability for 24, 48, and 72 h for d) D1 ORL UVA, e) HS-5, and f) Saos-2 cells. †$p \leq 0.05$; ‡$p \leq 0.01$; *$p \leq 0.001$ for each time point compared to negative control calculated by ANOVA followed by Dunnett's post hoc test.

Because of their anti-microbial properties and benefits as dietary supplements, phenolic diterpenes carnosol and carnosic acid can be used alone or in combination with commercial antibiotics [110]. It was previously reported that the minimal inhibitory concentration (MIC) of carnosic acid for both *S. aureus* (ATCC 25923) and *S. epidermidis* (DSM 1798) as 64 µg/mL, and it is not effective on *E.coli* and *K. pneumonia*, which was consistent with our results [101]. *In vivo* studies also supported the inhibitory effect of carnosic acid on *S. aureus* which was internalized by macrophages without any harm to macrophages [111]. These phenolic compounds have the potential to be used for the treatment of infections that occur at the bone defect sites due to their anti-microbial properties. In addition to their anti-microbial properties, the toxicity of these phenolic compounds on normal and cancer cells were also studied and carnosol treatment apparently decreased the viability of osteosarcoma cells more than marrow stromal and

bone marrow stem cells. The response of the same cells to carnosic acid was similar for the same conditions, with slightly higher cytotoxicity of carnosic acid on normal cells. The cytotoxicity of both phenolic compounds for the same concentrations was less than 2D for stem cells but remained similar for normal and cancer cells in 3D culture.

The IC50 values, which is defined as the concentration at which the cell viability decreased to the half of the population compared to the control group, obtained in this study for different cell types and culture conditions were comparable to previous studies (Table 2.2). IC50 values of carnosol for MCF7 breast cancer cells were reported as 25.6 μM [94] and 82 μM [90]. For normal cells, the IC50 values of carnosol were reported as 50 μM and 35.2 μM for BAEC and HUVEC cells, respectively, while these values were reported as 5.3 μM and 6.6 μM for HL60 (leukemia) and HT1080 (fibrosarcoma) cancer cell lines [93].

Table 2.2. IC50 values (μg/ml) of carnosol and carnosic acid calculated after 72h treatment of D1 ORL UVA, HS-5 and Saos-2 cells for different culture conditions. The values in parenthesis are μM equivalents of the concentrations.

	Carnosol	**Carnosic acid**
D1 ORL UVA (monolayer)	12 (36.4)	40 (120.7)
HS-5 (monolayer)	25 (78.9)	18 (54.6)
Saos-2 (monolayer)	18 (54.6)	18 (54.6)
D1 ORL UVA (osteo)	23 (69.8)	22 (60.3)
HS-5 (osteo)	64 (291.2)	6 (18.1)
Saos-2 (osteo)	24 (72.8)	9 (27.15)
D1 ORL UVA (3D)	64 (291.2)	35 (105.6)
HS-5 (3D)	25 (75.8)	23 (69.4)
Saos-2 (3D)	20 (60.7)	64 (193.1)

In another study, carnosol was reported to have no effect on breast, ovarian and colon cancer models at concentrations lower than 25 μM and had dose- and time-

dependent inhibitory effects for concentrations higher than 50 μM, while for healthy cells, viability reduction was only observed at concentrations higher than 200 μM [112].

Inhibitory effect of carnosol on the proliferation of adenocarcinomas was shown to be mediated by increasing intracellular cyclin B1, which regulates the progression from G_2 to M phase [95]. Carnosic acid that is extracted especially from rosemary, on the other hand, is reported to have anti-proliferative effects on various cancer cell lines such as HL-60 (myeloid leukemia), M14 and A375 (human melanoma), CaCo-2 (human colon carcinoma), HepG2 (hepatoma) and HCT-116 (colon cancer) and estrogen receptor negative human breast cancer cells by induction of G_1 cell cycle arrest [97-99]. Also, carnosic acid was reported to decrease the cell viability through apoptosis in RINm5F rat beta cells [99] and in human neuroblastoma IMR-32 cells [100]. In this research, we studied the response of normal and cancer cells that are derived from bone tissue to carnosol and carnosic acid treatment in 2D and 3D cell cultures. According to our results, the behavior of normal and cancer cells is different and concentration and time dependent upon treatment. We also observed that the response of the same cell type to the same concentration of carnosol or carnosic acid differs in 2D and in 3D. Exposure to carnosol in 3D cell culture conditions affected osteosarcoma cells in lower concentrations while normal cells appeared to tolerate the compound in concentrations closer to antimicrobial levels. Furthermore, carnosol and carnosic acid acted as proliferative agents for stem cells when applied in low doses for 3D culture, a trend that was not previously reported in related studies [113]. We believe that improved biomimicry in 3D culture may facilitate information on previously unknown molecular functions of phenolic compounds in osteogenesis.

In addition to their anti-microbial, anti-carcinogenic and anti-inflammatory properties, herbal extracts can also be utilized as osteogenic inducers for *in vitro* differentiation of stem cells in cell culture and in tissue engineering applications [114]. Phenolic diterpenes found in herbs are gaining much interest because of their anti-inflammatory, anti-microbial, anti-cancer and anti-oxidant properties. In addition to carnosol and carnosic acid, rosemary plants contain other phenolic diterpenes such as rosmanol and its isomers epi-rosmanol and epi-isorosmanol [115]. Rosmanol and epi-rosmanol were also reported to have anti-tumor effects especially on neuroblastoma cells [112]. Carnosic acid and carnosol are reported to be the most abundant and biologically most active components of rosemary plant [116], but the anti-oxidant effect of rosmanol

is much higher than carnosol [117]. Because of this, in order to combine both anti-microbial, anti-carcinogenic and anti-oxidant activities together at the highest level, the total extract of the plant or a mixture of all these phenolic compounds could be used simultaneously.

Encapsulation of the molecules is an alternative method to prevent the toxicity of the compound and to obtain a controlled and prolonged release system. It was previously reported that when *Calendula officinalis* extract was released from polymeric microspheres in collagen scaffolds, the toxicity of the extract on L929 fibroblasts was largely decreased and an extended release of the compound was achieved [118]. Another study showed that chlorophene loaded nanospheres decreased the toxic effect of chlorophene on human red blood cells, while keeping its anti-microbial activity on *S. aureus* and *C. albicans* [119]. Previous studies also showed that molecules with varying molecular weights were entrapped within polymeric films, and by changing the crosslinking degree of the films the release kinetics of the compounds were changed with no significant decrease in the anti-microbial properties [120]. In our study the most effective carnosol and carnosic acid concentration which has the only anti-microbial effect was highly toxic on normal bone cells; so the release properties of these phenolic compounds might be improved and the toxic effect might be decreased by incorporation of a controlled release system.

Bone infections are very difficult to treat. Especially implant-related infections increase the duration and the cost of treatment and sometimes may result in morbidity or mortality [121]. It is crucial to prevent the adhesion of bacteria to implant surface in order to prohibit the biofilm formation which complicates the recognition of the bacteria by the immune system and the antibiotics [122]. If the implant or the scaffold is aimed to be used after tumor resection surgeries, incorporation of an anti-carcinogenic compound that does not damage the normal tissues as much as chemotherapeutic agents will have advantages over the commercial products. It is reported previously that such a scaffold was produced by doping of hydroxyapatite nanoparticles with selenium that can be used after tumor resection [123]. Similarly, the phenolic compounds carnosol and carnosic acid used in this study could be incorporated in a tissue engineering scaffold with a more complex release system and be utilized as an internal fixation system after tumor resection operations.

In conclusion, our study showed that phenolic diterpenes carnosol and carnosic acid both have an anti-microbial effect on *S. aureus*, which is the most commonly observed microorganisms in bone infections. The concentration that inhibits the growth of this bacteria was cytotoxic for monolayer cultures in this study, but in more accurate 3D conditions normal cells were able to better tolerate higher carnosol concentrations which are close to concentrations that have anti-microbial activity. We also suggest that carnosol could be encapsulated in controlled release systems to engineer its capabilities for bone tissue engineering in the future. Together with their anti-microbial and chemopreventive properties, these phenolic diterpenes are promising compounds for use in the treatment of bone defects especially formed after tumor resections.

CHAPTER 3

LOW INTENSITY MECHANICAL VIBRATIONS ENHANCE OSTEOGENESIS OF MESENCHYMAL STEM CELLS ON PAPER BASED SCAFFOLDS

3.1. Biomechanical Cues

3.1.1. Effect of Mechanical Forces on Bone at Tissue Level

All the tissues in human body are subjected to different mechanical loads; such as the compression on bone and cartilage, tension on muscles and tendons, fluid shear in blood vessels and hydrodynamic pressure in the heart valves [124]. Bone adapts structurally and functionally to the mechanical demand it withstands. Julius Wolff, who was a German surgeon proposed a mathematical model to explain this functional adaptation process in 1892. According to his theory (later on called as Wolff's Law), mechanical loading triggers bone formation and an increase in the rigidity of bone. Conversely, unloading of bone such as experienced during prolonged bed rest, sedentary life style or weightlessness as a consequence of space flights, induces bone loss because of high resorption rate [125] and reduction in the bone volumetric formation [126]. Mechanical loading on bone tissue, similar to any given solid material, can be described with dimensionless stress and strain parameters [127]. Strain reflects the relative deformation of a material under applied mechanical load. Under normal circumstances, the strain caused by deformation during physical activities in bone is in the range of 0.1% to 0.35% (100-350 microstrain - με) [128]. Harold Frost, later in 1987 hypothesized the "mechanostat" theory that adaptation of bone tissue to mechanical loads depends on several thresholds [129]. According to this, bone modeling and remodeling are in homeostasis within a threshold range of mechanical loads; below a threshold value bone is resorbed and above another value excess bone mass is formed. It is usually suggested that the formation and resorption of bone are in equilibrium when the strain is between

200 and 2500 με [130]. The region between lower and upper threshold values is called as "lazy zone" and there is no net increase in bone mass or strength within this region [131]. In fact, there is not only one universal mechanostat [132], and skeletal adaptations to mechanical loads are heavily influenced with sex [133], race [134], age [135-137] and genetic disposition [138, 139].

In addition to biological factors, the physical properties of the mechanical loads also determine how the skeleton adapts to applied forces. The anabolic effect of the mechanical forces is dependent on the magnitude [140], frequency [140-143], rate, cycle number [144] and distribution of the mechanical loads [145]. The *in vivo* bone formation is promoted by dynamic loading with physiological frequencies rather than static loading [146]. The mechanical forces exerted on the whole body and at the cellular or tissue level are very different from each other in terms of scales. The magnitude of forces perceived at the cellular level are 10^9 to 10^{12} times smaller than the ones used in classical biomechanics [124]. Because of this the experimental setups and the devices for applying mechanical stimuli to whole body or to the cultured cells have different designs.

3.1.2. Effect of Mechanical Forces on Bone at Cellular Level

Cells are subjected to both intrinsic and extrinsic forces in the body and they sense and respond to these varying forces by changes in cellular biochemical signaling cascades, which is known as mechanotransduction [147]. The molecular response of the cells does not only depend on the externally applied forces. The geometry, topography and stiffness of the substrate that the cells adhere also regulate the molecular events such as growth, proliferation, differentiation, gene expression and apoptosis [148-150].

The main steps in cellular response formation to mechanical forces are i) mechanocoupling, ii) biochemical coupling, iii) signal transmission and iv) response of effector cells [151]. In the first step external mechanical load causes interstitial fluid flow within the lacunae and this fluid flow results with deformation of bone cells. In biochemical coupling the mechanical force is transformed to a biochemical signal through a pathway involving ECM, membrane and intracellular proteins and cytoskeletal elements. In signal transmission several molecules are transported from sensor cells such

as osteocytes and bone lining cells to effector cells such as osteoblasts and osteoclasts which results with the effector cell response as formation or removal of bone [151, 152].

Osteocytes are the cells that are primarily responsible from the transmission of mechanical stimuli within bone tissue and they are more sensitive to mechanical stimuli than pre-osteoblasts and osteoblasts [128, 153]. Osteocytes are situated in "lacunae", which are fluid filled spaces, inside the bone matrix. They interact with each other and with osteoblasts found at bone surface via their cellular processes through channels known as "canaliculi". It is still controversial how the mechanical forces act on cellular responses [146].

Osteocytes have cellular processes which are rigid because of the highly crosslinked actin fibers. These rigid structures facilitate the sensing of the mechanical stimuli and very small strains between the contact points of these processes and the bony wall is amplified to very high strain values which results with calcium influx and initiation of biological signaling [16]. Osteocytes have transverse tethering elements in the pericellular matrix which anchor them to the canalicular wall and the fluid flow causes a tensional force on them which is transmitted to cytoskeletal elements with a higher level strain than tissue level [154-156]. *In vitro* studies demonstrate that the strains that are needed to evoke a significant cellular response for osteocytes are around 10 000 με which is much higher than *in vivo* strains needed [157]. Osteocytes have other stiff protrusions that are made up of microtubules, originate from the cell body and extend to the ECM that are called as "primary cilia". Other researchers suggest that primary cilia are the main mechanosensors in the bone [158]. The length of primary cilia changes from 2 μm to 30 μm in different cell types and shorter cilia lengths cause higher rigidity which makes it harder to deflect under fluid flow. Because of this it is still contradictory whether these structures are the primary mechanosensing units or not [16].

3.1.3. Signal Transduction Pathways in Mechanotransduction

There are different hypotheses about force transmission and the response of the cells which are still under investigation. There is not only one explanatory pathway, but there are some common proteins that take place in the force transmission process. Focal

adhesions are the contact points of cells with the ECM. Integrins are heterodimeric transmembrane proteins that are connected to the ligands from one end in the ECM to actin filaments through protein complexes in the intracellular space [159]. They are composed of two non-covalently associated glycoproteins, α and β subunits. A common pathway for mechanotransduction is the coupling of integrins with ECM proteins fibronectin or vitronectin to initiate the mechanotransduction events. On the intracellular side different proteins are suggested to link to α or β subunits of integrin or to both subunits simultaneously, such as focal adhesion kinase (FAK), paxillin and caveolin that bind to other proteins which have actin binding sites [159, 160]. There are also other proteins that have both integrin and actin binding sites such as tensin, filamin and talin [160]. Many intracellular proteins (e.g. fimbrin, α-actinin and ERM (ezrin, radixin, moesin)) have more than one actin binging sites, so they take place in the crosslinking of actin fibers so that transmitting the force away from the focal adhesion points and regulate cytoskeletal strain (Figure 3.1).

Osteocytes are the main regulators of mechanotransduction in bone tissue. They release prostaglandin E_2 (PGE_2), which is a hormone-like molecule that controls contraction and relaxation of smooth muscle, regulation of inflammatory response and controls blood pressure. PGE_2 is needed for anabolic response of the bone [161]. There are several PGE_2 receptors that can activate Akt, which is a protein kinase B and prevents cells from apoptosis and promotes cell replication and proliferation in MSCs [161]. Akt takes place in the activation of WNT signaling. WNT is a family of secreted glycoproteins and function as growth factors. WNT/β-catenin pathway controls stem cell proliferation and differentiation and is required for bone formation. β-catenin is a protein that is responsible for regulation and coordination of cell-cell adhesion [162]. In the presence of WNT signals β-catenin is transferred to the nucleus and initiate transcription of osteoblast specific genes [162, 163]. WNT/β-catenin pathway has an important role in the expression of Runt-related transcription factor 2 (Runx 2) gene, which is essential for osteoblast differentiation [164]. Expression of several osteoblast specific genes such as osteocalcin, Col1α1, BSP and osteopontin is dependent on binding of Runx 2 to their promotor regions [165] (Figure 3.2).

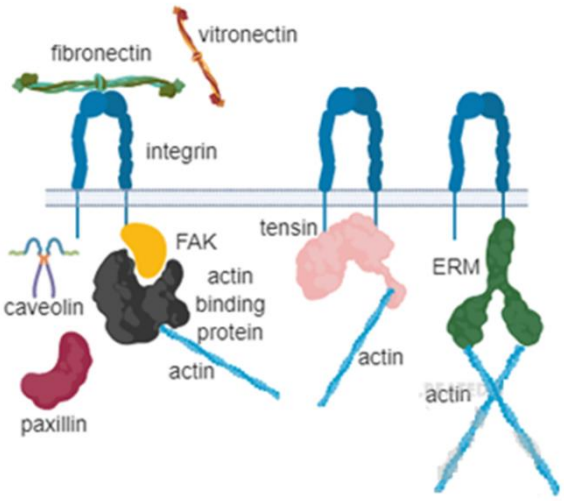

Figure 3.1. Transmission of the mechanical loads from ECM to intracellular space (The figure was drawn using Bio render software [25])

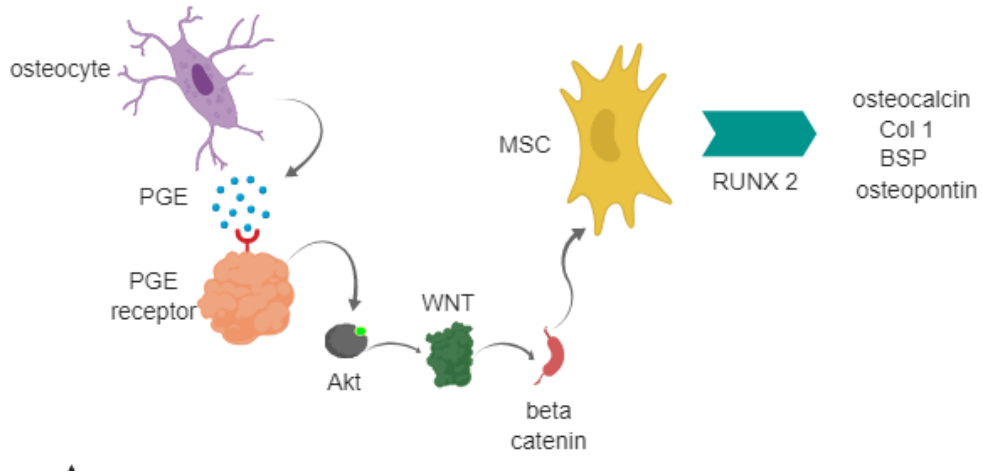

Figure 3.2. WNT/β-catenin pathway in MSC differentiation (The figure was drawn using Bio render software [25])

The molecules and their interaction in the signal transduction and osteoblastic differentiation are not limited to the ones that were described above. WNT/β-catenin is the most widely studied pathway in embryonic development, MSC differentiation and

drug design for bone diseases. The interaction of other molecules that have roles in mechanotransduction are still under investigation.

3.1.4. Mechanical Loading of Cells in Vitro

In order to understand how bone cells sense and respond to the specific mechanical loads, cellular deformations up to some extend should be formed in a system isolated from other environmental factors. *In vitro* mechanical loading models are used for studying the effects of forces within physiological or pathophysiological range at the cellular level within a controlled microenvironment. These models allow studying the effect of individual forces on individual cells at different differentiation states [166].

Researchers have long been studying the mechanical stimulation and mechanotransduction events by using pseudo physiological stimulation such as fluid shear, cellular membrane deformation by micropipette aspiration and hydrostatic pressure, but recently mechanical vibrations are also being used as a tool to study mechanotransduction pathways [167]. These systems can be designed for 2D cell cultures or 3D tissue engineered constructs. The most common models for fluid shear application in 2D cell cultures are parallel plate flow chambers. Most systems are derived from a chamber designed to provide a controlled fluid flow by hydrostatic pressure for cells grown on a glass slide and surrounded by a polycarbonate chamber that is sealed with a rubber gasket [168]. Fluid flow can be unidirectional, pulsatile or oscillatory [169]. These systems allow the application of very high shear rates, but the main drawback of them is the unsuitability of the system for long term cultivation and air bubble formation within the channels that alter the flow regime [169]. An alternative system for creating fluid shear is rocking “see-saw” setup for cells cultured in multiple well plates. These systems also have some drawbacks such as the generation of only low level of fluid shear stresses and the non-homogenity of the forces applied on cells depending on the location of cells and the amount of liquid in the wells of the plate [169].

In order to study the direct effect of matrix strain *in vitro* for 2D systems usually two models are used; stretching the substrate that cells are attached and four point bending

models to apply tension. These devices can be commercially purchased or produced home-made.

Since 2D systems have some drawbacks explained above, 3D *in vitro* models that mimic physiological conditions better are developed. As for monolayer cultures, mechanical loading can also be studied for 3D systems in specifically designed bioreactors to apply compression, tension or vibration [166].

In our research the mechanical forces were applied through vibration and fluid shear in a perfusion bioreactor, thus *in vitro* vibration and perfusion systems are discussed in more detail in the following sections.

3.1.5. Low Magnitude High Frequency Vibration

Low magnitude loads with high frequencies are commonly referred as "vibrations" [170]. It is known that instead of high magnitude forces, low magnitude forces with high frequencies are also anabolic for bone tissue [143]. High magnitude of loading can damage the bone and cause formation of cracks. Dynamic loading triggers anabolic reactions whereas static loading cause bone reduction [171]. Bone is subjected to high magnitude loading as a result of physical exercise or daily activities but in addition to that there is always a continuous low magnitude high frequency loading on bones because of muscle contraction [171]. The main idea behind application of vibration is to simulate the forces acting on bone tissue as a result of muscle action in the resting state [172].

Frequency, magnitude of the peak acceleration and total displacement are the parameters that are used to define a sinusoidal vibration. Frequency is the number of oscillations applied to the system per second and depicted with the unit Hertz (Hz). Acceleration is expressed as g, where 1 g=9.81 m/s^2 is the gravitational pull and total displacement is the peak to peak distance of the oscillating system expressed in μm, mm or cm [170]. Generally vibrations with smaller acceleration than 1g and frequency between 20 and 90 Hz are considered as low magnitude high frequency vibrations (LMHFV) and there are a lot of *in vitro* and *in vivo* studies regarding their supportive effects on musculoskeletal system in the literature [173].

As an example, in a previous study performed by our research group, it was observed that mouse bone marrow stem cells alter their cytoskeletal organization upon application of mechanical vibrations which is also a determinant of osteogenic differentiation [77]. LMHFVs with 0.15g magnitude and 90 Hz frequency for 15 min/day during 7 days, in the presence and absence of chemical inducers of *in vitro* osteogenesis, increased total actin content, actin fiber thickness, Runx 2 mRNA expression and cytoplasmic membrane roughness.

Another study by our group demonstrated that application of LMHFVs at the same magnitude, frequency and duration values with the previous study reverted back the effects of adipogenic induction of D1 ORL UVA cells in terms of cellular morphology and reduction in the expression of adipogenic genes [78].

In another research where diabetic rat models with type 2 diabetes were used it was observed that LMHFV accelerated the open foot wound healing by stimulating blood microcirculation and glucose uptake in muscles [174]. In another *in vivo* research it was reported that LMHFV with 35 Hz, 0.3g accelerated callus formation, mineralization and fracture healing in rats with closed femoral shaft fracture [175]. Another study showed that application of whole body vibrations to ovariectomized osteoporitic rats with bone implants enhanced osseointegration of the implant [176].

LMHFVs are also clinically applied for prevention of bone loss related to osteoporosis and improving muscle strength. In a study which LMHFVs were applied to post-menopausal women with 0.2 g acceleration and 30 Hz frequency for less than 20 min, it was shown that these vibrations inhibited bone loss in the femur and spine, especially for individuals with lower body mass [177]. In another extensive clinical trial LMHFVs (0.3 g, 35 Hz) were applied for 20 min, 5days/week for 18 months for elderly and it was reported that this alternative therapy reduced fall and fracture risks by improving muscle strength and balancing ability [178].

Since LMHFVs have stimulatory effects in prevention of bone loss and the application is rather easy compared to other mechanical loading systems, in this research vibrational loading has chosen for physical stimulation of stem cells together with fluid shear for induction of osteogenesis.

3.2. Methods

3.2.1. Generation of Stable Cell Lines Through Viral Infection

D1 ORL UVA (mouse bone marrow) cell line was infected with EGFP (enhanced green fluorescent protein) carrying retroviruses in order to produce fluorescently labelled stable cell lines for further imaging analysis of tissue engineering experiments. EGFP gene was transferred by pMIG viral vector (Addgene #9044, USA) (Figure 3.3).

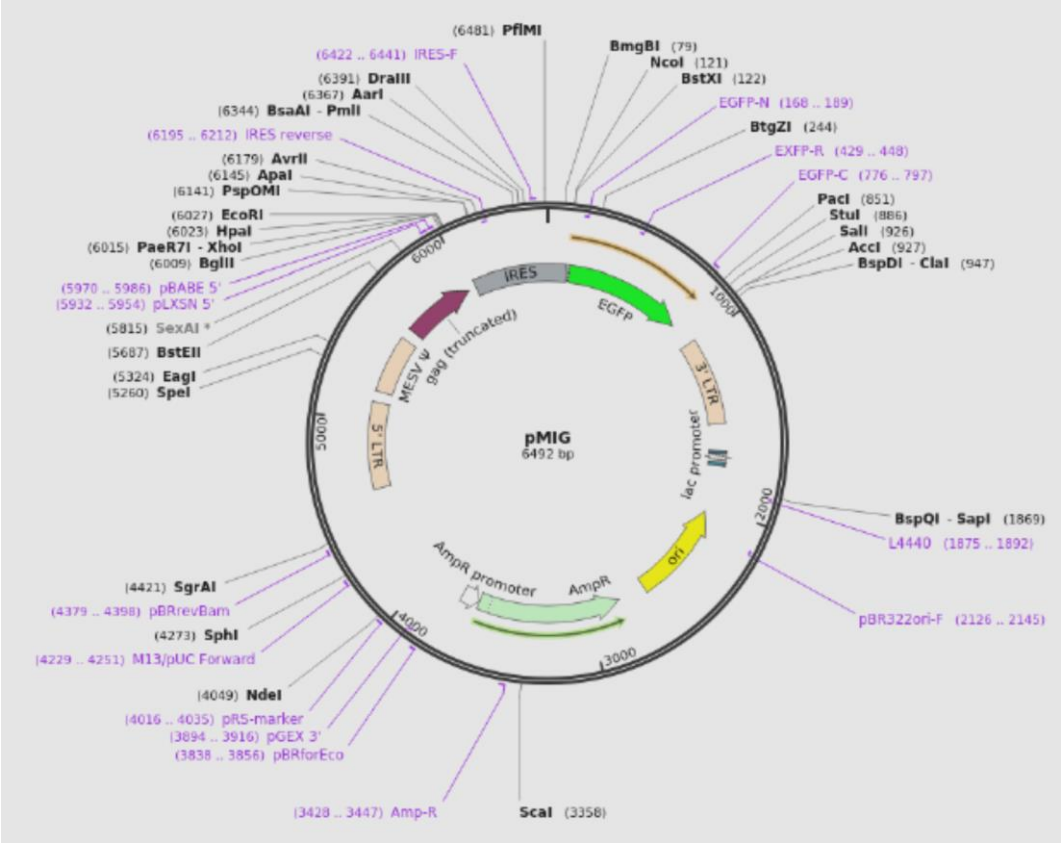

Figure 3.3. pMIG viral vector map

Viruses were kindly provided by Assoc. Prof. Dr. Özden YALÇIN ÖZUYSAL and kept as frozen suspension in the freezer. For infection D1 ORL UVA cells were first seeded in 6 well plates at a density of $3x10^5$ cells/well. Frozen virus suspensions were thawed.

Growth media of the cells in 6 well plates were discarded on the next day after cell seeding. For each 1 mL of virus suspension 1 µL of Polybrene, a polymer used for increasing the transduction efficiency of viruses, was added to prepare infection medium. Normal growth medium with Polybrene and without the virus was added to cells as a negative control (mock). This infection medium was added on cells instead of discarded growth medium and cells were incubated at 37 ^oC and 5% CO_2.

The next day, infection medium was discarded and normal growth medium was added. Cells were incubated in this medium for 2 days. Since the viral vectors contain Puromycin resistance genes, the successfully infected cells will be resistant to Puromycin antibiotic. For this purpose, selection medium with Puromycin (2 µg/mL) was prepared. Cells in 6 well plates were splitted in 10 cm Petri plates and incubated in the selection medium until all of the mock cells die.

After stable cells line that carry EGFP gene was produced, the media of cells were replaced with normal growth media. Green fluorescent labelled D1 ORL UVA cell stocks were prepared by freezing the cells.

3.2.2. Cell Culture and Osteogenic Induction

EGFP carrying D1 ORL UVA cells were seeded in directly 12 well plates, or on circular Whatman paper constructs at a density of 10^2 and 10^4 cells in 20 µL medium, respectively and 700 µL growth medium was added.

For osteogenic induction, on the next day of cell seeding the regular growth medium of cells was replaced with osteogenic induction medium (10 mM β-glycerophosphate, 50 µg/mL ascorbic acid and DMEM high glucose complete medium).

3.2.3. Application of Low Magnitude Mechanical Signals (LMMS)

D1 ORL UVA cells (with EGFP) seeded in 12 well plates and on Whatman paper scaffolds were exposed to LMMS daily at 90 Hz and 0.1 g (1 g = Earth's gravitational pull), for 15 min/day, 5 days/week at ambient conditions for 21 days. Control samples were hold outside the incubator for the same duration. LMMS was generated and delivered to cells by a custom-made platform in vertical direction (Figure 3.4).

Figure 3.4. Vibration platform and the computer system

3.2.4. Determination of Cell Viability on Whatman Paper

The effect of LMMS on the viability of cells seeded in tissue culture plates and on Whatman paper scaffolds were determined by MTT assay. MTT test was applied to the cells on days 1, 3, 7 and 10 after seeding. On the indicated time points, regular growth media of the samples were replaced by 10% MTT solution containing medium, incubated for 4 h at 37 ^{o}C and 5% CO_2. Tetrazolium salts were solubilized with DMSO and absorbance was measured at 570 and 650 nm wavelengths with a spectrophotometer (Thermo Fisher Scientific, Multiscan Spectrum, USA). Non-cell seeded Whatman paper that was incubated with the same amount of MTT containing medium for the same duration was used as the blank.

3.2.5. Total RNA Isolation from Paper Scaffolds and RT-PCR

For total RNA isolation from cells on Whatman paper scaffolds D1 ORL UVA cells (passage no<20) were seeded on scaffolds at a density of 10^5 cells/paper. RNA isolation was done on 14^{th} day of incubation. PureLink RNA Mini Kit (Invitrogen, USA) was used for RNA isolation.

Paper samples were washed with PBS once and then transferred into separate microcentrifuge tubes. The whole purification procedure was conducted on ice. Lysis buffer was prepared by adding 5 µL β-mercaptoethanol to each 500 µL lysis buffer of the commercial kit. The samples were homogenized with a tissue grinder (Isolab, Germany) by immersing the microcentrifuge tubes in ice to prevent the heating of the samples and denaturation of RNA. Samples were homogenized for a total of 1 min, with a break after 30 sec.

The cells were suspended by passing the suspension through insulin needles several times. After suspension 400 µL 70% ethanol was added to each sample and RNA purification was done according to the manufacturer's instructions. Isolated RNAs were kept at -80 ^oC. The concentration and purity of isolated RNAs were measured by Nanodrop spectrophotometer (NanoDrop 1000 Spectrophotometer, Thermo Scientific, USA).

Reverse transcription was done by using RevertAid First Strand cDNA Synthesis Kit (ThermoFisher Scientific, USA), according to the manufacturer's instructions with 220 ng template RNA. cDNAs were kept at -20 ^oC. For RT-PCR 55ng cDNA was used with the primers listed below. PCR was conducted at 95 ^oC for 30s, 60 ^oC for 30s and 72 ^oC for 30s for 45cycles. The annealing temperatures are given in (Table 3.1). Quantitative RT-PCR was done by Light Cycler 96 thermal cycler (Roche, Switzerland) with FastStart Essential DNA Green Master Kit (Roche, Switzerland).

The relative expression levels of the target genes were calculated by threshold cycle (ΔΔCt) method with GAPDH as reference gene and reported as $2^{-\Delta\Delta Ct}$, as relative folding changes to samples under static and growth medium conditions.

Table 3.1. Sequences of forward and reverse primers used for RT-qPCR reactions.

Gene	Forward primer	Reverse primer	Annealing Temperature (ºC)
OCN	CTG ACA AAG CCT TCA TGT CCA A	GCG CCG GAG TCT GTT CAC TA	55.9
ALP	TTT AGT ACT GGC CAT CGG CA	ATT GCC CTG AGT GGT GTT GCA	57.9
GAPDH	GAC ATG CCG CCT GGA GAA AC	AGC CCA GGA TGC CCT TTA GT	58

3.2.6. Determination of Mineralization on Whatman Paper

Cell seeded Whatman paper constructs and tissue culture plates were washed with 10 mM PBS three times and fixed with 4% paraformaldehyde (PFA) (Sigma-Aldrich, USA) for 20 min at room temperature. Then PFA was discarded and samples were rinsed with distilled water twice.

Alizarin red S dye solution (2% w/v) was prepared by dissolving the dye in distilled water and the pH of dye solution was adjusted between 4.1 and 4.3. Dark brown solution was filtered. Samples were stained with Alizarin red S dye, by incubating them at 37 ºC for 30 min. Then the samples in tissue culture plates were washed with distilled water three times.

For the samples with Whatman paper, a blank non-cell seeded paper was used as a reference to understand whether the non-specifically bound dye was removed or not. Additional rinsing was done by adding PBS and leaving the samples on a shaker overnight. The following day samples were washed with distilled water by leaving them in water for a total of 3h on the shaker and renewing the water at every hour. After aspiration of the water, the samples were stored at -20 ºC before extraction of the dye with CPC [179].

3.2.7. Quantification of Alizarin Red S Staining Through Cetylpyridinium Chloride (CPC) Extraction

CPC solution with 10% (w/v) concentration was prepared by dissolving CPC in 10 mM sodium phosphate (pH 7.0). Alizarin red S stained samples were incubated in 0.5 mL CPC solution in a 24 well plate for 1 h at room temperature on a shaker. 100 µL aliquots from each sample was transferred as triplicate to a 96-well plate and the absorbance was measured at 550 nm. Alizarin red concentration per sample was calculated and the values were normalized to total protein amount.

3.2.8. Total Protein Isolation and Determination of the Amount from Cells on Paper Scaffolds

Lysis buffer (10 mM Tris-HCl pH=7.5, 1 mM EDTA, 0.1% Triton X) was prepared. Protease inhibitor (1% v/v) and dithiothreitol (DTT, 0.1 % v/v) were added to this solution to prepare the complete lysis buffer. Paper scaffolds were washed with PBS and transferred to 1.5 mL microcentrifuge tubes which were placed in ice. Complete lysis buffer (250 µL) was added to each sample and the samples were vortexed 10 s with 5 min intervals during a total of 30 min. Lysates were centrifuged at 15000 rpm for 3 min and supernatants were transferred to fresh tubes.

Total protein contents were measured by Bradford assay. Bradford reagent (20 %, v/v) was diluted with distilled water (80 %, v/v). Diluted Bradford reagent was aliquoted in separate microcentrifuge tubes and 10 % (v/v) isolated protein was added to tubes, and 100 µL from each sample was transferred to a 96-well plate as triplicate and the absorbance was read at 595 nm.

3.2.9. FTIR Analyses for Detection of Mineralization

The composition of organic and inorganic components of ECM was detected by Fourier-transform infrared spectroscopy (FTIR) (Perkin Elmer Spectrum Version 10.4.3,

USA). The samples were fixed with 4% PFA and washed with distilled water several times. Then they were dried in the vacuum oven to remove the water. FTIR spectrometer with ATR attachment was used and the spectra was recorded in the range of 4000-400 cm^{-1} wavenumber with 4 cm^{-1} resolution. Water has a strong infrared absorbance [180], thus samples were dried in the vacuum oven to remove water prior to FTIR analysis. FTIR spectra of the samples were compared with empty paper that was treated with the same procedures for cell fixation and washing steps. Since the fingerprint peaks of bone originating from collagen and hydroxyapatite are within 400-1700 cm^{-1} region of the spectrum, the comparison between spectra of different samples was done by narrowing the wavenumber interval. Analyses were done by using Spectragryph 1.2 spectroscopy software.

3.2.10. Statistical Analyses

All the experiments were repeated in triplicates, and all results are displayed as the mean ± standard deviation. Statistical analyses for comparison between the groups were performed using ANOVA. In order to detect significant difference in growth Student's t-test was performed for each cell seeding density, between control and vibration groups of each condition. To demonstrate the differences between groups for gene expression and quantification of mineralization ANOVA followed by S-N-K post hoc test was done. Levels of significance were reported for 5%, 1%, and 0.1%.

3.3. Results

3.3.1. Generation of Stable Cell Lines Through Viral Infection

D1 ORL UVA cells were infected with EGFP gene carrying PMIG retroviral vector to be able to visualize the cells on the paper without any further staining. Fluorescent microscope images of infected D1 ORL UVA cells showed that a stable cell

line which produce EGFP protein was successfully obtained (Figure 3.5). These infected cells were used for cell viability, mineralization and gene expression analyses throughout the study.

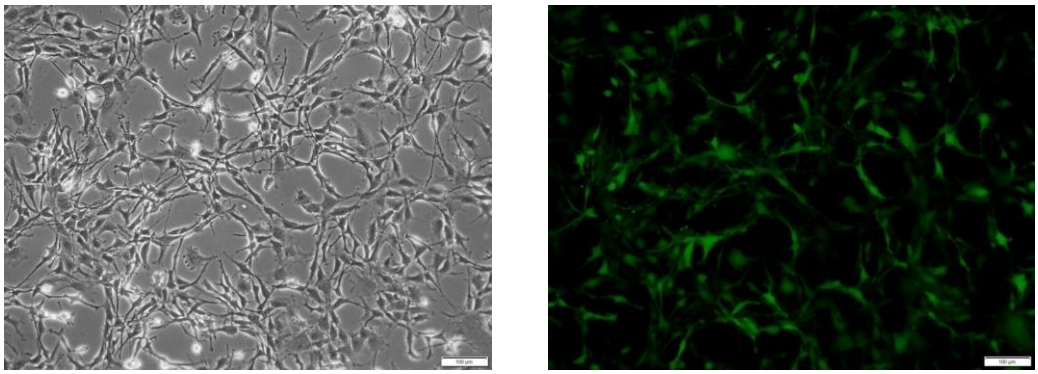

Figure 3.5. D1 ORL UVA cells that were infected with EGFP carrying PMIG retroviral vector. Left: phase contrast, right: fluorescent microscope images. Scale bar: 100 μm

3.3.2. Determination of Cell Viability

The viability of D1 ORL UVA stem cells that were seeded on filter paper scaffolds and incubated in standard growth medium or in osteogenic induction medium with or without exposure to vibration was determined via MTT cell viability test. It was observed that for each cell seeding density (10^3, 10^4 and 10^5 cells/paper) the cell number increased during 10 days for both standard growth and osteogenic induction conditions on paper scaffolds (Figure 3.6). According to cell viability test results, it was seen that the filter paper was biocompatible and an appropriate scaffold material for long term incubation of the cells. This data was also supported with fluorescent microscopic observation during 21 days of incubation (Figure 3.7). Together with biocompatibility assessment the aim of this test was also determination of the optimum cell seeding density.

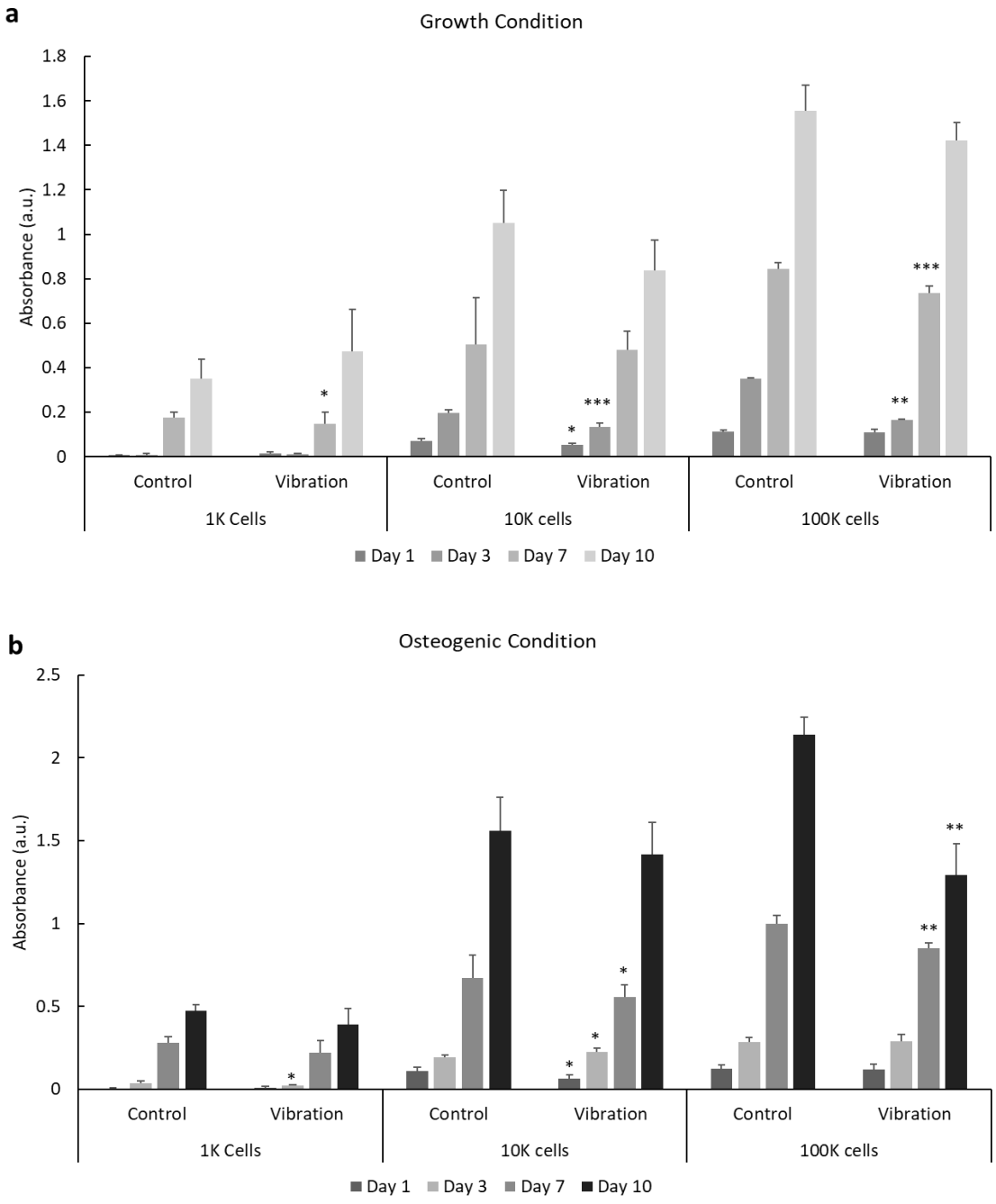

Figure 3.6. The viability of D1 ORL UVA cells on filter paper scaffolds was determined via MTT test. Cell viability under a) normal growth and b) ostogenic induction conditions during 10 days. *$p \leq 0.05$; **$p \leq 0.01$; ***$p \leq 0.001$ for each cell density and each time point compared to control calculated by Student's t-test.

According to the graph, it was seen that the trend in cell number increase was similar for each seeding density, but 10^3 cells/paper scaffold was not enough for further

gene expression and mineralization detection analyses. It was also seen that there was not an important difference between 10^4 and 10^5 cells/scaffold seeding densities in terms of cell viability and proliferation. For this reason, 10^4 cells/paper scaffold was used as the seeding density for the entire experiments.

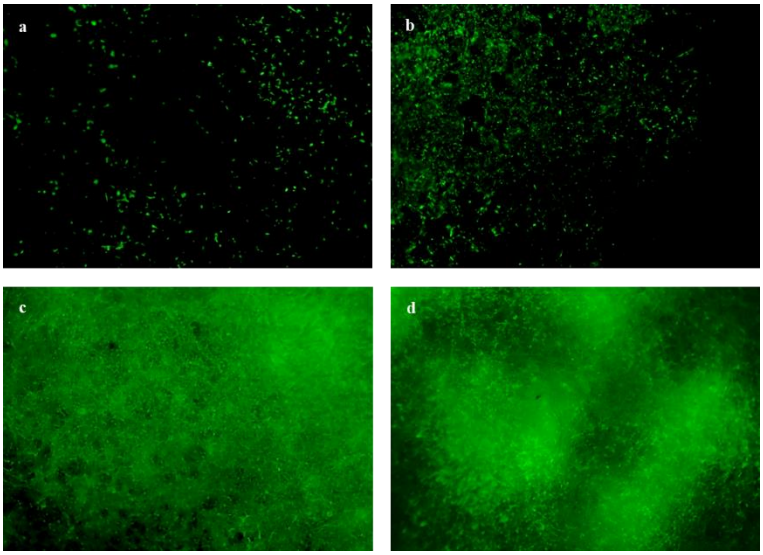

Figure 3.7. Fluorescent microscope images of D1 ORL UVA-EGFP cells showing proliferation of cells on filter paper scaffolds; a) day 1, b) day 7, c) day 14 and d) day 21after cell seeding. Magnification, 4X.

3.3.3. Determination of Osteogenic Differentiation

The osteogenic differentiation of stem cells was determined by gene expression at molecular level by RT-qPCR and by evaluation of mineralization through Alizarin red S staining and FT-IR spectroscopy.

3.3.3.1. Determination of Osteogenic Gene Expression

The expression levels of osteogenic genes alkaline phosphatase (ALP) and osteocalcin (OCN) from static and vibration applied D1 ORL UVA cells which were

incubated in osteogenic induction medium on paper scaffolds were compared to static samples grown in normal growth medium.

The gene expression analysis was done after 14 days of incubation. In order to determine the effect of the vibrational forces on the osteogenic differentiation, the change in mRNA expression levels of osteoblastic marker genes ALP and OCN were assessed by comparison to the mRNA expression level of the housekeeping gene GAPDH. Four experimental groups were tested; growth control (GC), osteogenic control (OC), growth vibration (GV) and osteogenic vibration (OV). The mRNA expression levels of all osteogenic markers for each group were normalized to the expression of the related gene of growth control group.It was observed that ALP and OCN expression profiles had different trends (Figure 3.8). The OCN expression level of OV was 2.8 fold higher than GC, whereas GV was almost 15% lower. Chemical osteogenic induction without vibration, on the other hand, increased the expression of OCN gene 1.8 fold. Induction of osteogenesis, whether chemical or mechanical, caused a decrease in ALP expression for all groups compared to GC at 14th day of osteogenic induction.

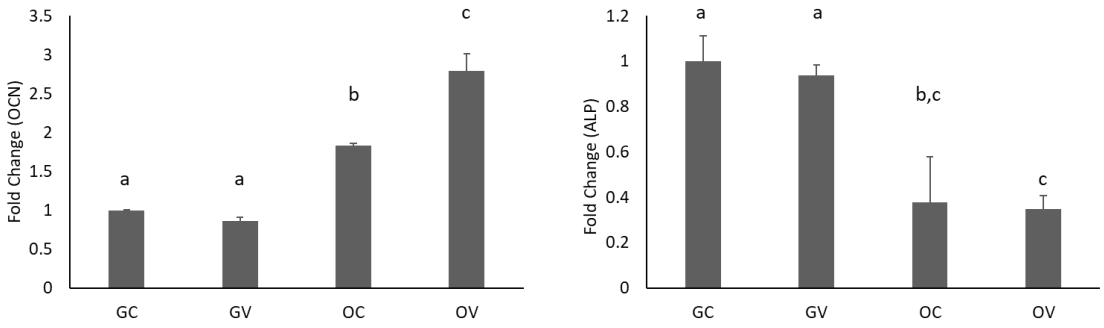

Figure 3.8. Gene expression levels of D1 ORL UVA stem cells that were either induced with application of vibration or with osteogenic induction medium treatment after 14 days. OCN expression was found to be higher for OC and OV groups, whereas ALP expression was lower for all groups compared to GC group. a, b, c: differences in gene expression level between groups calculated by ANOVA followed by S-N-K post hoc test. $p \leq 0.05$. GC: growth control, OC: osteogenic control, GV: growth vibration, OV: osteogenic vibration

3.3.3.2. Determination of Mineralization

Alizarin red S (ARS) staining, which evaluates calcium deposits in cells, was done on days 14 (for both plate and paper scaffold samples) and 21 (only for paper samples) of osteogenic induction. The experimental groups consist of cells seeded in directly to tissue culture plates and on Whatman paper scaffolds. Half of the samples within each group were incubated in regular growth medium and the remaining were incubated in osteogenic induction medium. These samples were subjected to LMMS, and each group also had static controls. According to the results obtained, mineralization was not observed for the cells grown in regular medium, but the cells that were treated with osteogenic supplements were stained densely on 14^{th} day of incubation (Figure 3.9a). When the ARS dye that bound to calcium deposits formed by the cells grown in culture plate was dissolved with CPC for quantification, the highest mineral deposition was observed in OV group (Figure 3.9b).

It was observed that, on both 14 and 21 days, only the cells which were treated with osteogenic induction medium on paper scaffolds deposited calcium (Figure 3.10a). The density of red color which is the indicator of mineralization was higher on day 21 compared to day 14 within both OC and OV groups (Figure 3.10b). Similar to 2D culture results, mineral calcium deposition was denser for OV group compared to OC group for both time points.

3.3.3.3. Detection of Extracellular Matrix Components by FTIR

The organic and inorganic components of bone give intense and separate peaks when analyzed with FTIR. Various important data such as mineral to matrix ratio, the mineral and collagen maturity and crystallinity can be obtained and calculated from FTIR spectra [181]. The typical FTIR spectra of the bone has specific peaks around 900-1200 cm^{-1} arising from symmetric (v_1) and asymmetric (v_3) stretch phosphate regions of hydroxyapatite and 900-910 cm^{-1} out-of-phase bending (v_2) carbonate regions, respectively [182]. The maturity of the collagen crosslinks in the ECM can also be detected by the changes in the secondary structure of the protein which is visible as bands

around 1650 (Amide I) and 1550 (Amide II) wavenumbers (cm^{-1}) [181]. Therefore, the spectra of paper constructs were obtained (Figure 3.11a) and the spectrum of empty paper (EP) was subtracted from each sample spectra (Figure 3.11b) to analyze the ECM composition for each condition on 14^{th} and 21^{st} days of osteogenic induction. It was observed that the samples which were stimulated by vibrational forces during 21 days, whether incubated in osteogenic induction medium or not, had peaks in Amide I and Amide II regions, as well as peaks in v_3 phosphate region. For the 14^{th} day, only the samples that were incubated in osteogenic induction medium with vibration had both amide and phosphate peaks, but vibration applied samples in normal growth media had not. Non-vibrated but osteogenically induced group for 21 days, on the other hand, had peaks only in Amide I and II regions without a phosphate peak. For both time points, days 14 and 21, chemical osteogenic induction resulted with protein deposition as can be seen from the peaks in the amide regions, but application of vibration together with osteogenic induction caused mineral deposition in addition to protein.

3.4. Discussion

Expression of osteoblast specific genes is an important determinant of osteogenic differentiation. At the early phase of differentiation, after an initial increase in cell proliferation, ALP and Collagen I gene expressions are upregulated, and this is followed by ECM deposition.

At later stages, expression of bone markers and mineralization related genes such as osteocalcin (OCN), osteopontin (OPN), osteonectin and bone sialoprotein (BSP) start to increase [183].

During cell proliferation phase, OCN secretion might not be detected in the medium, but its level start to increase with nodule formation and reaches the peak value when these nodules start to mineralize [184]. However, the time that these specific genes are expressed might differ according to cell type, culture conditions and physical factors [185]. Among the osteogenic marker genes, OCN is expressed only in osteoblasts [186]. There are contradictory evidences about the role of OCN in mineralization; proposing that OCN is responsible for the initiation of HAP crystal formation, and it also functions

as a mineralization inhibitor [187]. According to our results, OCN expression was highest for OV group, suggesting that vibrational forces together with chemical induction promoted the osteogenic differentiation of MSCs on filter paper scaffolds more than incubation of cells with osteogenic medium under static conditions. In addition to that, the mechanical forces applied for 14 days were not enough solely to induce osteogenic differentiation. In a previous research that was performed in our laboratory, it was demonstrated that the vibration did not have a significant effect on the expression of OCN in a 2D cell culture system [77]. Contrarily, in our research, when the same D1 ORL UVA bone marrow stem cells were subjected to the vibrational forces with the same magnitude and frequency on 3D paper scaffolds, the expression of OCN gene was found to be significantly ($p \leq 0.01$) increased compared to the cells incubated in osteogenic medium under static conditions. The expression of ALP gene, on the other hand, was downregulated upon treatment with osteogenic induction medium on 14^{th} day. ALP is an early marker of osteogenesis and its expression start to decrease in the mineral nodule formation phase [188]. In consistence with the ARS staining results, for OC and OV samples which were stained positively for ARS, a decrease in ALP expression was observed. This shows that osteogenically induced cells differentiated into mineral forming osteoblasts on paper scaffolds.

Mineralization process starts with the binding of calcium and phosphate ions to charged amino acid residues of collagen matrix [189-191]. During HAP formation, the composition of mineral phase changes and several different forms of calcium phosphate crystals such as amorphous calcium phosphate, octacalcium phosphate, β-tricalcium phosphate and dicalcium phosphate dehydrate can also be found in the medium [190, 192-194]. Calcium and all types of calcium phosphates are stained with ARS dye [195, 196]. ARS dye binds approximately 2 moles of Ca^{2+} per mole of dye in solution [197]. According to staining results, static samples that were incubated with osteogenic media (OC) stained positively for calcium, but no phosphate peak was observed for these samples when they were analyzed with FTIR. This can be explained with the initiation of amorphous calcium phosphate precipitates before mature HAP formation upon chemical osteogenic induction that can be detected with ARS staining, but cannot be determined through phosphate stretching in HAP region through FTIR. Additionally, osteocalcin is a calcium binding protein and it takes a role in the nucleation and propagation of HAP crystal formation [198]. It was previously shown that knockdown of OCN gene causes a

delay in the maturation of HAP crystals [190]. Our gene expression results together with mineralization studies also show that, OCN expression level was higher for OV samples and a denser staining of the minerals formed by these samples and the FTIR peak in phosphate region also prove that vibration had a positive effect on formation of more mature mineral crystals.

Bone is a composite material and its infrared spectrum contains a combination of bands from both native hydroxyapatite (at 500-700 cm^{-1} and 900-1200 cm^{-1}) and collagen (at 1200-1700 cm^{-1}) [199]. It also contains a band around 870 cm^{-1} which arises from carbonate and is a characteristic of type B apatite [199]. Data obtained from infrared spectroscopy provide valuable information about the localization of ions with asymmetric vibrations, and the mineral phase obtained from homogenized *in vitro* cultures [200]. In a research about the potential use of Runx 2 expressing dermal fibroblast cells for bone tissue engineering applications, FTIR was used for chemical characterization of the deposited mineral phase. Amide I/II bands at 1655 and 1550 cm^{-1}, together with an enhanced phosphate peak at 1100 cm^{-1} were reported for the cells with osteogenic capacity [201]. In another research, FTIR was used to determine the chemical composition of bone nodules formed by BMSCs on chitosan/PMMA scaffolds and it was reported that the spectra of the deposited material were almost identical to the spectra obtained from murine calvariae [202]. Another research for the characterization of ECM mineralization of MC3T3-E1 cells *in vitro* demonstrated that these cells had absorption bands at 1200-900 cm^{-1} range arising from phosphate group of the mineral in the ECM and amide I/II/III bands at 1650-1635 cm^{-1}, 1550-1535 cm^{-1} and 1240 cm^{-1}, respectively [203]. In our research, chemical characterization of the ECM with FTIR demonstrated that application of vibration for a longer period (21 days), caused the formation of phosphate peak from mineral phase and amide I/II peaks from the organic component collagen even in the absence of chemical induction. But for shorter duration (14 days) vibration alone was not enough for the formation of mineral phase denoted with a phosphate peak. Amide and phosphate bands observed together only for vibration applied samples with chemical induction through osteogenic medium. This might suggest that application of vibrational forces together with chemical osteogenic induction improved the mineral deposition of the cells. The lack of carbonate bands in our samples might be the result of shorter incubation durations and due to this less mature hydroxyapatite formation compared to similar studies in the literature [201].

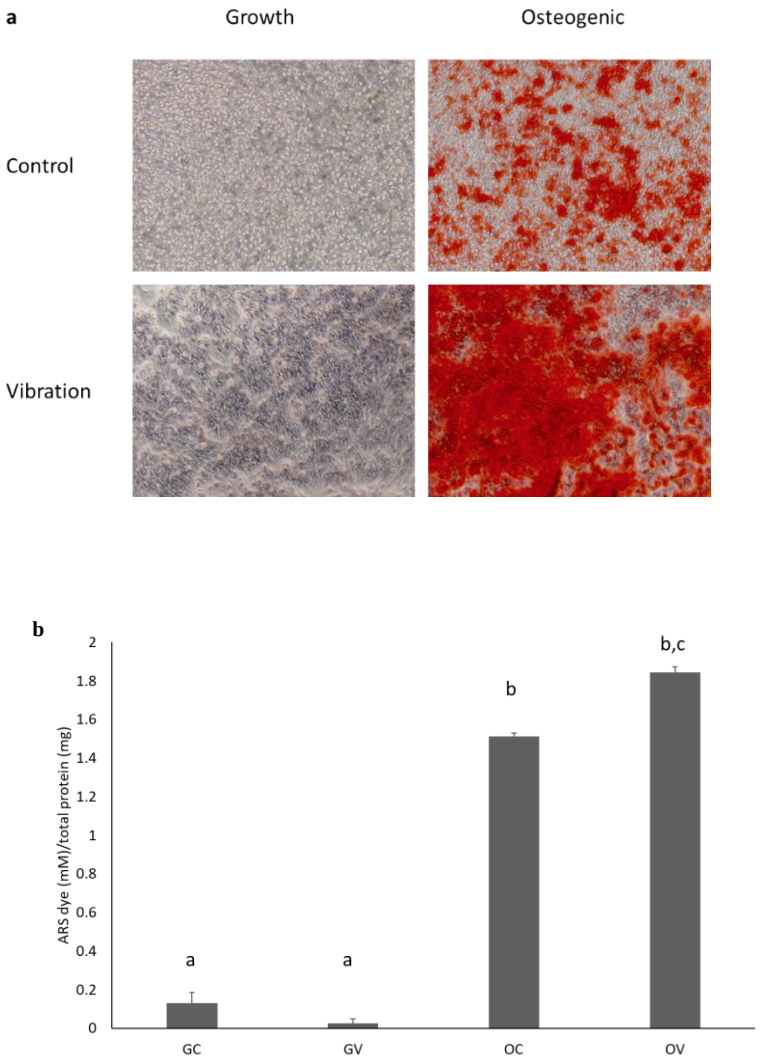

Figure 3.9. a) Phase contrast micrographs of D1 ORL UVA cells in tissue culture plates, stained with Alizarin red on day 14 (Magnification 10X). Red color indicates calcium deposits. b) Quantification of Alizarin red S (ARS) staining by CPC extraction. a, b, c: differences in dissolved ARS dye concentration between groups calculated by ANOVA followed by S-N-K post hoc test. GC: Growth control, GV: Growth vibration, OC: Osteogenic control, OV: Osteogenic vibration

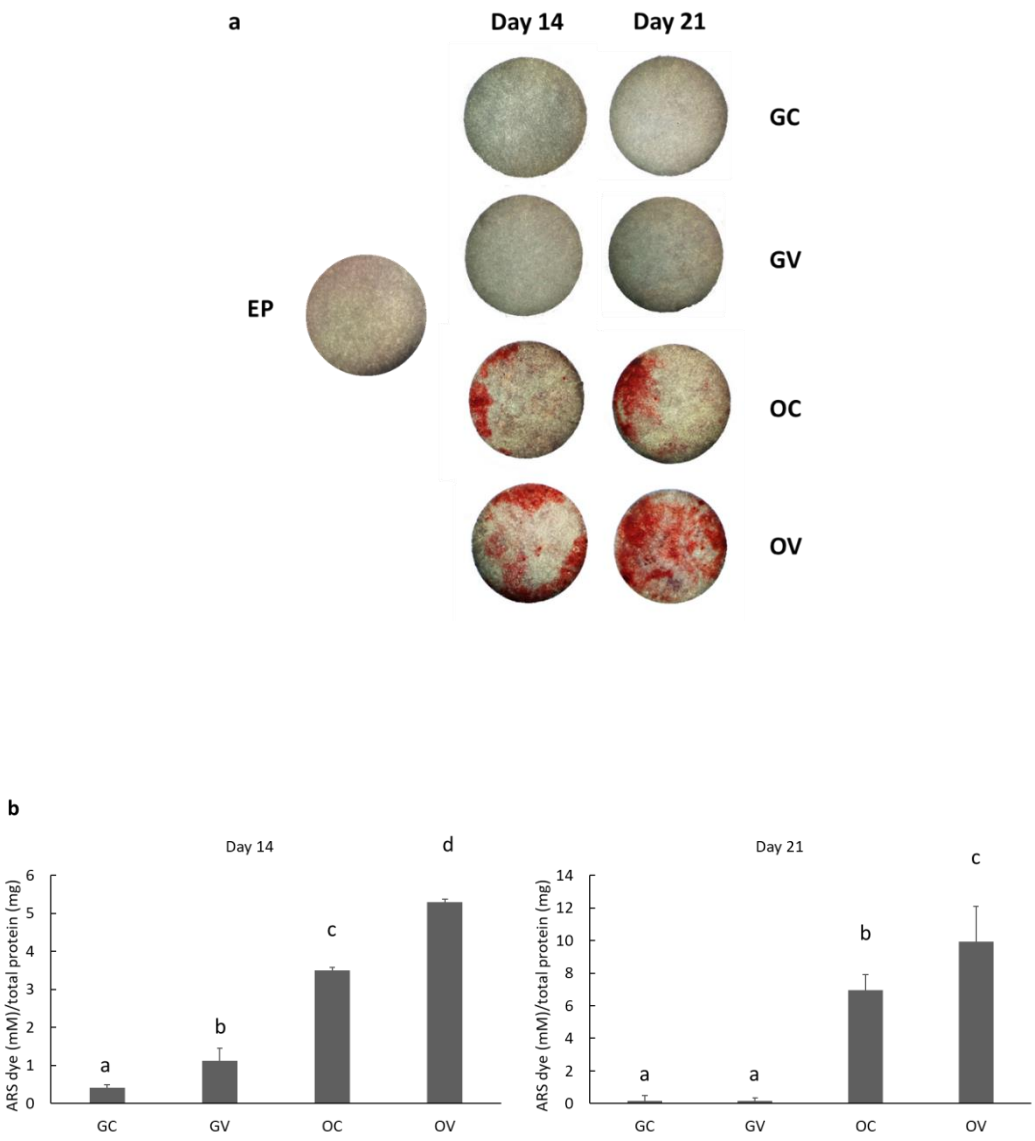

Figure 3.10. a) Stereomicroscope images of D1 ORL UVA cells seeded on paper scaffolds, incubated in regular growth medium or osteogenic induction medium and stained with Alizarin red on days 14 and 21. Red color indicates calcium deposits. b) Quantification of Alizarin red S (ARS) staining by CPC extraction. a, b, c: differences in dissolved ARS dye concentration between groups calculated by ANOVA followed by S-N-K post hoc test. GC: Growth control, GV: Growth vibration, OC: Osteogenic control, OV: Osteogenic vibration

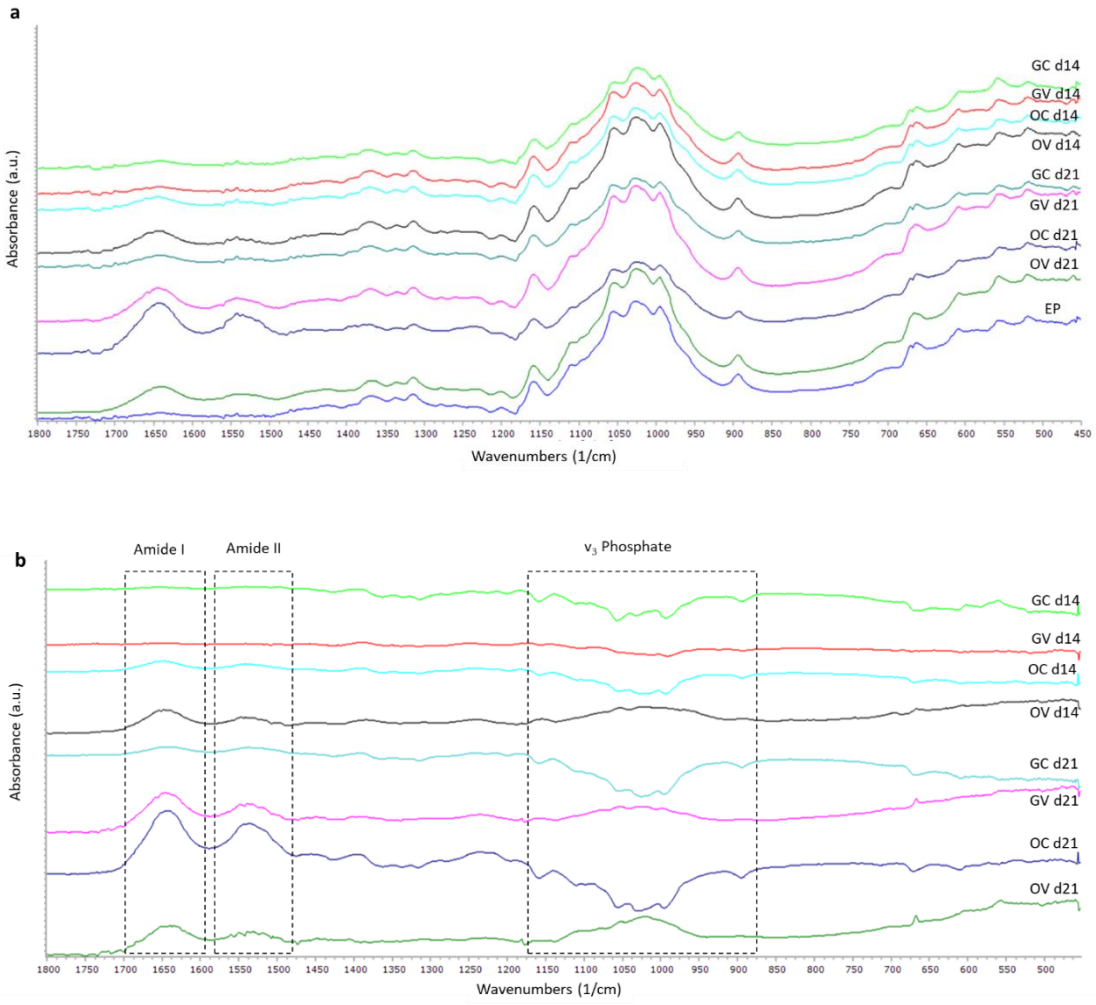

Figure 3.11. FTIR spectra of filter paper samples with D1 ORL UVA stem cells that were incubated in regular growth media or osteogenic media for 14 and 21 days with vibration or under static conditions. a) Spectra of each sample and the empty paper without cells, b) spectra of samples after the spectrum of empty paper was subtracted from each. GC: Growth control, GV: Growth vibration, OC: Osteogenic control, OV: Osteogenic vibration

CHAPTER 4

BIOREACTOR BASED CONTINUOUS APPLICATION OF MECHANICAL SIGNALS TO MESENCHYMAL STEM CELLS ON PAPER BASED SCAFFOLDS ENHANCE MINERALIZATION

4.1. Bioreactors in Bone Tissue Engineering

Bioreactors have been extensively used in many processes from production of biomass to waste water treatment and they are also adapted for tissue engineering applications [204]. Two dimensional culture conditions are not suitable for the production of centimeter scale bone tissue constructs for implantation because of diffusional limitations of oxygen and nutrients together with insufficient surface area to grow high number of cells. Under static cell culture conditions nutrients can only be transported through diffusion and because of mass transfer limitations in the center the cells tend to move to the periphery of the scaffold. [148]. Besides, bone progenitor cells need mechanical stimulation in addition to biochemical inducers to differentiate and form a functional tissue [148].

Use of bioreactors facilitate the mass transfer of nutrients and oxygen and removal of metabolic wastes, provide homogenous distribution of cells and expose cells to mechanical stimuli and ease the monitoring and controlling of the process [204, 205]. In bone tissue engineering field, the most widely used bioreactors are compression, perfusion, parallel plate, spinner flasks, magnetic force and rotating wall vessel bioreactors [148, 204, 205]. Different designs with combination of more than one type of physical stimulus are also used for tissue engineering purposes [148]. In this study a perfusion/vibration bioreactor was used for the incubation and mechanical stimulation of bone marrow MSCs. For this reason, a detailed information about perfusion bioreactors is given in the next section.

4.1.1. Perfusion Bioreactors

Perfusion bioreactors are designed to provide a controlled flow within the system [205]. These systems are used to overcome the limitations of spinner flask and rotating wall vessel bioreactors via providing a better controlled mixing and stimulating the cells with mechanical forces [206]. Perfusion bioreactors are composed of a media reservoir, a pump, a closed circuit of tubings and a chamber where the tissue engineered constructs are placed. They are divided into two types according to path of the flow as direct and indirect perfusion bioreactors. In direct perfusion, the media flow through the core of the scaffold and in indirect perfusion the scaffold is loosely placed into the chamber and media flow around it [148]. Optimal flow rate for stimulation of osteogenic differentiation and ECM mineralization depend on the fluid flow characteristics, scaffold and bioreactor design and it is usually optimized by trial and error for each bioreactor system [207].

Bone remodeling is related with the strain and strain is dependent on the interstitial fluid velocity [146]. The shear stress formed as a result of fluid flow in perfusion bioreactors depends on the scaffold geometry and architecture such as the porosity and interconnectivity of pores and this stress can be adjusted by changing the flow rate [208]. A perfusion bioreactor should provide sufficient flow through each scaffold, must be consistent, repeatable and controllable. In addition, all components pertaining to the bioreactor should withstand sterilization procedures that prevent contamination [209].

It is very challenging to measure the effects of fluid shear on cells for 3D scaffold systems. Perfusion of fluid decreases mass transfer limitations in the system, improves nutrient and oxygen transfer and removal of metabolic wastes which make it very difficult to distinguish the beneficial effect of fluid shear directly on cells. It is also challenging the calculation of shear force applied on cells because of the complex force distribution within the scaffold geometry [128]. Despite these challenges there is a wide range of studies in the literature demonstrating the positive effects of perfusion bioreactors on the production of tissue engineered bone constructs [210].

For example, in a study researchers applied computational fluid dynamics in combination with mechano-regulation theory for the optimization of various scaffold geometries such as pore size and porosity and fluid flow rates to obtain the optimum shear

stress for the maximized mineralization. It was reported that the optimal flow rate is dependent on the scaffold geometry, nevertheless the values are between 0.5 and 5 mL/min for various geometries [207]. In another study, the researchers used a flow perfusion bioreactor for 6 mm thick polyurethane scaffolds seeded with pre-osteoblasts and showed that after 8 days of incubation cell density was 76±3% at the core of scaffolds incubated in perfusion bioreactors, while cell density was 0.3±0.3% for the static control group claiming that flow perfusion can be used for production of large scale constructs by maintaining cell viability [211]. In a similar study, goat bone marrow stromal cells were seeded to calcium phosphate scaffolds which have 10 cc volume and incubated for 19 days in a perfusion bioreactor. They reported that the scaffolds were covered with a homogenous cell layer with a dense ECM and these scaffolds stimulated bone formation after 6 weeks when implanted in mice [212]. Another research reported that a perfusion bioreactor that was used for maintaining a fluid flow through decellularized bone scaffolds of 0.5 cm with human adipose tissue derived stem cells stimulated the production of bone matrix components such as collagen, BSP and osteopontin after 5 weeks incubation [213].

In this research we used a custom made vibration/perfusion bioreactor that was used previously to cultivate trabecular bone explants (Figure 4.1) for the incubation of mouse bone marrow stem cells that were seeded on filter paper constructs to study the combinatorial effect of two mechanical forces on the osteogenic differentiation. The importance of this research is the use of a novel, low-cost, reproducible and commercially available scaffold material in a complex bioreactor system with the possibility of studying different mechanical loads at the same time.

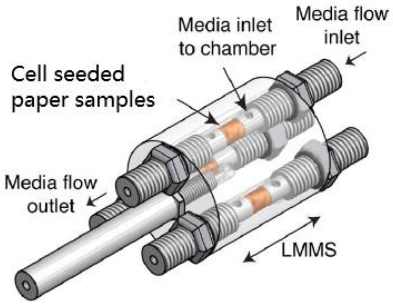

Figure 4.1. Schematic representation of custom made vibration/perfusion bioreactor [214].

4.2. Methods

4.2.1. Experimental Design for the Perfusion/Vibration Bioreactor

The perfusion/vibration bioreactor experiments were performed at Biomechanics and Mechanobiology Laboratory in National University of Ireland, Galway (NUIG), under supervision of Prof. Dr. Laoise McNamara.

The bioreactor consists of following parts (Figure 4.2):

- A voice coil linear actuator (an adapted Enduratec bioreactor, Bose Limited, Gillingham, UK) for vibration
- Polyether ether ketone (PEEK-1000) platens
- Custom made polyetherimide (PEI-1000) chamber (Riteway Engineering Limited, Galway)
- HelixMark® standard silicone tubing (inner diameter 1.58 mm, outer diameter 3.18 mm, wall thickness 0.80 mm) (Freudenberg Medical, Germany)
- Ismatec® 2 stop peristaltic pump tubing (inner diameter 1.52 mm) (Cole-Parmer, Germany)
- Peristaltic pump (Harvard Peristaltic Pump P70, USA)
- Media bottles
- Luer fittings
- Surge protector
- Linear variable differential transformer (LVDT)

D1 ORL UVA cells that were infected with PMIG retrovirus to insert GFP gene were seeded on 16 Whatman paper scaffolds without collagen at 10^5 cells in 20 μL/paper density for bioreactor studies. Cells were seeded on paper constructs in 12 well plates and the next day after seeding, for osteogenic induction growth media were replaced with osteogenic media for 8 of the samples. Five days after seeding 4 samples in normal growth media and 4 samples in osteogenic induction media were transferred into the bioreactor chamber. For comparison, paper scaffolds with the same cell seeding density were

incubated both in growth and osteogenic media for the same duration under static conditions.

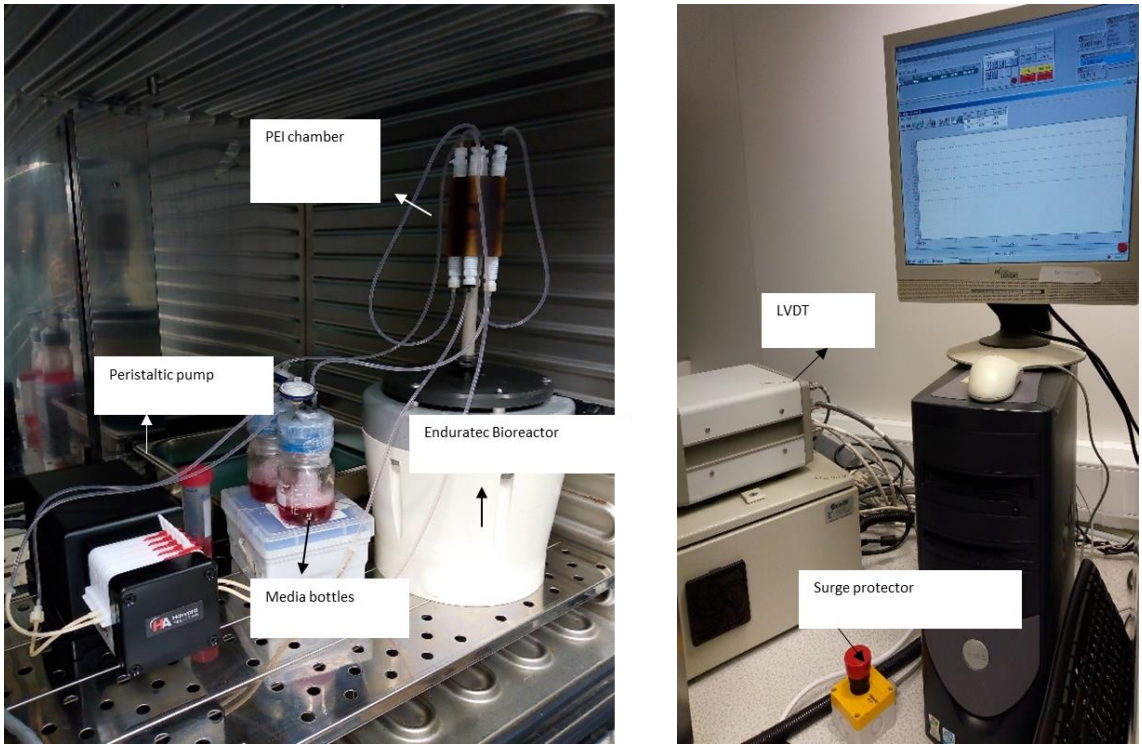

Figure 4.2. Parts of perfusion/vibration bioreactor and the controlling unit

Before assembling the bioreactor all the platens, chambers, tubings, media bottles and luer fittings were washed with 1% virkon, 70% ethanol and distilled water, respectively. PTFE tape was wrapped around the screws. Tubings were connected to media bottles. Two of the sample holes on the chamber were serially connected to each other with tubings; so that they were fed from the same medium bottle (Figure 4.3a). Each bottle and tubings were prepared as a closed loop system prior to autoclaving. All of the parts were then autoclaved. After sterilization with the autoclave, all parts were subjected to UV light in the laminar flow hood for 1h.

The bioreactor was assembled in the laminar flow hood. First the bottom screws were placed into the chamber holes. Then cell seeded samples were inserted into the holes in chamber (Figure 4.3c). Two samples were inserted into each hole. Afterwards top screws were placed and all of the tubings were connected. Then 40 mL media were put

into the bottles. Syringe filters were placed on top of the bottles (Figure 4.3b). With a syringe 20 mL medium from each bottle was taken and pumped through the tubings to check the connections.

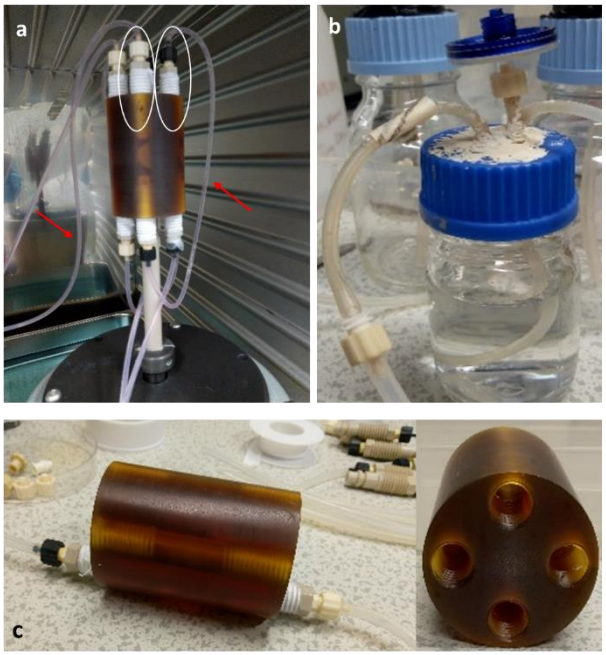

Figure 4.3. a) Serial connection of sample holes. White circles show two successive holes that are connected to each other, and red arrows show the connector tubing. b) Media bottles. Medium is perfused through the system and returns back to the same bottle. c) The sample chamber and the screws. The chamber consists of 4 sample holes.

The shelves of the incubator were removed and the Enduratec bioreactor and the peristaltic pump were sprayed with 70 % ethanol and inserted into the incubator. Then all of the media bottles and the chamber were carried into the incubator as well. The chamber was placed on top of the threaded bar on Enduratec bioreactor for further vibration application. The tubings were connected to the peristaltic pump. Media were constantly and continuously perfused through the system at a flow rate of 0.9 mL/min.

Vibration was applied to the system at 0.1g magnitude, 90 Hz frequency and 324000 cycles (1h/day) for 5 days/week. Media were changed twice a week by removing

half of the media from the bottles and adding same amount of fresh media. Samples were incubated in the bioreactor for 14 days.

4.2.2. Total RNA Isolation from Bioreactor Samples and RT-PCR

For total RNA isolation from cells on Whatman paper scaffolds RNeasy Mini Kit (Qiagen, The Netherlands) was used. Paper samples from the bioreactor and static culture were washed with PBS once, and transferred to wide bottom Eppendorf tubes. Lysis buffer was prepared by adding 1% (v/v) β-mercaptoethanol and 500 µL lysis buffer was added to each sample.

Samples were put on ice and homogenized with a mechanical homogenizer at the highest power for 1 min with an interval after 30 s. 500 µL 70% molecular grade ethanol was added to each sample. Lysate was passed 10 times through a blunt-end 20-gauge needle fitted to an RNase-free syringe for each sample and RNA isolation was done according to the manufacturer's instructions. Isolated RNAs were kept at -80 ^{o}C.

Reverse transcription was done by QuantiNova Reverse Transcription Kit (Qiagen, The Netherlands), according to the manufacturer's instructions. cDNAs were kept at -20 ^{o}C. For reverse transcription reaction 500 ng RNA template was used. For RT-PCR 50 ng cDNA was used with the primers listed below. The primer specificity was tested with Primer-BLAST tool. PCR was conducted at 90 ^{o}C for 5s, specific annealing temperatures for each primer pair for 10s and 72 ^{o}C for 20s for 40 cycles. The annealing temperatures are given in Table 4.1.

Quantitative RT-PCR was done by StepOne Plus thermal cycler (Applied Biosystems, USA) with QuantiNova SYBR Green PCR Kit (Qiagen, The Netherlands). The relative expression levels of the target genes were calculated by threshold cycle (ΔΔCt) method with GAPDH as reference gene and reported as $2^{-\Delta\Delta Ct}$, as relative folding changes to samples under static and growth medium conditions.

Table 4.1. Sequences of forward and reverse primers used for RT-qPCR reactions.

Gene	Forward primer	Reverse primer	Annealing Temperature (ºC)
ALP	ATCTTTGGTCTGGCTCCCATG	TTTCCCGTTCACCGTCCA	57.2
OPN	AGCAAGAAACTCTTCCAAGCAA	GTGAGATTCGTCAGATTCATCCG	55.2
Runx 2	CGCCCCTCCCTGAACTCT	TGCCTGCCTGGGATCTGTA	60
GAPDH	AGGTCGGTGTGAACGGATTT	GTGATGGGCTTCCCGTTGAT	58

4.2.3. FTIR Analyses for Detection of Mineralization

The composition of organic and inorganic components of ECM was detected by Fourier-transform infrared spectroscopy (FTIR) (Perkin Elmer Spectrum Version 10.4.3, USA). The samples were fixed with 4% PFA and washed with distilled water several times. Then they were dried in the vacuum oven to remove the water. FTIR spectrometer with ATR attachment was used and the spectra was recorded in the range of 4000-400 cm^{-1} wavenumber with 4 cm^{-1} resolution. Analyses were done by using Spectragryph 1.2 spectroscopy software.

4.2.4. Detection of Scaffold Mineralization with Micro Computed Tomography (µCT)

Micro CT allows to take stacked images from the inner side of the objects by using X-rays and reconstructs 3D views. It is a very useful tool for detection of *in vivo* [215, 216], *ex vivo* [217] and *in vitro* [218] bone formation and mineralization. The mineral formation was assessed using a micro computed tomography device (Scanco Medical µCT 100). A voxel size of 3.3 µm and 70 kVp X-ray source at 114 µA were used. Before

μCT scanning, the samples were fixed with 4% PFA. Fixation of the specimens in the μCT sample holder was achieved by placing a multi-layer sponge in the 14 mm holder, and fixing two specimens separated in between. The sample holder was then filled with 1X PBS, in which the scans were performed. Bone volume (BV, mm^3), total volume (TV, mm^3) and bone mineral density distribution (BMDD, mg HA/cm^3) were determined from the scans and histograms of samples were represented by using mg HA/cm^3 and % of TV data obtained from μCT scans. For heterogeneity of the samples, peak mineralization and mean mineralization values were calculated and full width at half maximum (FWHM) was measured [219].

4.2.5. Immunostaining for Osteogenic Differentiation Markers

Immunostaining for osteoblastic proteins bone sialoprotein (BSP) and osteopontin (OPN) was done to detect the differentiation of bone marrow MSCs upon osteogenic induction and mechanical stimulation. Samples from static culture and bioreactor were washed with PBS at day 19 (14 days in bioreactor with 5 days in tissue culture plate under static conditions prior to transferring the samples to the bioreactor) and fixed with 4% paraformaldehyde (PFA) for 15 min at room temperature and washed with PBS twice again. Permeabilization solution was prepared by adding 20 μL Triton-X to 10 mL distilled water and 500 μL of this solution was added on each sample and incubated for 5 min. Samples were washed with PBS once more and 1%BSA was added on each sample to prevent non-specific binding and incubated for 1h at room temperature. One sample from each group (St-g, St-o, Br-g and Br-o) were cut into two pieces and half of them were stained for BSP and DAPI (for the nucleus), and the remaining were stained for OPN and DAPI. BSP and OPN primary antibodies were produced in mice (Santa Cruz Biotechnology Inc, USA). BSP and OPN antibodies were diluted 1:100 in 1% BSA and samples were incubated with the primary antibodies at 4 ^oC overnight. Then primary antibodies were removed and the samples were washed with 1%BSA 3 times by incubating each wash for 10 min at room temperature. For BSP and OPN stainings, goat anti-mouse secondary antibody that was labelled with 549 nm Alexa Fluor fluorescent dye was used. The secondary antibody was diluted at a ratio of 1:200 in 1X PBS and the

samples were incubated with the secondary antibody in dark for 1.5 h at room temperature. After incubation samples were washed with PBS twice. For DAPI staining, 20 mg/mL DAPI stock solution was diluted to 200 ng/mL and the samples were incubated with this solution for 5 min at room temperature. Samples were washed with PBS twice afterwards and kept in PBS at 4 ^{o}C in dark until observation with the fluorescent microscope (Olympus IX83).

4.2.6. Statistical Analyses

Gene expression studies were repeated in triplicates, stainings and μCT scans were repeated in duplicates. All results are displayed as the mean ± standard deviation. Statistical analyses for comparison between the groups were performed using ANOVA. In order to detect significant difference between groups for osteoblastic gene expression levels ANOVA followed by S-N-K post hoc test was done. Levels of significance were reported for 5%.

4.3. Results

4.3.1. The Effect of Mechanical Stress on the Differentiation of MSCs at Gene Expression Level

The simultaneous effect of two mechanical forces, vibration and fluid shear, on the differentiation of mouse bone marrow MSCs on paper scaffolds was determined at gene expression level by quantitative reverse transcriptase polymerase chain reaction (RT-qPCR). In order to determine the effect of the mechanical forces on the osteogenic differentiation, the change in mRNA expression levels of osteoblastic marker genes ALP, Runx 2 and OPN were assessed by comparison to the mRNA expression level of the housekeeping gene GAPDH. For the assessment of mRNA expression levels, four experimental groups were tested; static growth (St-g), static osteogenic (St-o), bioreactor

growth (Br-g) and bioreactor osteogenic (Br-o). The mRNA expression levels of all osteogenic markers for each group were normalized to the expression of the related gene of static growth group.

It was observed that Runx 2 and ALP expression profiles were similar for each group, but OPN expression had a different trend (Figure 4.4).

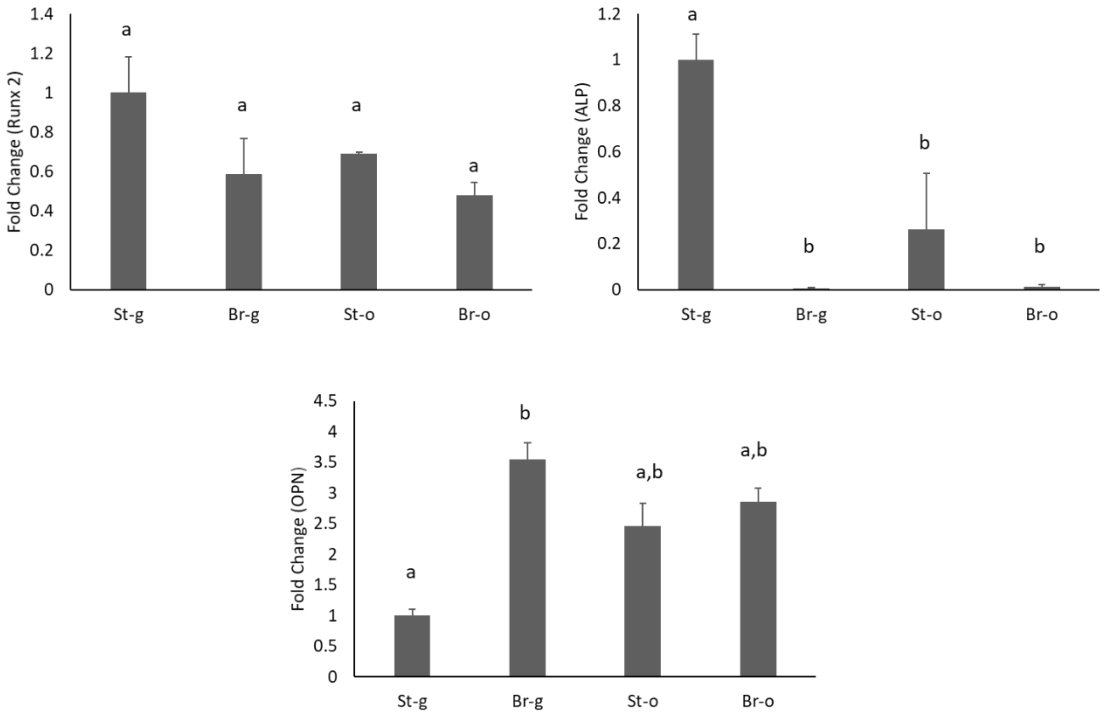

Figure 4.4. Gene expression levels of D1 ORL UVA stem cells that were either incubated in the bioreactor with regular growth medium or osteogenic medium (Br-g and Br-o), or under static culture conditions (St-g and St-o) after 19 days. OPN expression was found to be higher whereas Runx 2 and ALP expressions were lower for Br-o and Br-g compared to St-g group. a, b,: differences in gene expression levels between groups calculated by ANOVA followed by S-N-K post hoc test.

The expressions of Runx2 and ALP were lower, whereas OPN expression was higher for Br-o and Br-g when compared to St-g group. The Runx 2 and ALP expression levels of the samples incubated in osteogenic medium were less than their counterparts incubated in regular growth medium for both static and bioreactor samples, but OPN expression increased upon treatment with osteogenic medium.

4.3.2. Micro Computed Tomography (μCT) Analyses for Detection of Mineralization

According to data obtained from μCT scans, the highest degree of mineralization was observed for Br-o sample (Figure 4.5). Corresponding BV values are reported in Table 4.2. The quantification depending on BMDD parameters were calculated after the histograms of the samples were drawn (Figure 4.6). Only the histograms of St-o and Br-o samples displayed a Gaussian distribution, so BMDD parameters were calculated only for those samples (Table 4.3).

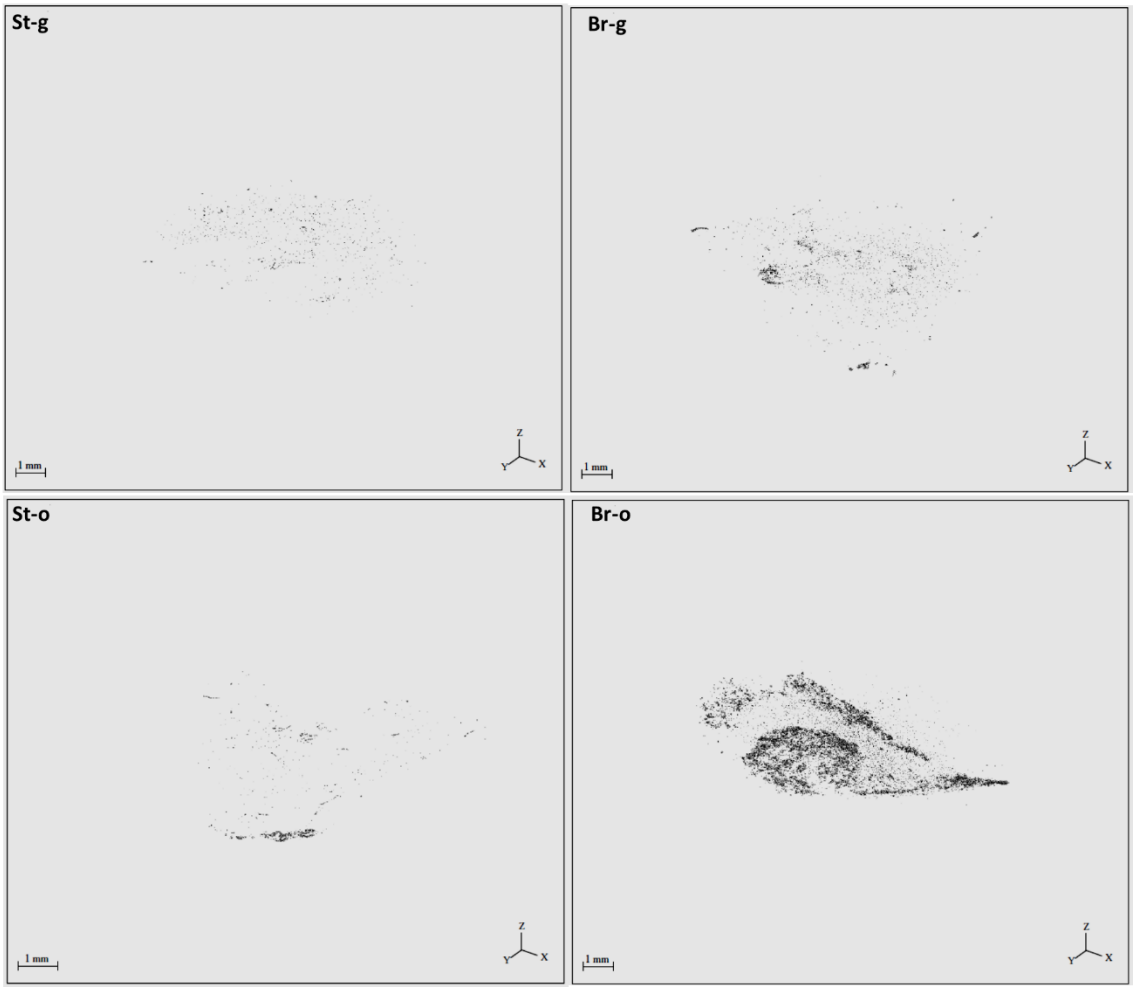

Figure 4.5. μCT images of the scanned paper samples. St-g: Static growth, Br-g: Bioreactor growth, St-o: Static osteogenic, Br-o: Bioreactor osteogenic

Table 4.2. Bone volume (BV) values of the samples obtained by μCT scans.

Sample	Bone Volume (BV) mm^3
St-g	0.0021
Br-g	0.0080
St-o	0.0026
Br-o	0.0988

Table 4.3. BMDD parameters calculated from the histograms of the samples

Sample	Mpeak	Mmean	FWHM
St-o	2.282	240.75	19.05
Br-o	1.942	277.75	140.34

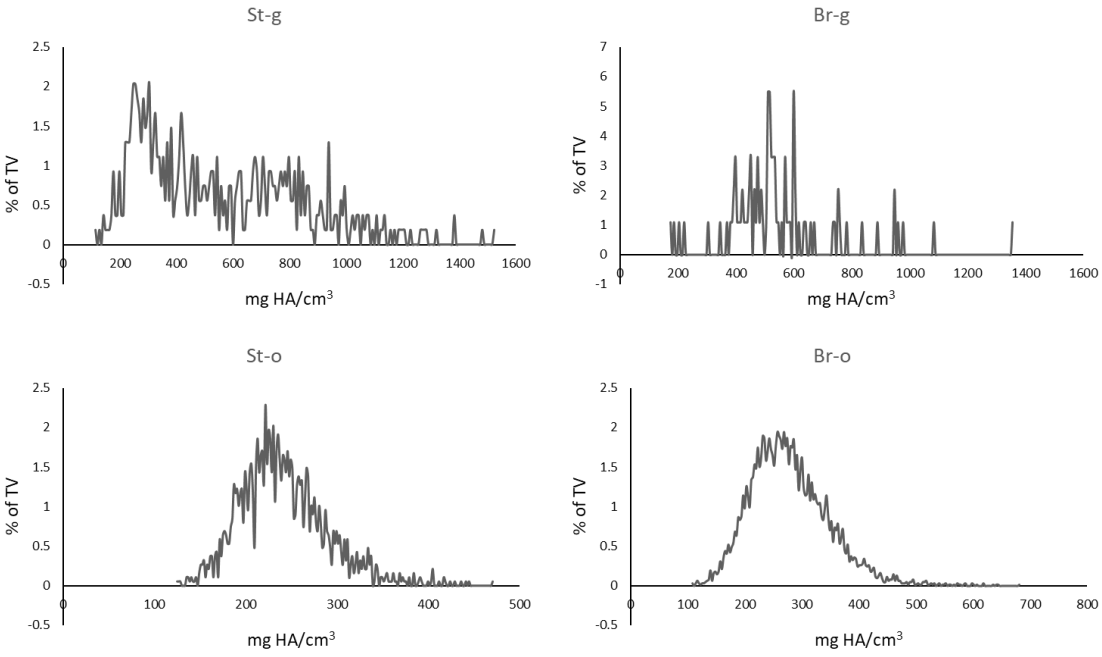

Figure 4.6. Histograms of each sample. St-g: Static growth, Br-g: Bioreactor growth, St-o: Static osteogenic, Br-o: Bioreactor osteogenic

4.3.3. Immunostaining for Osteogenic Differentiation Markers

D1 ORL UVA cells that were seeded on paper scaffolds and incubated in growth or osteogenic media under static conditions or in vibration/perfusion bioreactor were stained with antibodies against BSP 2 and OPN proteins to detect osteogenic differentiation at day 19 (14 days in bioreactor with 5 days static incubation priorly). It was observed that OPN expression was higher for the samples incubated in the bioreactor (Figure 4.7). The bioreactor growth group expressed more OPN than static osteogenic group, which was also consistence with the gene expression results. This shows that mechanical forces, fluid shear and vibration, acting on cells in the bioreactor triggered the expression of osteoblast specific genes even in the absence of chemical inducers.

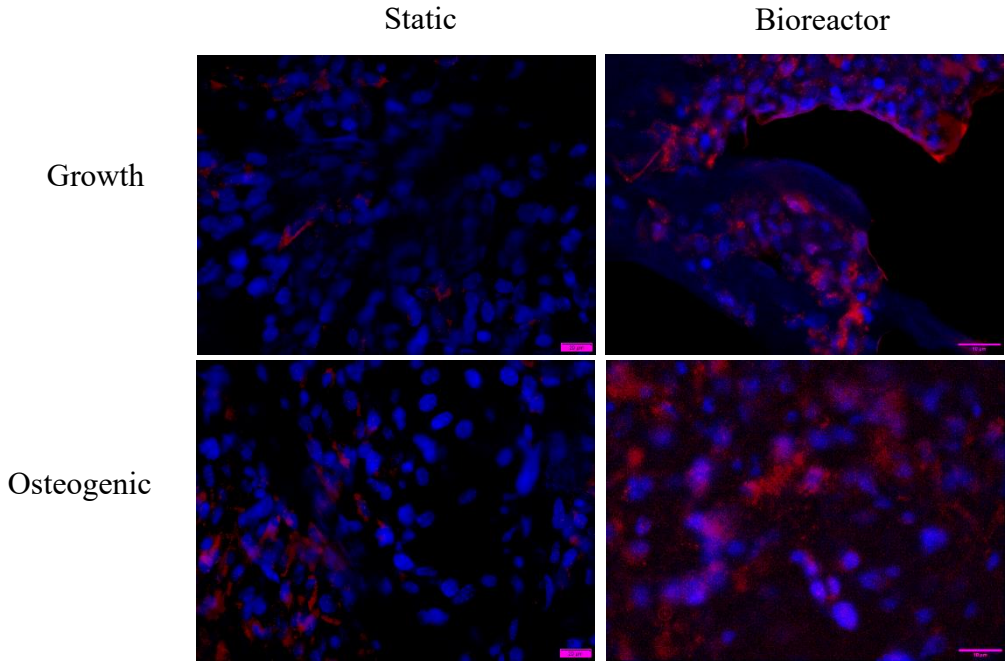

Figure 4.7. Expression of bone specific protein osteopontin (OPN) was detected by immunocytochemical staining. Samples were stained for OPN (red) on day 19 (14 days in vibration/perfusion bioreactor and 5 days in tissue culture plate before transferring into bioreactor, or 19 days in tissue culture plate for static condition) and counterstained with DAPI (blue) for nucleus. More OPN signal was detected for the samples incubated in the bioreactor compared to static cultures. Scale bar represents 10 μm.

According to another immunostaining result for a different osteogenic marker BSP 2, it was observed that more signal was detected for the samples in osteogenic induction group for both static cultures and the samples incubated in the bioreactor (Figure 4.8). BSP 2 was not observed in static culture for the growth group. However, BSP 2 in a small quantity was observed for bioreactor growth group, which can be concluded as like for OPN, mechanical forces caused an increase in the production of BSP 2.

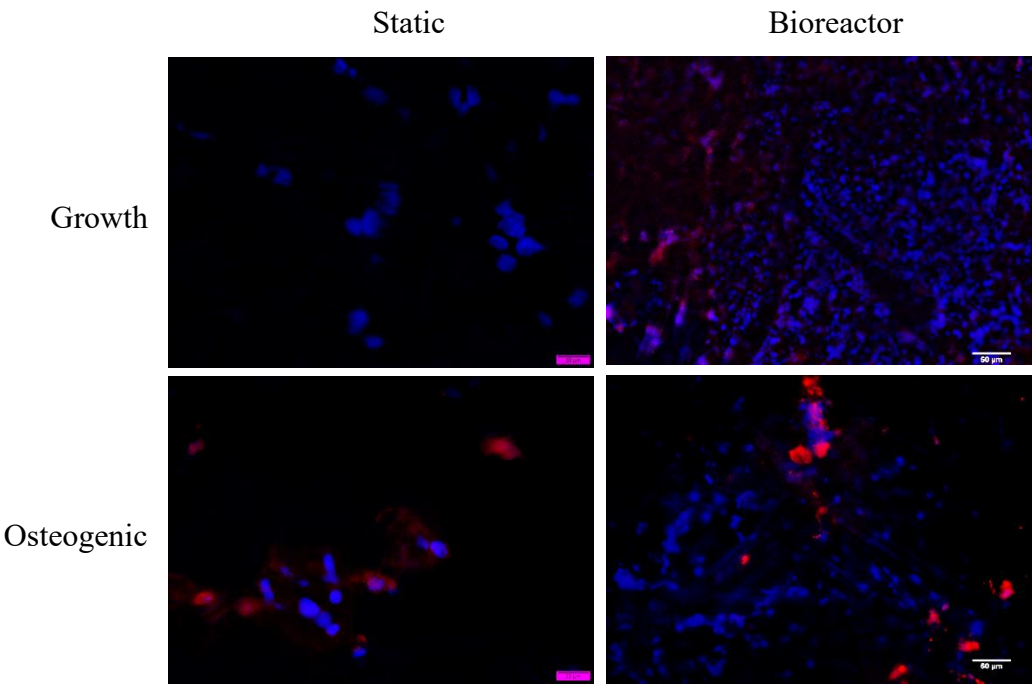

Figure 4.8. Production of bone specific protein bone sialoprotein 2 (BSP 2) was detected by immunocytochemical staining. Samples were stained for BSP 2 (red) on day 19 (14 days in vibration/perfusion bioreactor and 5 days in tissue culture plate before transferring into bioreactor, or 19 days in tissue culture plate for static condition) and counterstained with DAPI (blue) for nucleus. The signal for BSP 2 was found higher in osteogenic induction group, whether the samples were incubated in the bioreactor or under static culture conditions. Scale bar represents 20 μm for the left column, 50 μm for the right column.

4.3.4. Alizarin Red S Staining for Detection of Mineralization

The samples that were incubated in the bioreactor and under static culture conditions in tissue culture plates were stained with Alizarin red S dye to detect mineralization. Red color on Br-o and St-o groups indicates that calcium deposition started for these samples (Figure 4.9). However, St-g and Br-g groups were not stained. It was observed that Br-o sample stained more intensely suggesting that mechanical loading when used in combination with chemical inducers triggered osteogenic differentiation and ECM mineralization.

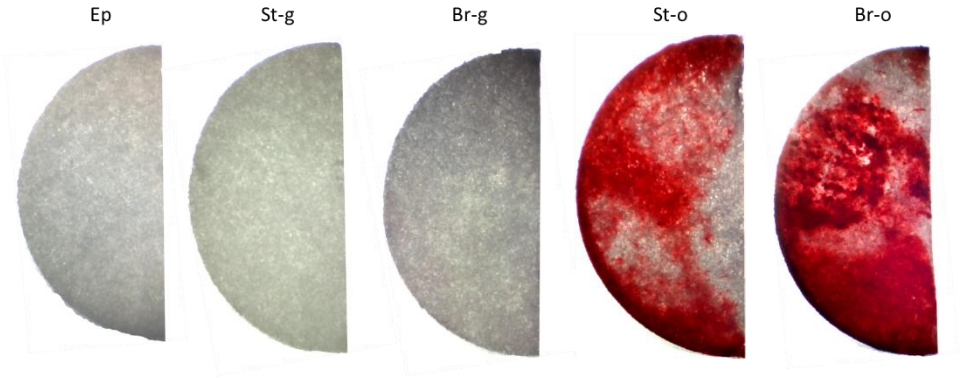

Figure 4.9. Stereomicrographs of Alizarin red S stained samples. Samples incubated in standard growth medium under static conditions (St-g) and in the bioreactor (Br-g) were not stained, but the ones incubated in osteogenic induction medium (Br-o) and (St-o) stained positively for calcium deposition.

4.3.5. FTIR Analyses for Detection of Mineralization

It was observed that all of the sample groups except Br-o had very similar spectra. However, Br-o group had peaks at 1237, 1453, 1548 and 1634 cm^{-1} wavelengths which were not observed in other samples. The peaks at 1237, 1548 and 1634 cm^{-1} originate from amide III band (1200-1300 cm^{-1}) [199], amide II of collagen moiety [199] and amide I β sheets [181], respectively. The peak at 1453 cm^{-1}, on the other hand, arises from carbonate substitutions in the HAp crystal lattice [199]. According to our results, the

bands that originate from the organic component of bone, collagen, was clearly visible for Br-o sample with a slight mineralization (Figure 4.10).

.

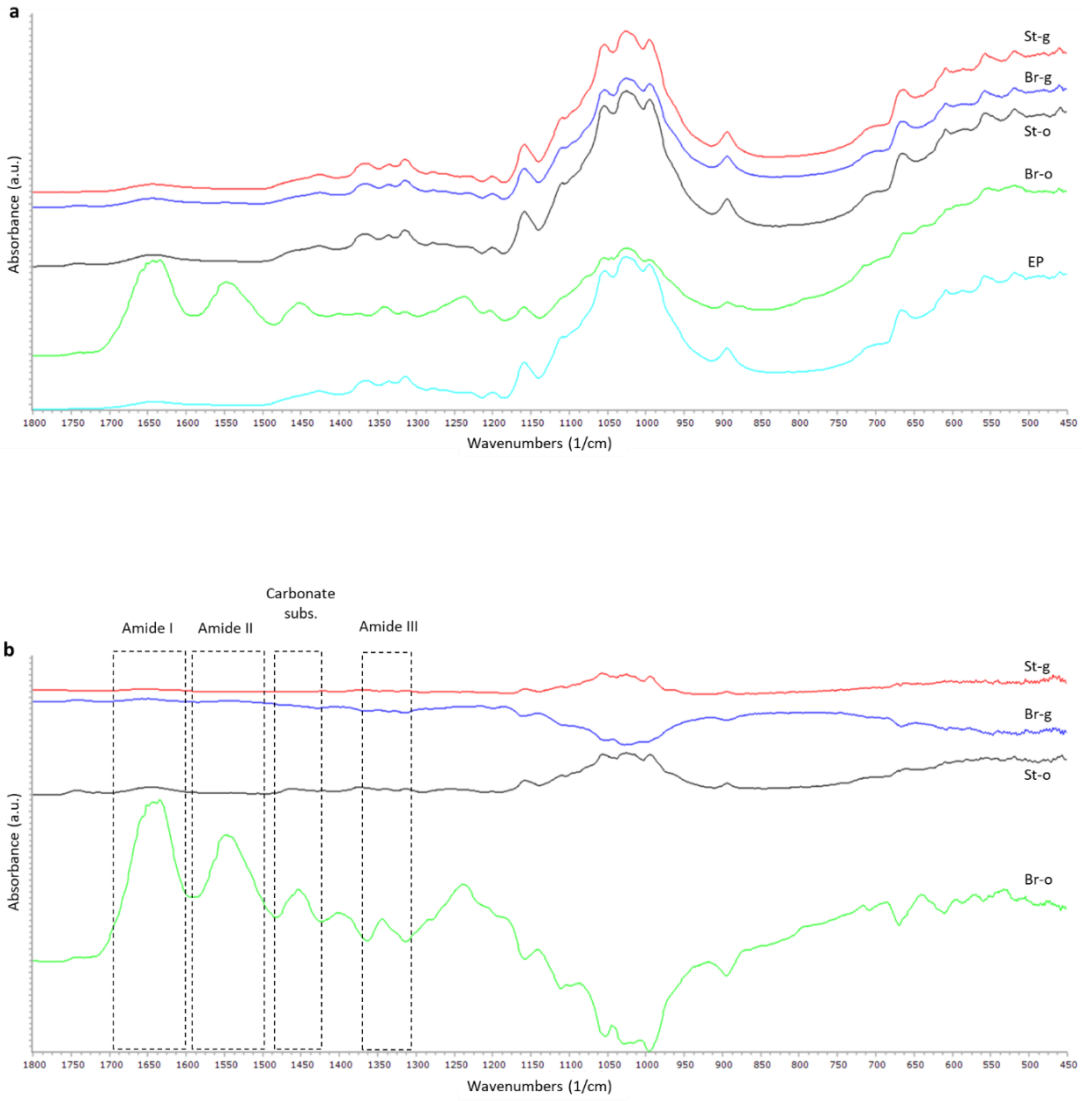

Figure 4.10. FTIR spectra of the samples between 450 and 1800 cm-1 wavenumbers. All of the samples had the same spectra with empty paper (Ep), except Br-o. a) Spectra of all samples demonstrating the distinct peaks of Br-o sample. b) Spectra of all samples after the spectrum of empty paper was subtracted.

4.4. Discussion

Osteoblast culture systems have their unique differentiation profiles [220], so the expression pattern of genes during each stage of differentiation might vary depending on cell type. Runx2 and ALP are among the most important early stage markers of osteogenic differentiation [221]. In the early phase of osteoblastic differentiation of progenitor cells or in multipotent stem cells, Runx2 expression is required for triggering the expression of mineralization related genes such as OCN, OPN and BSP in the later stages [222, 223]. During the differentiation of multipotent stem cells into osteoblasts, Runx2 expression decreases in time and this decrease is required for the maintenance of osteoblast function [224]. In this research, mRNA expression levels were measured at 19^{th} day of incubation, which corresponds to middle or late stage of osteogenic differentiation. According to our results the expression level of Runx2 gene was highest for St-g group and upon osteogenic induction a decrease in this level was observed. Previous reports show that Runx2 gene expression might be upregulated independently from osteoblastic differentiation [225], as the increase in mRNA level of St-g group in our study. It was also reported that Runx 2 plays a role in the early response of osteoblastic cells to mechanical induction [226].

ALP expression starts to decline after an initial peak [227] in a similar way to Runx2 expression [228]. However, there are two peaks of OPN expression at different time points during osteogenic differentiation; once at cell proliferation stage and again in later stages [221]. The expression of OPN gene also depends on the mechanical signals received by the cells [229, 230] and this results with the upregulation of OPN upon mechanical stimulation [231].

Our RT-PCR results might suggest that the decreased levels of Runx2 and ALP expressions together with an induction in OPN expression is the result of differentiation of D1 ORL UVA MSCs into immature osteoblasts upon osteogenic induction. In addition to that, the lowest expression levels of Runx2 and ALP genes, with the highest OPN expression that was observed for the bioreactor group suggest that a combination of mechanical vibrations and fluid shear forces induced the osteoblastic differentiation of cells most.

For the detection of osteogenic differentiation of bone morrow stem cells used in this research, in addition to gene expression analysis immunocytochemical stainings were

also performed. BSP 2 and OPN are non-collagenous extracellular matrix proteins which belong to SIBLING (small integrin binding ligand *N*-glycosylated) family and by interacting with hydroxyapatite (HAP) they take part in the mineralization of bone [232]. BSP has an important role in the nucleation of HAP in the bone matrix. It binds to HAP by polyglutamic acid residues and to cell surface integrins with arginine-glycine-aspartate (RGD) sequence [233, 234]. Similar to OPN, BSP is also an osteoblastic marker gene that is commonly used for studying MSC differentiation and its expression increases upon mechanical stimulation [235]. Previous studies about the localization of these proteins showed that BSP is found in mineralized regions of bone, whereas OPN accumulation was observed in both mineralized and non-mineralized tissue and stromal cells [236]. For the determination of mineral formation ARS staining was done and our results were similar to the previous reports. OPN expression was observed for non-mineralized samples that were incubated in the bioreactor without chemical induction. However, expression of BSP was only detected for the samples that were stained positively for calcium deposition. In a very recent research, it was reported that the *ex vivo* stretching of rat calvarial bones altered the osteoblastic gene expression pattern depending on the mechanical loading [237]. The expression sequence of non-collagenous proteins was BSP, OPN and OCN from the earliest time point to the later stages, respectively; whereas for some osteoblasts OCN expression was prior then OPN expression upon mechanical induction. Briefly, mechanical stimulation and the magnitude of the load applied might alter the gene expression patterns during osteoblastic differentiation process.

Detection of mineralization is an important tool for the determination of osteogenic differentiation and it occurs under several defined conditions. A matrix is required for the specific orientation of ions that will take part in the mineral crystal formation under physiological conditions [238]. When anchored to the matrix BSP and OPN are involved in the crystal nucleation [238]. The mineralization of bone is still under investigation and different hypothesis exist about the formation and maturation of the inorganic phase. According to matrix vesicle formation hypothesis, for the initiation of mineralization, calcium and inorganic phosphate nucleate within the matrix vesicles first and then they are transported to ECM. In the following steps this process continues with the formation of HAP crystals and association of the inorganic phase with collagen fibers [239]. Mechanical loads are also very important for the differentiation of stem cells into osteoblasts. In a previous research, it was reported that higher matrix protein production

and calcium release levels were observed for PLLA scaffolds which were carrying Bay K8644, a voltage operated calcium channel agonist, and mechanically induced via a compression/perfusion bioreactor compared to static controls [240]. According to our results, for the initiation of calcium deposition application of mechanical forces via the bioreactor was not sufficient, but upon loading with chemical induction the highest mineral formation was observed. ARS staining results showed that induction with osteogenic medium under static conditions also resulted with the formation of the mineralized matrix. However, for the samples that were not subjected to mechanical loading the FTIR peaks that arise from the inorganic component of bone was not observed. This might be due to formation of immature mineral crystals by the cells. ARS dye binds calcium ions and forms a complex. St-o samples were stained with ARS, but no peak was observed in the phosphate region of the FTIR data for those samples. The mineral phase of the St-o sample might not be mature enough for detection with FTIR; calcium accumulation might have started but HAP formation has not been completed yet. Briefly, this can be explained with the faster differentiation of MSCs upon application of mechanical loading. Incubation of the samples in regular growth medium without any osteogenic supplements but with mechanical loading did not result with mineral formation which was demonstrated both with ARS staining and FTIR analysis, suggesting that mechanical loading without chemical induction was also not enough to stimulate crystal formation.

CHAPTER 5

CONCLUSION

This research thesis can be mainly divided into two parts: The first part was designed to understand the cytotoxic effects of two potential phenolic compounds for prevention of carcinogenesis and more importantly the effect of culture conditions, monolayer or 3D, on the cytotoxic response of mesenchymal stem cells (MSCs) upon administration of these compounds. The second part was designed for understanding the effects of single and simultaneous mechanical forces on the osteogenic differentiation of MSCs. The entire research concerns about the improvement of cell and scaffold systems for bone tissue engineering applications.

As indicated in Chapter 2, phenolic diterpenes carnosol and carnosic acid had antimicrobial properties on Gram positive bacteria, but the concentrations to cease the bacterial activity was cytotoxic when bone derived cells were incubated in monolayer cultures. However, when the cells were subjected to these phenols in 3D culture systems, they were able to tolerate the cytotoxicity better, which shows the importance of mimicking the real 3D tissue organizations through tissue engineering principles.

In Chapter 3, single type of mechanical force was applied as vibration and its effect on osteogenic differentiation was determined at molecular level as gene expression and mineralization. Although the application of mechanical forces induced a faster osteoblastic differentiation, without addition of osteogenic supplements into the culture media these forces were not sufficient to trigger osteogenesis. In this research, single acceleration, frequency and duration value was tested depending on the results of previous researches in the literature. For a further prospect, a range of different values might be tested to optimize the osteoblastic differentiation and maturation of MSCs.

In order to approach more reliable *in vitro* conditions, it is very crucial to simulate *in vivo* parameters as close as possible. Our bones are subjected to more than one type of mechanical force in real life. For this reason, in Chapter 4, the effects of simultaneously applied fluid shear and vibration forces on osteogenesis were studied. However, this part of the research was conducted in a limited duration, since it was a short term research

project, the incubation time of the constructs could not exceed 14 days in the bioreactor. Longer incubation duration might better mimic the *in vivo* conditions. Besides, as a further prospect, paper scaffolds might be constructed from multiple layers to mimic the 3D structure of bone more closely and subjected to mechanical forces.

The entire research demonstrated how important the environmental stimuli for osteogenic differentiation and how important to use a 3D system rather than monolayer culture in terms of cellular behavior. Additionally, it was also demonstrated that filter paper is a good candidate for construction of bone tissue engineering scaffolds even without any further modifications.

For a future projection, the filter paper scaffold systems in this research can be used for studying the effects of vibrational forces on the differentiation of stem cells on 3D scaffold systems by preparing a mathematical model. Varying acceleration and frequency values can be essayed experimentally to understand whether the mathematical model fits real conditions or not. Additionally, paper based scaffolds can be implanted in vivo and local vibrations or whole body vibration can be applied externally for the stimulation of osteogenesis. For the bioreactor studies, shear forces acting on the samples can be modeled and calculated for varying flow rates of the culture medium and experimentally tested when the shear force is applied vertically or horizontally to the samples.

CHAPTER 6

REFERENCES

[1] S.M. Ott, Cortical or Trabecular Bone: What's the Difference?, American Journal of Nephrology 47(6) (2018) 373-375.

[2] L.M. Biga, S. Dawson, A. Harwell, R. Hopkins, J. Kaufmann, M. LeMaster, P. Matern, K. Morrison-Graham, D. Quick, J. Runyeon, Bone Classification, in: L.M. Biga, S. Dawson, A. Harwell, R. Hopkins, J. Kaufmann, M. LeMaster, P. Matern, K. Morrison-Graham, D. Quick, J. Runyeon (Eds.), Anatomy & Physiology, Open Oregon State, Oregon State University2019.

[3] A. Hoppe, Bioactive Glass Derived Scaffolds with Therapeutic Ion Releasing Capability for Bone Tissue Engineering Dreidimensionale bioaktive Glasgerüste mit therapeutischer Doktor-Ingenieur, 2014.

[4] J.A. Buckwalter, R.R. Cooper, Bone structure and function, Instructional course lectures 36 (1987) 27-48.

[5] A.M. Parfitt, Misconceptions (2): turnover is always higher in cancellous than in cortical bone, Bone 30(6) (2002) 807-9.

[6] J.R. Dwek, The periosteum: what is it, where is it, and what mimics it in its absence?, Skeletal radiology 39(4) (2010) 319-323.

[7] S.W. and, H.D. Wagner, THE MATERIAL BONE: Structure-Mechanical Function Relations, Annual Review of Materials Science 28(1) (1998) 271-298.

[8] J.Y. Rho, L. Kuhn-Spearing, P. Zioupos, Mechanical properties and the hierarchical structure of bone, Medical engineering & physics 20(2) (1998) 92-102.

[9] D.B. Burr, O. Akkus, Chapter 1 - Bone Morphology and Organization, in: D.B. Burr, M.R. Allen (Eds.), Basic and Applied Bone Biology, Academic Press, San Diego, 2014, pp. 3-25.

[10] N. Rosenberg, O. Rosenberg, M. Soudry, Osteoblasts in bone physiology-mini review, Rambam Maimonides medical journal 3(2) (2012) e0013-e0013.

[11] H. Nakamura, Morphology, Function, and Differentiation of Bone Cells, Journal of Hard Tissue Biology 16(1) (2007) 15-22.

[12] H. Tenenbaum, J. Heersche, Differentiation of osteoblasts and formation of mineralized bone In Vitro Calcif, 1982.

[13] I. Matic, B.G. Matthews, X. Wang, N.A. Dyment, D.L. Worthley, D.W. Rowe, D. Grcevic, I. Kalajzic, Quiescent Bone Lining Cells Are a Major Source of Osteoblasts During Adulthood, Stem cells (Dayton, Ohio) 34(12) (2016) 2930-2942.

[14] S.C. Miller, L. de Saint-Georges, B.M. Bowman, W.S. Jee, Bone lining cells: structure and function, Scanning microscopy 3(3) (1989) 953-60; discussion 960-1.

[15] L.F. Bonewald, The amazing osteocyte, J Bone Miner Res 26(2) (2011) 229-238.

[16] M.B. Schaffler, W.-Y. Cheung, R. Majeska, O. Kennedy, Osteocytes: master orchestrators of bone, Calcified tissue international 94(1) (2014) 5-24.

[17] E.M. Aarden, E.H. Burger, P.J. Nijweide, Function of osteocytes in bone, Journal of cellular biochemistry 55(3) (1994) 287-99.

[18] F. Arai, T. Miyamoto, O. Ohneda, T. Inada, T. Sudo, K. Brasel, T. Miyata, D.M. Anderson, T. Suda, Commitment and differentiation of osteoclast precursor cells by the sequential expression of c-Fms and receptor activator of nuclear factor kappaB (RANK) receptors, The Journal of experimental medicine 190(12) (1999) 1741-1754.

[19] B.F. Boyce, Z. Yao, L. Xing, Osteoclasts have multiple roles in bone in addition to bone resorption, Critical reviews in eukaryotic gene expression 19(3) (2009) 171-80.

[20] W.J. Boyle, W.S. Simonet, D.L. Lacey, Osteoclast differentiation and activation, Nature 423(6937) (2003) 337-342.

[21] M.R. Allen, D.B. Burr, Chapter 4 - Bone Modeling and Remodeling, in: D.B. Burr, M.R. Allen (Eds.), Basic and Applied Bone Biology, Academic Press, San Diego, 2014, pp. 75-90.

[22] H.M. Frost, Skeletal structural adaptations to mechanical usage (SATMU): 2. Redefining Wolff's law: the remodeling problem, The Anatomical record 226(4) (1990) 414-22.

[23] J.M. Delaisse, T.L. Andersen, M.T. Engsig, K. Henriksen, T. Troen, L. Blavier, Matrix metalloproteinases (MMP) and cathepsin K contribute differently to osteoclastic activities, Microscopy research and technique 61(6) (2003) 504-13.

[24] J.S. Kenkre, J.H.D. Bassett, The bone remodelling cycle, Annals of Clinical Biochemistry 55(3) (2018) 308-327.

[25] S. Aoki, K. Shteyn, R. Marien, Bio render, (2019).

[26] A. Cacchioli, B. Spaggiari, F. Ravanetti, F.M. Martini, P. Borghetti, C. Gabbi, THE CRITICAL SIZED BONE DEFECT: MORPHOLOGICAL STUDY OF BONE HEALING STUDIO MORFOLOGICO DELLA RIPARAZIONE OSSEA IN UN DIFETTO OSSEO CRITICO, 2007.

[27] Y. Khan, M.J. Yaszemski, A.G. Mikos, C.T. Laurencin, Tissue engineering of bone: material and matrix considerations, The Journal of bone and joint surgery. American volume 90 Suppl 1 (2008) 36-42.

[28] N. Shayesteh Moghaddam, M. Taheri Andani, A. Amerinatanzi, C. Haberland, S. Huff, M. Miller, M. Elahinia, D. Dean, Metals for bone implants: safety, design, and efficacy, Biomanufacturing Reviews 1(1) (2016) 1.

[29] M. Orciani, M. Fini, R. Di Primio, M. Mattioli-Belmonte, Biofabrication and Bone Tissue Regeneration: Cell Source, Approaches, and Challenges, Frontiers in bioengineering and biotechnology 5 (2017) 17-17.

[30] O. Duchamp de Lageneste, A. Julien, R. Abou-Khalil, G. Frangi, C. Carvalho, N. Cagnard, C. Cordier, S.J. Conway, C. Colnot, Periosteum contains skeletal stem cells with high bone regenerative potential controlled by Periostin, Nature Communications 9(1) (2018) 773.

[31] S. Debnath, A.R. Yallowitz, J. McCormick, S. Lalani, T. Zhang, R. Xu, N. Li, Y. Liu, Y.S. Yang, M. Eiseman, J.H. Shim, M. Hameed, J.H. Healey, M.P. Bostrom, D.A. Landau, M.B. Greenblatt, Discovery of a periosteal stem cell mediating intramembranous bone formation, Nature 562(7725) (2018) 133-139.

[32] B.C. Heng, C. Zhang, X. Deng, Y. Xiao, A. Pisciotta, F. Kidwai, T.A. Mitsiadis, Biomedical Applications of Dental and Oral-Derived Stem Cells, Stem Cells International 2017 (2017) 2.

[33] M. Orciani, R. Di Primio, Skin-Derived Mesenchymal Stem Cells: Isolation, Culture, and Characterization, in: K. Turksen (Ed.), Skin Stem Cells: Methods and Protocols, Humana Press, Totowa, NJ, 2013, pp. 275-283.

[34] O. Karadas, D. Yucel, H. Kenar, G.T. Kose, V. Hasirci, Collagen scaffolds with in situ-grown calcium phosphate for osteogenic differentiation of Wharton's jelly and menstrual blood stem cells, J Tissue Eng Regen M 8(7) (2014) 534-545.

[35] Y. Liu, R. Niu, F. Yang, Y. Yan, S. Liang, Y. Sun, P. Shen, J. Lin, Biological characteristics of human menstrual blood-derived endometrial stem cells, Journal of Cellular and Molecular Medicine 22(3) (2018) 1627-1639.

[36] L. Chen, J. Qu, C. Xiang, The multi-functional roles of menstrual blood-derived stem cells in regenerative medicine, Stem Cell Research & Therapy 10(1) (2019) 1.

[37] D. Marolt, M. Knezevic, G.V. Novakovic, Bone tissue engineering with human stem cells, Stem Cell Res Ther 1(2) (2010) 10.

[38] C.M. Verfaillie, Adult stem cells: assessing the case for pluripotency, Trends in cell biology 12(11) (2002) 502-8.

[39] V. Kartsogiannis, K. Ng, Cell Lines and Primary Cell Cultures in the Study of Bone Cell Biology, 2005.

[40] Y. Honda, X. Ding, F. Mussano, A. Wiberg, C.-M. Ho, I. Nishimura, Guiding the osteogenic fate of mouse and human mesenchymal stem cells through feedback system control, Scientific reports 3 (2013) 3420-3420.

[41] S.X. Hsiong, T. Boontheekul, N. Huebsch, D.J. Mooney, Cyclic arginine-glycine-aspartate peptides enhance three-dimensional stem cell osteogenic differentiation, Tissue engineering. Part A 15(2) (2009) 263-272.

[42] B.A. Roecklein, B. Torok-Storb, Functionally distinct human marrow stromal cell lines immortalized by transduction with the human papilloma virus E6/E7 genes, Blood 85(4) (1995) 997-1005.

[43] S.K. Malyala, Y. Ravi Kumar, C.S.P. Rao, Organ Printing With Life Cells: A Review, Materials Today: Proceedings 4(2, Part A) (2017) 1074-1083.

[44] L. Moroni, J.H. Elisseeff, Biomaterials engineered for integration, Materials Today 11(5) (2008) 44-51.

[45] D.-C. Chen, Y.-L. Lai, S.-Y. Lee, S.-L. Hung, H.-L. Chen, Osteoblastic response to collagen scaffolds varied in freezing temperature and glutaraldehyde crosslinking, Journal of Biomedical Materials Research Part A 80A(2) (2007) 399-409.

[46] K.F. Leong, C.K. Chua, N. Sudarmadji, W.Y. Yeong, Engineering functionally graded tissue engineering scaffolds, Journal of the mechanical behavior of biomedical materials 1(2) (2008) 140-52.

[47] I. Drosse, E. Volkmer, R. Capanna, P. De Biase, W. Mutschler, M. Schieker, Tissue engineering for bone defect healing: an update on a multi-component approach, Injury 39 Suppl 2 (2008) S9-20.

[48] K. Rezwan, Q.Z. Chen, J.J. Blaker, A.R. Boccaccini, Biodegradable and bioactive porous polymer/inorganic composite scaffolds for bone tissue engineering, Biomaterials 27(18) (2006) 3413-31.

[49] Y. Ikada, Tissue engineering : fundamentals and applications, Academic Press/Elsevier, Amsterdam; Boston, 2006.

[50] J.A. Roether, J.E. Gough, A.R. Boccaccini, L.L. Hench, V. Maquet, R. Jerome, Novel bioresorbable and bioactive composites based on bioactive glass and polylactide foams for bone tissue engineering, Journal of materials science. Materials in medicine 13(12) (2002) 1207-14.

[51] J.S. Carson, M.P. Bostrom, Synthetic bone scaffolds and fracture repair, Injury 38 Suppl 1 (2007) S33-7.

[52] J.I. Dawson, D.A. Wahl, S.A. Lanham, J.M. Kanczler, J.T. Czernuszka, R.O. Oreffo, Development of specific collagen scaffolds to support the osteogenic and chondrogenic differentiation of human bone marrow stromal cells, Biomaterials 29(21) (2008) 3105-16.

[53] J.C. Courtenay, R.I. Sharma, J.L. Scott, Recent Advances in Modified Cellulose for Tissue Culture Applications, Molecules (Basel, Switzerland) 23(3) (2018) 654.

[54] G. Camci-Unal, A. Laromaine, E. Hong, R. Derda, G.M. Whitesides, Biomineralization Guided by Paper Templates, Scientific Reports 6 (2016).

[55] K. Ng, B. Gao, K.W. Yong, Y. Li, M. Shi, X. Zhao, Z. Li, X. Zhang, B. Pingguan-Murphy, H. Yang, F. Xu, Paper-based cell culture platform and its emerging biomedical applications, Materials Today 20(1) (2017) 32-44.

[56] F. Deiss, A. Mazzeo, E. Hong, D.E. Ingber, R. Derda, G.M. Whitesides, Platform for high-throughput testing of the effect of soluble compounds on 3D cell cultures, Analytical chemistry 85(17) (2013) 8085-8094.

[57] B. Mosadegh, B.E. Dabiri, M.R. Lockett, R. Derda, P. Campbell, K.K. Parker, G.M. Whitesides, Three-dimensional paper-based model for cardiac ischemia, Advanced healthcare materials 3(7) (2014) 1036-1043.

[58] G. Camci-Unal, D. Newsome, B.K. Eustace, G.M. Whitesides, Fibroblasts Enhance Migration of Human Lung Cancer Cells in a Paper-Based Coculture System, Advanced Healthcare Materials 5(6) (2016) 641-647.

[59] S.-H. Kim, H.R. Lee, S.J. Yu, M.-E. Han, D.Y. Lee, S.Y. Kim, H.-J. Ahn, M.-J. Han, T.-I. Lee, T.-S. Kim, S.K. Kwon, S.G. Im, N.S. Hwang, Hydrogel-laden paper scaffold system for origami-based tissue engineering, Proceedings of the National Academy of Sciences of the United States of America 112(50) (2015) 15426-15431.

[60] O. Karadas, G. Mese, E. Ozcivici, Cytotoxic Tolerance of Healthy and Cancerous Bone Cells to Anti-microbial Phenolic Compounds Depend on Culture Conditions, Applied biochemistry and biotechnology 188(2) (2019) 514-526.

[61] P. Hassanzadeh, Tissue engineering and growth factors: Updated evidence, 2012.

[62] J.O. Hollinger, T.A. Einhorn, B.A. Doll, C. Sfeir, Bone tissue enginering 1st Edition ed., CRC Press, Florida, 2005.

[63] C.J. Bishop, J. Kim, J.J. Green, Biomolecule delivery to engineer the cellular microenvironment for regenerative medicine, Ann Biomed Eng 42(7) (2014) 1557-1572.

[64] T.-M. De Witte, L.E. Fratila-Apachitei, A.A. Zadpoor, N.A. Peppas, Bone tissue engineering via growth factor delivery: from scaffolds to complex matrices, Regen Biomater 5(4) (2018) 197-211.

[65] C. Vater, P. Kasten, M. Stiehler, Culture media for the differentiation of mesenchymal stromal cells, Acta biomaterialia 7(2) (2011) 463-77.

[66] H. Kim, H. Suh, S.A. Jo, H.W. Kim, J.M. Lee, E.H. Kim, Y. Reinwald, S.H. Park, B.H. Min, I. Jo, In vivo bone formation by human marrow stromal cells in biodegradable

scaffolds that release dexamethasone and ascorbate-2-phosphate, Biochemical and biophysical research communications 332(4) (2005) 1053-60.

[67] R. A. Depprich, Biomolecule Use in Tissue Engineering, 2009.

[68] K. Hu, B.R. Olsen, The roles of vascular endothelial growth factor in bone repair and regeneration, Bone 91 (2016) 30-8.

[69] D.D. Bikle, C. Tahimic, W. Chang, Y. Wang, A. Philippou, E.R. Barton, Role of IGF-I signaling in muscle bone interactions, Bone 80 (2015) 79-88.

[70] C.G. Tahimic, Y. Wang, D. Bikle, Anabolic effects of IGF-1 signaling on the skeleton, Frontiers in Endocrinology 4(6) (2013).

[71] S. Advani, D. LaFrancis, E. Bogdanovic, P. Taxel, L.G. Raisz, B.E. Kream, Dexamethasone suppresses in vivo levels of bone collagen synthesis in neonatal mice, Bone 20(1) (1997) 41-6.

[72] S. Takamizawa, Y. Maehata, K. Imai, H. Senoo, S. Sato, R. Hata, Effects of ascorbic acid and ascorbic acid 2-phosphate, a long-acting vitamin C derivative, on the proliferation and differentiation of human osteoblast-like cells, Cell biology international 28(4) (2004) 255-65.

[73] D. Le Nihouannen, J.E. Barralet, J.E. Fong, S.V. Komarova, Ascorbic acid accelerates osteoclast formation and death, Bone 46(5) (2010) 1336-43.

[74] K.M. Choi, Y.K. Seo, H.H. Yoon, K.Y. Song, S.Y. Kwon, H.S. Lee, J.K. Park, Effect of ascorbic acid on bone marrow-derived mesenchymal stem cell proliferation and differentiation, Journal of bioscience and bioengineering 105(6) (2008) 586-94.

[75] M.J. Coelho, M.H. Fernandes, Human bone cell cultures in biocompatibility testing. Part II: effect of ascorbic acid, beta-glycerophosphate and dexamethasone on osteoblastic differentiation, Biomaterials 21(11) (2000) 1095-102.

[76] C.C. Wyles, M.T. Houdek, S.P. Wyles, E.R. Wagner, A. Behfar, R.J. Sierra, Differential cytotoxicity of corticosteroids on human mesenchymal stem cells, Clinical orthopaedics and related research 473(3) (2015) 1155-64.

[77] L. Demiray, Bone marrow stem cells adapt to low-magnitude vibrations by altering their cytoskeleton during quiescence and osteogenesis Turkish Journal of Biology 39 (2015) 88-97.

[78] O. Baskan, G. Mese, E. Ozcivici, Low-intensity vibrations normalize adipogenesis-induced morphological and molecular changes of adult mesenchymal stem cells, Proc Inst Mech Eng H 231(2) (2017) 160-168.

[79] R. Dorati, A. DeTrizio, T. Modena, B. Conti, F. Benazzo, G. Gastaldi, I. Genta, Biodegradable Scaffolds for Bone Regeneration Combined with Drug-Delivery Systems in Osteomyelitis Therapy, Pharmaceuticals (Basel) 10(4) (2017) 96.

[80] D.P. Lew, F.A. Waldvogel, Osteomyelitis, New England Journal of Medicine 336(14) (1997) 999-1007.

[81] D.P. Lew, F.A. Waldvogel, Use of Quinolones in Osteomyelitis and Infected Orthopaedic Prosthesis, Drugs 58(2) (1999) 85-91.

[82] N. Rao, B.H. Ziran, B.A. Lipsky, Treating osteomyelitis: antibiotics and surgery, Plastic and reconstructive surgery 127 Suppl 1 (2011) 177s-187s.

[83] H.S. Fraimow, Systemic antimicrobial therapy in osteomyelitis, Semin Plast Surg 23(2) (2009) 90-99.

[84] Y. Boakye, N. Osafo, C. Amaning Danquah, F. Adu, C. Agyare, Antimicrobial Agents: Antibacterial Agents, Anti-biofilm Agents, Antibacterial Natural Compounds, and Antibacterial Chemicals, 2019, pp. 1-24.

[85] S.M. Mandal, R.O. Dias, O.L. Franco, Phenolic Compounds in Antimicrobial Therapy, Journal of medicinal food 20(10) (2017) 1031-1038.

[86] G. Nieto, G. Ros, J. Castillo, Antioxidant and Antimicrobial Properties of Rosemary (Rosmarinus officinalis, L.): A Review, Medicines (Basel) 5(3) (2018) 98.

[87] R. Puupponen-Pimiä, L. Nohynek, C. Meier, M. Kähkönen, M. Heinonen, A. Hopia, K.-M. Oksman-Caldentey, Antimicrobial properties of phenolic compounds from berries, 2001.

[88] L. Sanhueza, R. Melo, R. Montero, K. Maisey, L. Mendoza, M. Wilkens, Synergistic interactions between phenolic compounds identified in grape pomace extract with antibiotics of different classes against Staphylococcus aureus and Escherichia coli, PLOS ONE 12(2) (2017) e0172273.

[89] J. Bauer, S. Kuehnl, J.M. Rollinger, O. Scherer, H. Northoff, H. Stuppner, O. Werz, A. Koeberle, Carnosol and Carnosic Acids from Salvia officinalis Inhibit Microsomal Prostaglandin E-2 Synthase-1, J Pharmacol Exp Ther 342(1) (2012) 169-176.

[90] J.J. Johnson, Carnosol: A promising anti-cancer and anti-inflammatory agent, Cancer Lett 305(1) (2011) 1-7.

[91] M.J. Jordan, V. Lax, M.C. Rota, S. Loran, J.A. Sotomayor, Relevance of Carnosic Acid, Carnosol, and Rosmarinic Acid Concentrations in the in Vitro Antioxidant and Antimicrobial Activities of Rosmarinus officinalis (L.) Methanolic Extracts, J Agr Food Chem 60(38) (2012) 9603-9608.

[92] D. Vergara, P. Simeone, S. Bettini, A. Tinelli, L. Valli, C. Storelli, S. Leo, A. Santino, M. Maffia, Antitumor activity of the dietary diterpene carnosol against a panel of human cancer cell lines, Food Funct 5(6) (2014) 1261-1269.

[93] M.G. Caballero, A.L. Jimenez, M.A.M. Torres, A.R. Quesada, Anti-angiogenic properties of carnosol and carnosic acid, two major dietary compounds from rosemary, Febs J 279 (2012) 92-92.

[94] J.J. Johnson, D.N. Syed, Y. Suh, C.R. Heren, M. Saleem, I.A. Siddiqui, H. Mukhtar, Disruption of Androgen and Estrogen Receptor Activity in Prostate Cancer by a Novel Dietary Diterpene Carnosol: Implications for Chemoprevention, Cancer Prev Res 3(9) (2010) 1112-1123.

[95] J.M. Visanji, D.G. Thompson, P.J. Padfield, Induction of G(2)/M phase cell cycle arrest by carnosol and carnosic acid is associated with alteration of cyclin A and cyclin B1 levels, Cancer Lett 237(1) (2006) 130-136.

[96] S. Birtic, P. Dussort, F.X. Pierre, A.C. Bily, M. Roller, Carnosic acid, Phytochemistry 115 (2015) 9-19.

[97] M.V. Barni, M.J. Carlini, E.G. Cafferata, L. Puricelli, S. Moreno, Carnosic acid inhibits the proliferation and migration capacity of human colorectal cancer cells, Oncol Rep 27(4) (2012) 1041-1048.

[98] L.S. Einbond, H.A. Wu, R. Kashiwazaki, K. He, M. Roller, T. Su, X.M. Wang, S. Goldsberry, Carnosic acid inhibits the growth of ER-negative human breast cancer cells and synergizes with curcumin, Fitoterapia 83(7) (2012) 1160-1168.

[99] V.G. Kontogianni, G. Tomic, I. Nikolic, A.A. Nerantzaki, N. Sayyad, S. Stosic-Grujicic, I. Stojanovic, I.P. Gerothanassis, A.G. Tzakos, Phytochemical profile of Rosmarinus officinalis and Salvia officinalis extracts and correlation to their antioxidant and anti-proliferative activity, Food Chem 136(1) (2013) 120-129.

[100] C.W. Tsai, C.Y. Lin, H.H. Lin, J.H. Chen, Carnosic Acid, a Rosemary Phenolic Compound, Induces Apoptosis Through Reactive Oxygen Species-Mediated p38 Activation in Human Neuroblastoma IMR-32 Cells, Neurochem Res 36(12) (2011) 2442-2451.

[101] S. Weckesser, K. Engel, B. Simon-Haarhaus, A. Wittmer, K. Pelz, C.M. Schempp, Screening of plant extracts for antimicrobial activity against bacteria and yeasts with dermatological relevance, Phytomedicine 14(7-8) (2007) 508-516.

[102] E. Torre, G. Iviglia, C. Cassinelli, M. Morra, Potentials of Polyphenols in Bone-Implant Devices, in: J. Wong (Ed.), Polyphenols2018.

[103] K.R. Hixon, T. Lu, S.H. McBride-Gagyi, B.E. Janowiak, S.A. Sell, A Comparison of Tissue Engineering Scaffolds Incorporated with Manuka Honey of Varying UMF, Biomed Res Int 2017 (2017) 4843065-4843065.

[104] Z.-C. Xing, W. Meng, J. Yuan, S. Moon, Y. Jeong, I.-K. Kang, In Vitro Assessment of Antibacterial Activity and Cytocompatibility of Quercetin-Containing PLGA Nanofibrous Scaffolds for Tissue Engineering, Journal of Nanomaterials 2012 (2012) 7.

[105] X. Xie, F. Pei, H. Wang, Z. Tan, Z. Yang, P. Kang, Icariin: A promising osteoinductive compound for repairing bone defect and osteonecrosis, Journal of biomaterials applications 30(3) (2015) 290-9.

[106] Y. Ji, L. Wang, D.C. Watts, H. Qiu, T. You, F. Deng, X. Wu, Controlled-release naringin nanoscaffold for osteoporotic bone healing, Dental materials : official publication of the Academy of Dental Materials 30(11) (2014) 1263-73.

[107] S. Osasan, M.Y. Zhang, F. Shen, P.J. Paul, S. Persad, C. Sergi, Osteogenic Sarcoma: A 21st Century Review, Anticancer Res 36(9) (2016) 4391-4398.

[108] C. Balachandran, Y. Arun, V. Duraipandiyan, S. Ignacimuthu, K. Balakrishna, N.A. Al-Dhabi, Antimicrobial and cytotoxicity properties of 2,3-dihydroxy-9,10-anthraquinone isolated from Streptomyces galbus (ERINLG-127), Applied biochemistry and biotechnology 172(7) (2014) 3513-28.

[109] S. Birtić, P. Dussort, F.-X. Pierre, A.C. Bily, M. Roller, Carnosic acid, Phytochemistry 115 (2015) 9-19.

[110] S. Moreno, T. Scheyer, C.S. Romano, A.A. Vojnov, Antioxidant and antimicrobial activities of rosemary extracts linked to their polyphenol composition, Free Radical Research 40(2) (2006) 223-231.

[111] A.M.O.S. Silvia Moreno, Mauro Gaya, María Verónica Barni, Olga A. Castro, Catalina van Baren, Rosemary Compounds as Nutraceutical Health Products, (2012).

[112] M.K. KEIICHI TABATA, MITSUKO MAKINO, MITSURU SATOH, YOSHIO SATOH, TAKASHI SUZUKI, Phenolic Diterpenes Derived from Hyptis incana Induce Apoptosis and G2/M Arrest of Neuroblastoma Cells, Anticancer Res. 32(11) (2012) 4781-9.

[113] E. Yildiz-Ozturk, S. Gulce-Iz, M. Anil, O. Yesil-Celiktas, Cytotoxic responses of carnosic acid and doxorubicin on breast cancer cells in butterfly-shaped microchips in comparison to 2D and 3D culture, Cytotechnology 69(2) (2017) 337-347.

[114] V.L. Udalamaththa, C.D. Jayasinghe, P.V. Udagama, Potential role of herbal remedies in stem cell therapy: proliferation and differentiation of human mesenchymal stromal cells, Stem Cell Research & Therapy 7(1) (2016) 110.

[115] I. Borrás-Linares, Z. Stojanović, R. Quirantes-Piné, D. Arráez-Román, J. Švarc-Gajić, A. Fernández-Gutiérrez, A. Segura-Carretero, Rosmarinus Officinalis Leaves as a Natural Source of Bioactive Compounds, International Journal of Molecular Sciences 15(11) (2014) 20585-20606.

[116] S. Habtemariam, The Therapeutic Potential of Rosemary (Rosmarinus officinalis) Diterpenes for Alzheimer's Disease, Evidence-based Complementary and Alternative Medicine : eCAM 2016 (2016) 2680409.

[117] N. Nakatani, R. Inatani, Structure of Rosmanol, A New Antioxidant from Rosemary (Rosmarinus officinalis L.), Agricultural and Biological Chemistry 45(10) (1981) 2385-2386.

[118] R.A. Jiménez, D. Millán, E. Suesca, A. Sosnik, M.R. Fontanilla, Controlled release of an extract of Calendula officinalis flowers from a system based on the incorporation of gelatin-collagen microparticles into collagen I scaffolds: design and in vitro performance, Drug Delivery and Translational Research 5(3) (2015) 209-218.

[119] H. Phuengkham, V. Teeranachaideekul, M. Chulasiri, N. Nasongkla, Preparation and optimization of chlorophene-loaded nanospheres as controlled release antimicrobial delivery systems, Pharmaceutical Development and Technology 21(1) (2016) 8-13.

[120] G.G. BUONOCORE, M. SINIGAGLIA, M.R. CORBO, A. BEVILACQUA, E.L. NOTTE, M.A.D. NOBILE, Controlled Release of Antimicrobial Compounds from Highly Swellable Polymers, Journal of Food Protection 67(6) (2004) 1190-1194.

[121] F.A. Al-Mulhim, M.A. Baragbah, M. Sadat-Ali, A.S. Alomran, M.Q. Azam, Prevalence of Surgical Site Infection in Orthopedic Surgery: A 5-year Analysis, International Surgery 99(3) (2014) 264-268.

[122] M. Ribeiro, F.J. Monteiro, M.P. Ferraz, Infection of orthopedic implants with emphasis on bacterial adhesion process and techniques used in studying bacterial-material interactions, Biomatter 2(4) (2012) 176-194.

[123] Y. Wang, J. Wang, H. Hao, M. Cai, S. Wang, J. Ma, Y. Li, C. Mao, S. Zhang, In Vitro and in Vivo Mechanism of Bone Tumor Inhibition by Selenium-Doped Bone Mineral Nanoparticles, ACS nano 10(11) (2016) 9927-9937.

[124] F.-C. Su, C.-C. Wu, S. Chien, Roles of Microenvironment and Mechanical Forces in Cell and Tissue Remodeling, 2011.

[125] P.J. Prendergast, R. Huiskes, The biomechanics of Wolff's law: recent advances, Irish journal of medical science 164(2) (1995) 152-4.

[126] E. Seeman, Age- and Menopause-Related Bone Loss Compromise Cortical and Trabecular Microstructure, The Journals of Gerontology: Series A 68(10) (2013) 1218-1225.

[127] E. Ozcivici, R. Garman, S. Judex, High-frequency oscillatory motions enhance the simulated mechanical properties of non-weight bearing trabecular bone, J Biomech 40(15) (2007) 3404-11.

[128] B.P. Hung, D.L. Hutton, W.L. Grayson, Mechanical control of tissue-engineered bone, Stem cell research & therapy 4(1) (2013) 10-10.

[129] J.M. Hughes, M.A. Petit, Biological underpinnings of Frost's mechanostat thresholds: the important role of osteocytes, Journal of musculoskeletal & neuronal interactions 10(2) (2010) 128-35.

[130] S.J. Mellon, K.E. Tanner, Bone and its adaptation to mechanical loading: a review, International Materials Reviews 57(5) (2012) 235-255.

[131] T. Sugiyama, L.B. Meakin, W.J. Browne, G.L. Galea, J.S. Price, L.E. Lanyon, Bones' adaptive response to mechanical loading is essentially linear between the low strains associated with disuse and the high strains associated with the lamellar/woven bone transition, J Bone Miner Res 27(8) (2012) 1784-1793.

[132] T.M. Skerry, One mechanostat or many? Modifications of the site-specific response of bone to mechanical loading by nature and nurture, Journal of musculoskeletal & neuronal interactions 6(2) (2006) 122-7.

[133] T. Steiniche, E.F. Eriksen, Chapter 15 - Age-Related Changes in Bone Remodeling, in: E.S. Orwoll (Ed.), Osteoporosis in Men, Academic Press, San Diego, 1999, pp. 299-312.

[134] B. Zhou, J. Wang, E.M. Stein, Z. Zhang, K.K. Nishiyama, C.A. Zhang, T.L. Nickolas, E. Shane, X.E. Guo, Bone density, microarchitecture and stiffness in Caucasian and Caribbean Hispanic postmenopausal American women, Bone Research 2 (2014) 14016.

[135] H. Razi, A.I. Birkhold, R. Weinkamer, G.N. Duda, B.M. Willie, S. Checa, Aging Leads to a Dysregulation in Mechanically Driven Bone Formation and Resorption, J Bone Miner Res 30(10) (2015) 1864-73.

[136] O. Demontiero, C. Vidal, G. Duque, Aging and bone loss: new insights for the clinician, Therapeutic advances in musculoskeletal disease 4(2) (2012) 61-76.

[137] A.L. Boskey, R. Coleman, Aging and bone, Journal of dental research 89(12) (2010) 1333-1348.

[138] S. Judex, W. Zhang, L.R. Donahue, E. Ozcivici, Genetic Loci That Control the Loss and Regain of Trabecular Bone During Unloading and Reambulation, Journal of Bone and Mineral Research 28(7) (2013) 1537-1549.

[139] E. Ozcivici, W. Zhang, L.R. Donahue, S. Judex, Quantitative trait loci that modulate trabecular bone's risk of failure during unloading and reloading, Bone 64 (2014) 25-32.

[140] E. Ozcivici, Y. Kim Luu, B. Adler, Y.-X. Qin, J. Rubin, S. Judex, C. Rubin, Mechanical signals as anabolic agent in bone, 2010.

[141] Y.F. Hsieh, C.H. Turner, Effects of loading frequency on mechanically induced bone formation, J Bone Miner Res 16(5) (2001) 918-24.

[142] B.R. Beck, K. Kent, L. Holloway, R. Marcus, Novel, high-frequency, low-strain mechanical loading for premenopausal women with low bone mass: early findings, Journal of bone and mineral metabolism 24(6) (2006) 505-7.

[143] M. Olcum, O. Baskan, O. Karadas, E. Ozcivici, Application of low intensity mechanical vibrations for bone tissue maintenance and regeneration, Turkish Journal of Biology 40(2) (2016) 300-307.

[144] S. Srinivasan, D.A. Weimer, S.C. Agans, S.D. Bain, T.S. Gross, Low-magnitude mechanical loading becomes osteogenic when rest is inserted between each load cycle, J Bone Miner Res 17(9) (2002) 1613-1620.

[145] J. Rubin, C. Rubin, C.R. Jacobs, Molecular pathways mediating mechanical signaling in bone, Gene 367 (2006) 1-16.

[146] J.F. Stoltz, D. Dumas, X. Wang, E. Payan, D. Mainard, F. Paulus, G. Maurice, P. Netter, S. Muller, Influence of mechanical forces on cells and tissues, Biorheology 37(1-2) (2000) 3-14.

[147] J.H.-C. Wang, B.P. Thampatty, An Introductory Review of Cell Mechanobiology, Biomechanics and Modeling in Mechanobiology 5(1) (2006) 1-16.

[148] M. Sladkova, G.M. de Peppo, Bioreactor Systems for Human Bone Tissue Engineering, 2014.

[149] I.A. Janson, A.J. Putnam, Extracellular matrix elasticity and topography: material-based cues that affect cell function via conserved mechanisms, Journal of biomedical materials research. Part A 103(3) (2015) 1246-1258.

[150] S.J. Mousavi, M. Hamdy Doweidar, Role of Mechanical Cues in Cell Differentiation and Proliferation: A 3D Numerical Model, PLOS ONE 10(5) (2015) e0124529.

[151] R.L. Duncan, C.H. Turner, Mechanotransduction and the functional response of bone to mechanical strain, Calcif Tissue Int 57(5) (1995) 344-58.

[152] C.H. Turner, F.M. Pavalko, Mechanotransduction and functional response of the skeleton to physical stress: the mechanisms and mechanics of bone adaptation, Journal of orthopaedic science : official journal of the Japanese Orthopaedic Association 3(6) (1998) 346-55.

[153] M. Mullender, A.J. El Haj, Y. Yang, M.A. van Duin, E.H. Burger, J. Klein-Nulend, Mechanotransduction of bone cells in vitro: mechanobiology of bone tissue, Medical & biological engineering & computing 42(1) (2004) 14-21.

[154] Y. Wang, L.M. McNamara, M.B. Schaffler, S. Weinbaum, A model for the role of integrins in flow induced mechanotransduction in osteocytes, Proceedings of the National Academy of Sciences of the United States of America 104(40) (2007) 15941-15946.

[155] L.D. You, S. Weinbaum, S.C. Cowin, M.B. Schaffler, Ultrastructure of the osteocyte process and its pericellular matrix, The anatomical record. Part A, Discoveries in molecular, cellular, and evolutionary biology 278(2) (2004) 505-13.

[156] L.M. McNamara, R.J. Majeska, S. Weinbaum, V. Friedrich, M.B. Schaffler, Attachment of osteocyte cell processes to the bone matrix, Anatomical record (Hoboken, N.J. : 2007) 292(3) (2009) 355-363.

[157] S.W. Verbruggen, T.J. Vaughan, L.M. McNamara, Strain amplification in bone mechanobiology: a computational investigation of the in vivo mechanics of osteocytes, Journal of The Royal Society Interface 9(75) (2012) 2735-2744.

[158] S. Temiyasathit, C.R. Jacobs, Osteocyte primary cilium and its role in bone mechanotransduction, Annals of the New York Academy of Sciences 1192 (2010) 422-428.

[159] H. Huang, R.D. Kamm, R.T. Lee, Cell mechanics and mechanotransduction: pathways, probes, and physiology, American journal of physiology. Cell physiology 287(1) (2004) C1-11.

[160] M.A. Schwartz, Integrins and extracellular matrix in mechanotransduction, Cold Spring Harbor perspectives in biology 2(12) (2010) a005066.

[161] C. Deng, G. Liu, The PI3K/Akt Signalling Pathway Plays Essential Roles in Mesenchymal Stem Cells, British Biomedical Bulletin 5(2) (2017).

[162] C. Galli, G. Passeri, G.M. Macaluso, Osteocytes and WNT: the Mechanical Control of Bone Formation, Journal of Dental Research 89(4) (2010) 331-343.

[163] M.P. Yavropoulou, J.G. Yovos, The role of the Wnt signaling pathway in osteoblast commitment and differentiation, Hormones (Athens, Greece) 6(4) (2007) 279-94.

[164] T. Gaur, C.J. Lengner, H. Hovhannisyan, R.A. Bhat, P.V. Bodine, B.S. Komm, A. Javed, A.J. van Wijnen, J.L. Stein, G.S. Stein, J.B. Lian, Canonical WNT signaling promotes osteogenesis by directly stimulating Runx2 gene expression, The Journal of biological chemistry 280(39) (2005) 33132-40.

[165] M. Bruderer, R.G. Richards, M. Alini, M.J. Stoddart, Role and regulation of RUNX2 in osteogenesis, European cells & materials 28 (2014) 269-86.

[166] R. Michael Delaine-Smith, B. Javaheri, J. Helen Edwards, M. Vazquez, R.M. Rumney, Preclinical models for in vitro mechanical loading of bone-derived cells, BoneKEy reports 4 (2015) 728.

[167] T. Shikata, T. Shiraishi, K. Tanaka, S. Morishita, R. Takeuchi, Effects of Acceleration Amplitude and Frequency of Mechanical Vibration on Osteoblast-Like Cells, 2007.

[168] J.A. Frangos, S.G. Eskin, L.V. McIntire, C.L. Ives, Flow effects on prostacyclin production by cultured human endothelial cells, Science (New York, N.Y.) 227(4693) (1985) 1477-9.

[169] C. Wittkowske, G.C. Reilly, D. Lacroix, C.M. Perrault, In Vitro Bone Cell Models: Impact of Fluid Shear Stress on Bone Formation, Frontiers in Bioengineering and Biotechnology 4(87) (2016).

[170] S. Judex, C.T. Rubin, Is bone formation induced by high-frequency mechanical signals modulated by muscle activity?, Journal of musculoskeletal & neuronal interactions 10(1) (2010) 3-11.

[171] W.R. Thompson, S.S. Yen, J. Rubin, Vibration therapy: clinical applications in bone, Current opinion in endocrinology, diabetes, and obesity 21(6) (2014) 447-453.

[172] J.H. Edwards, G.C. Reilly, Vibration stimuli and the differentiation of musculoskeletal progenitor cells: Review of results in vitro and in vivo, World J Stem Cells 7(3) (2015) 568-82.

[173] E. Lau, S. Al-Dujaili, A. Guenther, D. Liu, L. Wang, L. You, Effect of low-magnitude, high-frequency vibration on osteocytes in the regulation of osteoclasts, Bone 46(6) (2010) 1508-1515.

[174] C.O.-L. Yu, K.-S. Leung, J.L. Jiang, T.B.-Y. Wang, S.K.-H. Chow, W.-H. Cheung, Low-Magnitude High-Frequency Vibration Accelerated the Foot Wound Healing of n5-streptozotocin-induced Diabetic Rats by Enhancing Glucose Transporter 4 and Blood Microcirculation, Scientific Reports 7(1) (2017) 11631.

[175] K.S. Leung, H.F. Shi, W.H. Cheung, L. Qin, W.K. Ng, K.F. Tam, N. Tang, Low-magnitude high-frequency vibration accelerates callus formation, mineralization, and fracture healing in rats, Journal of orthopaedic research : official publication of the Orthopaedic Research Society 27(4) (2009) 458-65.

[176] B. Chen, Y. Li, D. Xie, X. Yang, Low-magnitude high-frequency loading via whole body vibration enhances bone-implant osseointegration in ovariectomized rats, Journal of Orthopaedic Research 30(5) (2012) 733-739.

[177] C. Rubin, R. Recker, D. Cullen, J. Ryaby, J. McCabe, K. McLeod, Prevention of Postmenopausal Bone Loss by a Low-Magnitude, High-Frequency Mechanical Stimuli: A Clinical Trial Assessing Compliance, Efficacy, and Safety, Journal of Bone and Mineral Research 19(3) (2004) 343-351.

[178] K.S. Leung, C.Y. Li, Y.K. Tse, T.K. Choy, P.C. Leung, V.W.Y. Hung, S.Y. Chan, A.H.C. Leung, W.H. Cheung, Effects of 18-month low-magnitude high-frequency vibration on fall rate and fracture risks in 710 community elderly—a cluster-randomized controlled trial, Osteoporosis International 25(6) (2014) 1785-1795.

[179] C.A. Gregory, W.G. Gunn, A. Peister, D.J. Prockop, An Alizarin red-based assay of mineralization by adherent cells in culture: comparison with cetylpyridinium chloride extraction, Anal Biochem 329(1) (2004) 77-84.

[180] A. Boskey, N. Pleshko Camacho, FT-IR imaging of native and tissue-engineered bone and cartilage, Biomaterials 28(15) (2007) 2465-2478.

[181] E.P. Paschalis, R. Mendelsohn, A.L. Boskey, Infrared assessment of bone quality: a review, Clinical orthopaedics and related research 469(8) (2011) 2170-8.

[182] H.M. Aydin, B. Hu, J. Sulé-Suso, A. Haj, Y. Yang, Study of tissue engineered bone nodules by Fourier transform infrared spectroscopy, 2011.

[183] H. Hanna, L.M. Mir, F.M. Andre, In vitro osteoblastic differentiation of mesenchymal stem cells generates cell layers with distinct properties, Stem cell research & therapy 9(1) (2018) 203-203.

[184] P. Collin, J.R. Nefussi, A. Wetterwald, V. Nicolas, M.L. Boy-Lefevre, H. Fleisch, N. Forest, Expression of collagen, osteocalcin, and bone alkaline phosphatase in a mineralizing rat osteoblastic cell culture, Calcif Tissue Int 50(2) (1992) 175-83.

[185] Y.-H.K. Yang, C.R. Ogando, C. Wang See, T.-Y. Chang, G.A. Barabino, Changes in phenotype and differentiation potential of human mesenchymal stem cells aging in vitro, Stem Cell Research & Therapy 9(1) (2018) 131.

[186] S.C. Moser, B.C.J. van der Eerden, Osteocalcin—A Versatile Bone-Derived Hormone, Frontiers in Endocrinology 9(794) (2019).

[187] M.L. Zoch, T.L. Clemens, R.C. Riddle, New insights into the biology of osteocalcin, Bone 82 (2016) 42-49.

[188] E. Golub, K. Boesze-Battaglia, The role of alkaline phosphatase in mineralization, Current Opinion in Orthopaedics 18 (2007) 444-448.

[189] W.J. Landis, R. Jacquet, Association of calcium and phosphate ions with collagen in the mineralization of vertebrate tissues, Calcif Tissue Int 93(4) (2013) 329-37.

[190] Y.-T. Tsao, Y.-J. Huang, H.-H. Wu, Y.-A. Liu, Y.-S. Liu, O.K. Lee, Osteocalcin Mediates Biomineralization during Osteogenic Maturation in Human Mesenchymal Stromal Cells, International journal of molecular sciences 18(1) (2017) 159.

[191] J. An, S. Leeuwenburgh, J. Wolke, J. Jansen, 4 - Mineralization processes in hard tissue: Bone, in: C. Aparicio, M.-P. Ginebra (Eds.), Biomineralization and Biomaterials, Woodhead Publishing, Boston, 2016, pp. 129-146.

[192] A.L. Boskey, Mineral-matrix interactions in bone and cartilage, Clinical orthopaedics and related research (281) (1992) 244-74.

[193] M.S. Johnsson, G.H. Nancollas, The role of brushite and octacalcium phosphate in apatite formation, Critical reviews in oral biology and medicine : an official publication of the American Association of Oral Biologists 3(1-2) (1992) 61-82.

[194] B. Xie, T.J. Halter, B.M. Borah, G.H. Nancollas, Tracking Amorphous Precursor Formation and Transformation during Induction Stages of Nucleation, Crystal Growth & Design 14(4) (2014) 1659-1665.

[195] H. Paul, A.J. Reginato, H.R. Schumacher, Alizarin red S staining as a screening test to detect calcium compounds in synovial fluid, Arthritis and rheumatism 26(2) (1983) 191-200.

[196] H. PUCHTLER, S.N. MELOAN, M.S. TERRY, ON THE HISTORY AND MECHANISM OF ALIZARIN AND ALIZARIN RED S STAINS FOR CALCIUM, Journal of Histochemistry & Cytochemistry 17(2) (1969) 110-124.

[197] C.M. Stanford, P.A. Jacobson, E.D. Eanes, L.A. Lembke, R.J. Midura, Rapidly forming apatitic mineral in an osteoblastic cell line (UMR 106-01 BSP), The Journal of biological chemistry 270(16) (1995) 9420-8.

[198] P. Simon, D. Grüner, H. Worch, W. Pompe, H. Lichte, T. El Khassawna, C. Heiss, S. Wenisch, R. Kniep, First evidence of octacalcium phosphate@osteocalcin nanocomplex as skeletal bone component directing collagen triple–helix nanofibril mineralization, Scientific Reports 8(1) (2018) 13696.

[199] M.M. Figueiredo, J. Gamelas, G. Martins, Characterization of Bone and Bone-Based Graft Materials Using FTIR Spectroscopy, 2012.

[200] A.L. Boskey, R. Roy, Cell culture systems for studies of bone and tooth mineralization, Chem Rev 108(11) (2008) 4716-4733.

[201] J.E. Phillips, D.W. Hutmacher, R.E. Guldberg, A.J. Garcia, Mineralization capacity of Runx2/Cbfa1-genetically engineered fibroblasts is scaffold dependent, Biomaterials 27(32) (2006) 5535-45.

[202] A. Kumar, C. Young, J. Farina, A. Witzl, E.D. Marks, Novel nanocomposite biomaterial to differentiate bone marrow mesenchymal stem cells to the osteogenic lineage for bone restoration, Journal of Orthopaedic Translation 3(3) (2015) 105-113.

[203] W.N. Addison, V. Nelea, F. Chicatun, Y.C. Chien, N. Tran-Khanh, M.D. Buschmann, S.N. Nazhat, M.T. Kaartinen, H. Vali, M.M. Tecklenburg, R.T. Franceschi, M.D. McKee, Extracellular matrix mineralization in murine MC3T3-E1 osteoblast cultures: an ultrastructural, compositional and comparative analysis with mouse bone, Bone 71 (2015) 244-56.

[204] J. Rauh, F. Milan, K.-P. Günther, M. Stiehler, Bioreactor Systems for Bone Tissue Engineering, 2011.

[205] A. Haj, S. Cartmell, Bioreactors for bone tissue engineering, 2010.

[206] D.A. Gaspar, V. Gomide, F.J. Monteiro, The role of perfusion bioreactors in bone tissue engineering, Biomatter 2(4) (2012) 167-175.

[207] F. Zhao, B. van Rietbergen, K. Ito, S. Hofmann, Flow rates in perfusion bioreactors to maximise mineralisation in bone tissue engineering in vitro, Journal of Biomechanics 79 (2018) 232-237.

[208] B. Bhaskar, R. Owen, H. Bahmaee, P.S. Rao, G.C. Reilly, Design and Assessment of a Dynamic Perfusion Bioreactor for Large Bone Tissue Engineering Scaffolds, Applied biochemistry and biotechnology 185(2) (2018) 555-563.

[209] G.N. Bancroft, V.I. Sikavitsas, A.G. Mikos, Design of a flow perfusion bioreactor system for bone tissue-engineering applications, Tissue engineering 9(3) (2003) 549-54.

[210] H. Nokhbatolfoghahaei, M.R. Rad, M.M. Khani, S. Shahriari, N. Nadjmi, A. Khojasteh, Application of Bioreactors to Improve Functionality of Bone Tissue Engineering Constructs: A Systematic Review, Current stem cell research & therapy 12(7) (2017) 564-599.

[211] A.M. Sailon, A.C. Allori, E.H. Davidson, D.D. Reformat, R.J. Allen, S.M. Warren, A Novel Flow-Perfusion Bioreactor Supports 3D Dynamic Cell Culture, Journal of Biomedicine and Biotechnology 2009 (2009).

[212] F.W. Janssen, J. Oostra, A.v. Oorschot, C.A. van Blitterswijk, A perfusion bioreactor system capable of producing clinically relevant volumes of tissue-engineered bone: In vivo bone formation showing proof of concept, Biomaterials 27(3) (2006) 315-323.

[213] M. Fröhlich, W.L. Grayson, D. Marolt, J.M. Gimble, N. Kregar-Velikonja, G. Vunjak-Novakovic, Bone Grafts Engineered from Human Adipose-Derived Stem Cells in Perfusion Bioreactor Culture, Tissue Engineering Part A 16(1) (2010) 179-189.

[214] T.R. Coughlin, J. Schiavi, M. Alyssa Varsanik, M. Voisin, E. Birmingham, M.G. Haugh, L.M. McNamara, G.L. Niebur, Primary cilia expression in bone marrow in response to mechanical stimulation in explant bioreactor culture, European cells & materials, 2016, pp. 111-122.

[215] Y.K. Luu, S. Lublinsky, E. Ozcivici, E. Capilla, J.E. Pessin, C.T. Rubin, S. Judex, In vivo quantification of subcutaneous and visceral adiposity by micro-computed tomography in a small animal model, Medical engineering & physics 31(1) (2009) 34-41.

[216] S. Judex, Y.K. Luu, E. Ozcivici, B. Adler, S. Lublinsky, C.T. Rubin, Quantification of adiposity in small rodents using micro-CT, Methods (San Diego, Calif.) 50(1) (2010) 14-9.

[217] G.M. Campbell, A. Sophocleous, Quantitative analysis of bone and soft tissue by micro-computed tomography: applications to ex vivo and in vivo studies, BoneKEy reports 3 (2014) 564-564.

[218] S.R. Stock, K.I. Ignatiev, S.A. Foster, L.A. Forman, P.H. Stern, MicroCT quantification of in vitro bone resorption of neonatal murine calvaria exposed to IL-1 or PTH, Journal of structural biology 147(2) (2004) 185-99.

[219] M. Mashiatulla, R.D. Ross, D.R. Sumner, Validation of cortical bone mineral density distribution using micro-computed tomography, Bone 99 (2017) 53-61.

[220] M.-H. Choi, W.-C. Noh, J.-W. Park, J.-M. Lee, J.-Y. Suh, Gene expression pattern during osteogenic differentiation of human periodontal ligament cells in vitro, J Periodontal Implant Sci 41(4) (2011) 167-175.

[221] W. Huang, S. Yang, J. Shao, Y.-P. Li, Signaling and transcriptional regulation in osteoblast commitment and differentiation, Frontiers in bioscience : a journal and virtual library 12 (2007) 3068-3092.

[222] Y. Li, C. Ge, J.P. Long, D.L. Begun, J.A. Rodriguez, S.A. Goldstein, R.T. Franceschi, Biomechanical stimulation of osteoblast gene expression requires phosphorylation of the RUNX2 transcription factor, J Bone Miner Res 27(6) (2012) 1263-74.

[223] T. Komori, Regulation of osteoblast differentiation by transcription factors, Journal of cellular biochemistry 99(5) (2006) 1233-1239.

[224] J. Xu, Z. Li, Y. Hou, W. Fang, Potential mechanisms underlying the Runx2 induced osteogenesis of bone marrow mesenchymal stem cells, American journal of translational research 7(12) (2015) 2527-2535.

[225] M. Mizuno, Y. Kuboki, Osteoblast-Related Gene Expression of Bone Marrow Cells during the Osteoblastic Differentiation Induced by Type I Collagen, The Journal of Biochemistry 129(1) (2001) 133-138.

[226] T. Kanno, T. Takahashi, T. Tsujisawa, W. Ariyoshi, T. Nishihara, Mechanical stress-mediated Runx2 activation is dependent on Ras/ERK1/2 MAPK signaling in osteoblasts, Journal of cellular biochemistry 101(5) (2007) 1266-1277.

[227] E. Birmingham, G.L. Niebur, P.E. McHugh, G. Shaw, F.P. Barry, L.M. McNamara, Osteogenic differentiation of mesenchymal stem cells is regulated by osteocyte and osteoblast cells in a simplified bone niche, European cells & materials 23 (2012) 13-27.

[228] M.H. Lee, A. Javed, H.J. Kim, H.I. Shin, S. Gutierrez, J.Y. Choi, V. Rosen, J.L. Stein, A.J.v. Wijnen, G.S. Stein, J.B. Lian, H.M. Ryoo, Transient upregulation of CBFA1 in response to bone morphogenetic protein-2 and transforming growth factor β1 in C2C12 myogenic cells coincides with suppression of the myogenic phenotype but is not sufficient for osteoblast differentiation, Journal of cellular biochemistry 73(1) (1999) 114-125.

[229] C.D. Toma, S. Ashkar, M.L. Gray, J.L. Schaffer, L.C. Gerstenfeld, Signal Transduction of Mechanical Stimuli Is Dependent on Microfilament Integrity: Identification of Osteopontin as a Mechanically Induced Gene in Osteoblasts, Journal of Bone and Mineral Research 12(10) (1997) 1626-1636.

[230] J. Sodek, J. Chen, T. Nagata, S. Kasugai, R. Todescan, Jr., I.W. Li, R.H. Kim, Regulation of osteopontin expression in osteoblasts, Ann N Y Acad Sci 760 (1995) 223-41.

[231] S. Wongkhantee, T. Yongchaitrakul, P. Pavasant, Mechanical Stress Induces Osteopontin Expression in Human Periodontal Ligament Cells Through Rho Kinase, Journal of Periodontology 78(6) (2007) 1113-1119.

[232] A.L. Boskey, Chapter 1 - The Biochemistry of Bone: Composition and Organization, in: E.S. Orwoll, J.P. Bilezikian, D. Vanderschueren (Eds.), Osteoporosis in Men (Second Edition), Academic Press, San Diego, 2010, pp. 3-13.

[233] B. Ganss, R.H. Kim, J. Sodek, Bone Sialoprotein, Critical Reviews in Oral Biology & Medicine 10(1) (1999) 79-98.

[234] Y. Ogata, Bone sialoprotein and its transcriptional regulatory mechanism, 2008.

[235] L. Malaval, N.M. Wade-Guéye, M. Boudiffa, J. Fei, R. Zirngibl, F. Chen, N. Laroche, J.-P. Roux, B. Burt-Pichat, F. Duboeuf, G. Boivin, P. Jurdic, M.-H. Lafage-Proust, J. Amédée, L. Vico, J. Rossant, J.E. Aubin, Bone sialoprotein plays a functional role in bone formation and osteoclastogenesis, The Journal of experimental medicine 205(5) (2008) 1145-1153.

[236] J. Chen, M.D. McKee, A. Nanci, J. Sodek, Bone sialoprotein mRNA expression and ultrastructural localization in fetal porcine calvarial bone: comparisons with osteopontin, The Histochemical journal 26(1) (1994) 67-78.

[237] M. Ikegame, S. Ejiri, H. Okamura, Expression of Non-collagenous Bone Matrix Proteins in Osteoblasts Stimulated by Mechanical Stretching in the Cranial Suture of Neonatal Mice, Journal of Histochemistry & Cytochemistry 67(2) (2019) 107-116.

[238] A.L. Boskey, Matrix proteins and mineralization: an overview, Connective tissue research 35(1-4) (1996) 357-63.

[239] J.P. Bonjour, Calcium and phosphate: a duet of ions playing for bone health, Journal of the American College of Nutrition 30(5 Suppl 1) (2011) 438s-48s.

[240] M.A. Wood, Y. Yang, P.B. Thomas, A.J. Haj, Using dihydropyridine-release strategies to enhance load effects in engineered human bone constructs, Tissue engineering 12(9) (2006) 2489-97.

VITA

Date and place of birth: 14/04/1984 Edirne

Education:

MSc: Middle East Technical University, Biotechnology

BSc: Ege University, Bioengineering

Fellowships & Honors:

EMBO Short Term Fellowship, National University of Ireland, Galway, November 2018-February 2019

Course Performance Award, METU, 2008

Erasmus Scholarship, Åbo Akademi University, 2005 August-2006 August

Publications:

Thesis:

Collagen Scaffolds with In Situ Grown Calcium Phosphate for Osteogenic Differentiation of Wharton's Jelly and Menstrual Blood Stem Cells. Msc.Thesis, Department of Biotechnology, METU, 2011

Articles in International Journals:

O. Karadas, G. Mese, E. Ozcivici. Cytotoxic Tolerance of Healthy and Cancerous Bone Cells to Anti-microbial Phenolic Compounds Depend on Culture Conditions. Applied Biochemistry and Biotechnology, 188 (2), pages 534-545, June 2019

O. Baskan, O. Karadas, G. Mese, E. Ozcivici. Applicability of Low-Intensity Vibrations as a Regulatory Factor on Stem and Progenitor Cell Populations. Current Stem Cell Research & Therapy (2019) 14: 1, DOI: 10.2174/1574888X14666191212155647

M. Olcum, O. Baskan, O. Karadas, E. Ozcivici. Application of Mechanical Vibrations for Bone Tissue Maintenance and Regeneration. Turkish Journal of Biology, Volume 40, pages 300-307, February 2016

O. Karadas, D. Yucel, H. Kenar, G. T. Kose, V. Hasirci. Collagen scaffolds with in situ grown calcium phosphate for osteogenic differentiation of Wharton's jelly and menstrual blood stem cells. Journal of Tissue Engineering and Regenerative Medicine, Volume 8, Issue 7, pages 534-545, July 2014